CONTROLLING THE PROPERTIES OF A LIQUID CRYSTALLINE EPOXY THROUGH MAGNETIC FIELD PROCESSING

BY

DEREK M. LINCOLN

A THESIS PRESENTED TO THE GRADUATE SCHOOL
OF THE UNIVERSITY OF FLORIDA IN PARTIAL FULFILLMENT
OF THE REQUIREMENTS FOR THE DEGREE OF
MASTER OF SCIENCE

UNIVERSITY OF FLORIDA

1998

REPORT DOCUMENTATION PAGE	Form Approved OMB No. 0704-0188

1. AGENCY USE ONLY *(Leave blank)*	2. REPORT DATE	3. REPORT TYPE AND DATES COVERED
	2 October 1998	

4. TITLE AND SUBTITLE
CONTROLLING THE PROPERTIES OF A LIQUID CRYSTALLINE EPOXY THROUGH MAGNETIC FIELD PROCESSING

5. FUNDING NUMBERS

6. AUTHOR(S)
DEREK M. LINCOLN

7. PERFORMING ORGANIZATION NAME(S) AND ADDRESS(ES)
UNIVERSITY OF FLORIDA

8. PERFORMING ORGANIZATION REPORT NUMBER
98-068

9. SPONSORING/MONITORING AGENCY NAME(S) AND ADDRESS(ES)
THE DEPARTMENT OF THE AIR FORCE
AFIT/CIA, BLDG 125
2950 P STREET
WPAFB OH 45433

10. SPONSORING/MONITORING AGENCY REPORT NUMBER

11. SUPPLEMENTARY NOTES

12a. DISTRIBUTION AVAILABILITY STATEMENT
Unlimited Distribution
In Accordance With 35-205/AFIT Sup 1

12b. DISTRIBUTION CODE

13. ABSTRACT *(Maximum 200 words)*

14. SUBJECT TERMS

15. NUMBER OF PAGES
116

16. PRICE CODE

17. SECURITY CLASSIFICATION OF REPORT	18. SECURITY CLASSIFICATION OF THIS PAGE	19. SECURITY CLASSIFICATION OF ABSTRACT	20. LIMITATION OF ABSTRACT

Abstract of Thesis Presented to the Graduate School
of the University of Florida in Partial Fulfillment of the
Requirements for the Degree of Master of Science

CONTROLLING THE PROPERTIES OF A LIQUID CRYSTALLINE EPOXY THROUGH MAGNETIC FIELD PROCESSING

By

Derek M. Lincoln

August 1998

Chairman: Dr. Elliot P. Douglas
Major Department: Materials Science and Engineering

It has been demonstrated recently that the physical and mechanical properties of liquid crystalline thermosets can be altered via processing in a magnetic field. Magnetic field processing imparts a degree of macromolecular anisotropy on the material. This anisotropy has been shown to cause a favorable change in some of these mechanical and physical properties. However, the degree of control over these property changes has yet to be studied in depth. The focus of this research is to explore the effects of the processing variables and determine the amount of control that exists over the final properties of the material.

A liquid crystalline epoxy, 4, 4'-diglycidyloxy-α-methylstilbene, and tetrafunctional diamine crosslinking agent, sulfanilamide, were used as the resin system for this study. The process variables that were determined to be the largest effectors of

the reorientation process are the magnetic field strength, the time in the field, and the amount of b-staging, or precuring, of the material. The response variable chosen to be studied was the second moment of the orientation function, or orientation parameter, determined by wide angle x-ray scattering (WAXS).

A statistical experimental design was employed using CARD® (Computer Aided Research and Development) software to investigate the interaction effects of the variables. The design used was a modified fractional factorial design to reduce the total number of samples required but still included several pairs of replicates to determine the experimental error not associated with the variation of the variables described above.

The samples were prepared and cured in a magnetic field at the National High Magnetic Field Laboratory. Wide angle x-ray scattering (WAXS) experiments were conducted to determine the amount of orientation imparted in the samples. The orientation parameter calculated was used as the response variable for the statistical experimental design.

The results form the experimental design showed the amount of B-staging and field strength to be the largest effectors of the orientation process. The time in the field was also shown to have an effect on the orientation process but not to the extent of the other two. A model constructed to model the response variables had a very good fit, R^2, of 0.8577. The experimental error is estimated to be 5.82%, which indicates that small effects of the variables can be predicted with the model.

Abstract of Thesis Presented to the Graduate School
of the University of Florida in Partial Fulfillment of the
Requirements for the Degree of Master of Science

CONTROLLING THE PROPERTIES OF A LIQUID CRYSTALLINE EPOXY THROUGH MAGNETIC FIELD PROCESSING

By

Derek M. Lincoln

August 1998

Chairman: Dr. Elliot P. Douglas
Major Department: Materials Science and Engineering

It has been demonstrated recently that the physical and mechanical properties of liquid crystalline thermosets can be altered via processing in a magnetic field. Magnetic field processing imparts a degree of macromolecular anisotropy on the material. This anisotropy has been shown to cause a favorable change in some of these mechanical and physical properties. However, the degree of control over these property changes has yet to be studied in depth. The focus of this research is to explore the effects of the processing variables and determine the amount of control that exists over the final properties of the material.

A liquid crystalline epoxy, 4, 4'-diglycidyloxy-α-methylstilbene, and tetrafunctional diamine crosslinking agent, sulfanilamide, were used as the resin system for this study. The process variables that were determined to be the largest effectors of

the reorientation process are the magnetic field strength, the time in the field, and the amount of b-staging, or precuring, of the material. The response variable chosen to be studied was the second moment of the orientation function, or orientation parameter, determined by wide angle x-ray scattering (WAXS).

A statistical experimental design was employed using CARD® (Computer Aided Research and Development) software to investigate the interaction effects of the variables. The design used was a modified fractional factorial design to reduce the total number of samples required but still included several pairs of replicates to determine the experimental error not associated with the variation of the variables described above.

The samples were prepared and cured in a magnetic field at the National High Magnetic Field Laboratory. Wide angle x-ray scattering (WAXS) experiments were conducted to determine the amount of orientation imparted in the samples. The orientation parameter calculated was used as the response variable for the statistical experimental design.

The results form the experimental design showed the amount of B-staging and field strength to be the largest effectors of the orientation process. The time in the field was also shown to have an effect on the orientation process but not to the extent of the other two. A model constructed to model the response variables had a very good fit, R^2, of 0.8577. The experimental error is estimated to be 5.82%, which indicates that small effects of the variables can be predicted with the model.

BIOGRAPHICAL SKETCH

Derek Lincoln was born in Denver, Colorado on 20 January 1974. He lived in Colorado from birth until coming to the University of Florida for work on his Master of Science degree in August 1996 degree. Prior to that he earned his Bachelor of Science degree and a commission as a second lieutenant in the United States Air Force form the United States Air Force Academy in Colorado Springs, Colorado.

Following graduation from the University of Florida he was assigned to the Air Force Material labs at Wright-Patterson Air Force Base, Dayton Ohio to work in the Materials and Manufacturing Directorate, Non-metallic materials division, Polymer branch.

LIST OF REFERENCES

Adm78 Admur, S; Chang, A.; Wong, C.; Ehrlich, P.; Allendoerfer, D. *J. Polym. Sci. Polym. Chem. Ed.* **1978**, *16*, 407

Alt95 Alt, David J.; Hudson, Steven D.; Garag, R. O.; Fujishiro, K. *Macromolecules.* **1995**, *28*, 1575

Anw91 Anwer, Afzana; Windle, Alan H. *Polymer.* **1991**, *32*, 103

Anw93 Anwer, A.; Windle, A. H. *Polymer.* **1993**, *34*, 3347

Arr72 Arridge, R. G. C.; Speake, J. H. *Polymer.* **1972**, *13*, 443

Ass97 Assender, Hazel E.; Windle, Alan H. *Polymer.* **1997**, *38*, 677

Avi76 Aviram, A. *Polym. Sci.: Polym. Lett. Ed.* **1976**, *14*, 757

Bar92 Barclay, G. G.; McNamee, S. G.; Ober, C. K.; Papathoms, K. I.; Wang, D. W. *J. Polym. Sci.: Part A: Polym. Chem.* **1992**, *30*, 1845

Bee96 Beekmans, F.; Posthuma de Boer, A. *Macromolecules.* **1996**, *29*, 8726

Bel90 Bellenger, V.; Dhoui, W.; Verdu, J.; Boye, J.; Lacabanne, C. *Polym. Eng. Sci.* **1990**, *30*, 321

Ben92 Benicewicz, Brian C.; Hoyt, Andrea E. U.S. Patent 5,114,612 1992.

Ben98 Benicewicz, Brian C.; Smith, Mark E.; Earls, Jim D.; Priester, Ralph D.; Setz, Stefan M.; Duran, Randolph S.; Douglas, Elliot P. *Macromolecules.* submitted

Bli97 Blinov, L. M. in *Handbook of liquid Crystal Research.* Collings, Peter J.; Patel, Jay S. ed. Oxford University Press: New York, 1997, p. 125.

Car70 Carr, E. F. *Phys. Rev. Lett.* **1970**, *24*, 807

Car93 Carfagna, C.; Amendola, E.; Giamberini, M.; Filippov, A. G.; Bauer, R. S. *Liquid Crystals.* **1993**, *13*, 571

Car94a Carfagna, C.; Amendola, E; Giamberini, M. *Composite Structures.* **1994**, *27*, 37

Car94b Carfagna, C.; Amendola, E; Giamberini, M. *J. Mat. Sci. Lett.* **1994**, *13*, 126

Car94c Carfagna, C.; Amendola, E.; Giamberini, M. *Liquid Crystalline Polymers: Proceedings of the International Workshop of Liquid Crystalline Polymers*. Capri, Italy, June 1-4, 1993, Carfagna, C. Ed.; Pergamon Press: Oxford, UK, 1994; pp. 69-85.

Car94d Carfagna, Cosimo; Amendola, Eugenio; Giamberini, Marta. *Macromol. Rapid Commun.* **1994**, *195*, 279

Car94e Carfagna, Cosimo; Amendola, Eugenio; Giamberini, Marta. *Macromol. Chem. Phys.* **1994**, *195*, 2307

Car95 Carfagna, C.; Amendola, E.; Giamberini, M.; Mensitieri, G.; Del Nobile, M. A.; Filippov, A. G. *Polym. Eng. Sci.* **1995**, *35*, 137

Cha94 Chang, Rong-yeu; Sjiao, Fu-chia; Yang, Wen-lii. *J. Non-Newtonian Fluid Mech.* **1994**, *55*, 1

Col97 Collings, Peter J.; Patel, Jay S. in *Handbook of Liquid Crystal Research*. Collings, Peter J.; Patel, Jay S. ed.; Oxford University Press; New York, 1997, p. 1.

Cre92 Crevecour, G.; Groeninckx, G. *Polymer Composites*. **1992**, *13*, 244

deG93 de Gennes, P. G.; Prost, J. *The Physics of Liquid Crystals*. Clarendon Press: Oxford, 1993.

Dem80 Demus, D.; Richter, L. *Texture of Liquid Crystals*. VEB Deutscher Verlag für Grundstoff Industrie: Leipzig, 1980.

Dre98 Dreher, S.; Seifert, S.; Zachmann, H. G.; Moszner, N.; Mercoli, P.; Zanghellini, G. *J. Appl. Polym. Sci.* **1998**, *67*, 531

Dut90 Dutta, D.; Fruitwala, H.; Kohli, A.; Weiss, R. A. *Polym. Eng. Sci.* **1990**, *30*, 1005

Eck96 Eckert, Tobias; Finklemann, Heino. *Macromol. Rapid Commun.* **1996**, *17*, 767

Eic96 Eichorn, Klaus J.; Sahre, Karin; Jahnichen, Diefer; Tobisch, Josef; Häbler, Liane. *Macromol. Chem. Phys.* **1996**, *197*, 3729

Eng94 Engberg, K.; Strömberg, O.; Martinsson, J.; Gedde, U. W. *Polym. Sci. Eng.* **1994**, *34*, 1336

Enn83 Enns, John B.; Gillham, John K. *J. Appl. Polym. Sci.* **1983**, *28*, 2831

Fer97 Ferri, D.; Laus, M. *Macromolecules.* **1997**, *30*, 6007

Ger91 Gerzeski, Roger H. *Int. SAMPE Symp.* **1991**, *36*, 1368

Gia95 Giamberini, Marta; Amendola, Eugenio; Carfagna, Cosimo. *Macromol. Rapid Commun.* **1995**, *16*, 97

Gra83 Gray, M. E.; Harrison, I. R. *J. Appl. Polym. Sci.* **1983**, *28*, 3603

Gri91 Grillet, Anne Cecile; Galy, Jocelyne; Gerard, Jean-Francois; Pascault, Jean-Pierre. *Polymer.* **1991**, *32*, 1885

Gul72 Gul', V. E.; Trifel', Yu. B.; Abdullaev, N. A. *Mekhanika Polimerov.* **1972**, *5*, 923

Gup85 Gupta, V. B.; Drzal, L. T.; Lee, C. Y. C. *Polym. Eng. Sci.* **1985**, *25*, 812

Han96 Hanabusa, Kenji; Hashimoto, Masami; Kimura, Mutsumi; Koyama, Toshiki; Shirai, Hirofusa. *Macromol. Chem. Phys.* **1996**, *197*, 1853

Her80 Hergenrother, P. M. *J. Macromol. Chem.* **1980**, *C19*, 1

Hey93 Heynderickx, I; Paridaans, F. *Polymer.* **1993**, *34*, 4068

Hik91 Hikmet, R. A.; Broer, D. J. *Polymer.* **1991**, *32*, 1627

Hik93 Hikmet, R. A. M.; Lub, J.; Higgins, J. A. *Polymer.* **1993**, *34*, 1736

Hoy90a Hoyt, Andrea E.; Benicewicz, Brian C.; Huang, Samuel J. in *ACS Symposium Series 435.* Weiss, R. A.; Ober, C. K. ed.; American Chemical Society: Washington, D. C., 1990, p. 198.

Hoy90b Hoyt, Andrea E.; Benicewicz, Brian C. *J. Polym. Sci.: Part A: Polym. Chem.* **1990**, *28*, 3403

Hoy90c Hoyt, Andrea E.; Benicewicz, Brian C. *J. Polym. Sci.: Part A: Polym. Chem.* **1990**, *28*, 3417

Hud90 Hudson, Steven D.; Thomas, Edwin L. *Polymer Preprints*. **1990**, *31*, 379

Iiz85 Iizuka, Eisaku. *J. of Appl. Polym. Sci.: Appl. Polym. Symp*. **1985**, *41*, 131

Jen73 Jen, S.; Clark, N. A.; Pershan, P. S.; Priestly, E. B. *Phys. Rev. Lett.* **1973**, *31*, 1552

Kis78 Kishore, P. R.; Rao, N. V. S.; Sarma, P. B. K.; Raj, T. F. S.; Avadhanlu, M. N.; Murty, C. R. K. *Mol. Cryst. Liq. Cryst.* **1978**, *45*, 231

Kis87 Kiss, Gabor. *Polym. Eng. Sci.* **1987**, *27*, 410

Kee79 Keenan, Joseph D.; Seferis, James C.; Quinlivan, John T. *J. Appl. Polym. Sci.* **1979**, *24*, 2375

Kos97 Kossikhina, S.; Kimura, T.; Ito, E.; Kawahara, M. *Polym. Eng. and Sci.* **1997**, *37*, 396

Koz89 Kozak, A.; Simon, G. P.; Williams, G. *Polym. Commun.* **1989**, *30*, 102

Kra76 Kramarenko, N. L.; Kurnosov, I. V.; Naboikin, Yu. V. *Phys. Stat. Sol. (A)*. **1976**, *33*, 773

Li96 Li, Jianlin; Anderson, James E.; Hoke, Charles D.; Nose, Toshiaki; Bos, Philip J. *Jpn. J. Appl. Phys*. **1996**, *35*, 1342

Lin94 Lin, Qinghuang; Yee, Albert F.; Earls, Jimmy D.; Hefner Jr., Robert E.; Sue, Hung-Jue. *Polymer*. **1994**, *35*, 2679

Lin97 Lin, Q.; Yee, A. F.; Sue, H-J.; Earls, J. D.; Hefner Jr., R. E. *J. Polym. Sci. Part B: Polym. Phys*. **1997**, *35*, 2363

Lit93 Litt, Morton H.; Whang, Wha-Tzong; Yen, Kung-Ti; Qian, Xue-Jun. *J. Polym. Sci.: Part A: Polym Chem*. **1993**, *31*, 183

Liu97 Liu, Jingping; Wang, Chicheng; Campbell, Gregory A.; Earls, Jim D.; Priester Jr., Ralph D. *J. Polym. Sci.: Part A: Polym. Chem*. **1997**, *35*, 1105

Mar82 Maret, G.; Blumstein, A. *Mol. Cryst. Liq. Cryst*. **1982**, *88*, 295

Mar91 Marrucci, Giuseppe; Grizzuti, Nino. *Makromol. Chem. Macromol. Symp.* **1991**, *181*

Mel94 Melissaris, Anastasios P.; Litt, Morton H. *Macromolecules*. **1994**, *27*, 2675

Mel95 Melissaris, Anastsios P.; Sutter, James K.; Litt, Morton H.; Scheiman, Daniel A.; Schuerman, Marla A. *Macromolecules*. **1995**, *28*, 860

Mic86 Michl, J.; Thulstrup, E. W. *Spectroscopy with Polarized Light*. VCH Publishers: Deerfield Beach, FL, 1986.

Mik87 Mikolajczak, G.; Cavaille, J. Y.; Johari, G. P. *Polymer*. **1987**, *28*, 2023

Miy78 Miyano, K. *J. Chem Phys*. **1978**, *69*, 4807

Moo85 Moore, R. C.; Denn, M. M.; Marrucci, G. *Polym. Mat. Sci. Eng*. **1985**, *52*, 84

Moo87 Moore, J. S.; Stupp, S. I. *Macromolecules*. **1987**, *20*, 282

Moo96 Moon, Hyuk-soo; Park, Jung-ki; Liu, Ju-hwan. *J. Appl. Polym. Sci*. **1996**, *59*, 489

Och85 Ochi, Mitsukazu; Iesako, Hiroshi; Shimbo, Masakis. *Polymer*. **1985**, *26*, 457

Pog70 Pogany, G. A. *Polymer*. **1970**, *11*, 66

Rao76 Rao, N. V. S.; Kishore, P. R.; Raj, T. F. S.; Avadhanlu, M. N.; Murty, C. R. K. *Mol. Cryst. Liq. Cryst*. **1976**, *36*, 65

Rat80 Rato, J.; Dynes, P.; Hamermesh, C. J. *J. Polym. Sci. Polym. Chem. Ed*. **1980**, *18*, 1035

Rod91 Rodin, Yu P. *Mekhanika Kompozitnykh Metrialov*. **1991**, *3*, 490

San95 Sanz, G.; Garmendia, J.; Andes, M. A.; Mondragon, I. *J. Appl. Polym. Sci*. **1995**, *55*, 75

Sas91 Sasuga, Tsuneo; Udagawa, Akira. *Polymer*. **1991**, *32*, 402

Saw86 Sawyer, Linda C.; Jaffe, Michael. *J. of Mat. Sci*. **1986**, *21*, 1897

Shi96 Shiota, Atsushi; Ober, Christopher K. *J. Polym. Sci.: Part A: Polym. Chem.* **1996**, *34*, 1291

Shi97a Shimoda, Toshiyuki; Kimura, Tsuehisa; Ito, Eiko. *Macromolecules.* **1997**, *30*, 5045

Shi97b Shiota, Atsushi; Ober, Christopher K. *Macromolecules.* **1997**, *30*, 4278

Shi97c Shiota, Atsushi; Ober, Christopher K. *Polymer.* **1997**, *38*, 5857

Smi96 Smith, M. E.; Douglas, E. P.; Benicewicz B. C.; Earls, J. D.; Priester Jr., R. D. *Mater. Res. Soc. Proc.* **1996**, *425*, 167

Tal93 Tal'roze, R. V.; Plate, N. A. in *Liquid-Crystal Polymers*. Plate, N. A. ed. Plenum Press: New York, 1993, p. 303.

Ven95a Venditti, R. A.; Gillham, J. K.; Jean, Y. C.; Lou, Y. *J. Appl. Polym. Sci.* **1995**, *56*, 1207

Ven95b Venditti, R. A.; Gillham, J. K. *J. Appl. Polym. Sci.* **1995**, *56*, 1687

Yam89 Yamagishi, Akio; Takeuchi, Tetsuya; Higashi, Terumasa; Date, Muneyuki. *J. Phys. Soc. Jpn.* **1989**, *58*, 2280

Yos96 Yoshiki, Kazumasa; Nakayama, Kazuo; Kyotani, Mutsumasa. *J. Appl. Polym. Sci.* **1996**, *62*, 1331

Zen85 Zentel, Rudolf; Strobl, Gert R.; Ringsdorf, Helmut. *Macromolecules.* **1985**, *18*, 960

Zha96 Zhao, Yue; Roche, Philippe; Yuan, Guoxiong. *Macromolecules.* **1996**, *29*, 4619

This work is dedicated to my family. For without their love and support, I would not be where I am today

ACKNOWLEDGMENTS

Funding for this project was provided by the National High Magnetic Field Laboratory. The liquid crystalline epoxy was provided was by The Dow Chemical Company. Magnetic field work was accomplished at the NHMFL.

I would like express my sincere gratitude to my advisor, Dr. Elliot Douglas, for his guidance and support on this project. I would also like to thank my committee members, Dr. Anthony Brennan and Dr. Christopher Batich, for their time and inputs. Special thanks go to Dr. Randolph Duran and the George and Josephine Butler Polymer Research Laboratory for the use of the Siemens x-ray equipment, and to Dr. Stefan Setz and Gayanga Weerasekera for their seemingly endless knowledge and help in conducting the x-ray analysis. Finally, I thank the folks down at the NHMFL for the facilities and help.

I would also like to thank the following colleagues for their patience and support: Dr. Jesse Arnold and Dr. Tom Miller for their know how and knowledge of seemingly everything; the rest of the Brennan group: Jeanne Hampton, Jeremy Mehlem, Luxsamee Plangsangmas, Xiaomei (Susie) Qian, Jennifer Russo, Mark Schwarz, Dr. Mike Zamora, Licheng Zhao for their help with just about everything; Jaime Rhodes and Kevin Powers for their technical support; Gwen Clark for the help and use of the microscope; and Drew Amery for keeping everything running smoothly.

I would like to extend special thanks to my group members Vishal Agarwal, Seunghyun Cho, and Arthur Gavrin for putting up with me and keeping me on track.

Finally, I would like to thank those behind-the-scenes people who basically keep everything held together and make things possible, the secretaries Jackie Hulsey and Debbie Malis, and Mary Swanson for making sure I graduate.

TABLE OF CONTENTS

page

LIST OF TABLES

LIST OF FIGURES

Abstract of Thesis Presented to the Graduate School
of the University of Florida in Partial Fulfillment of the
Requirements for the Degree of Master of Science

CONTROLLING THE PROPERTIES OF A LIQUID CRYSTALLINE EPOXY THROUGH MAGNETIC FIELD PROCESSING

By

Derek M. Lincoln

August 1998

Chairman: Dr. Elliot P. Douglas
Major Department: Materials Science and Engineering

It has been demonstrated recently that the physical and mechanical properties of liquid crystalline thermosets can be altered via processing in a magnetic field. Magnetic field processing imparts a degree of macromolecular anisotropy on the material. This anisotropy has been shown to cause a favorable change in some of these mechanical and physical properties. However, the degree of control over these property changes has yet to be studied in depth. The focus of this research is to explore the effects of the processing variables and determine the amount of control that exists over the final properties of the material.

A liquid crystalline epoxy, 4, 4'-diglycidyloxy-α-methylstilbene, and tetrafunctional diamine crosslinking agent, sulfanilamide, were used as the resin system for this study. The process variables that were determined to be the largest effectors of

the reorientation process are the magnetic field strength, the time in the field, and the amount of b-staging, or precuring, of the material. The response variable chosen to be studied was the second moment of the orientation function, or orientation parameter, determined by wide angle x-ray scattering (WAXS).

A statistical experimental design was employed using CARD® (Computer Aided Research and Development) software to investigate the interaction effects of the variables. The design used was a modified fractional factorial design to reduce the total number of samples required but still included several pairs of replicates to determine the experimental error not associated with the variation of the variables described above.

The samples were prepared and cured in a magnetic field at the National High Magnetic Field Laboratory. Wide angle x-ray scattering (WAXS) experiments were conducted to determine the amount of orientation imparted in the samples. The orientation parameter calculated was used as the response variable for the statistical experimental design.

The results form the experimental design showed the amount of B-staging and field strength to be the largest effectors of the orientation process. The time in the field was also shown to have an effect on the orientation process but not to the extent of the other two. A model constructed to model the response variables had a very good fit, R^2, of 0.8577. The experimental error is estimated to be 5.82%, which indicates that small effects of the variables can be predicted with the model.

CHAPTER 1
INTRODUCTION

The need for light weight, high strength materials for structural applications has prompted researchers to look to liquid crystalline polymers for a solution. This research has led to the push to create polymeric materials with high degrees of anisotropy at the molecular level. A prime example of these materials is polymer fibers. Liquid crystalline (LC) based polyaramid and polyester fibers possess excellent tensile properties due to the high degree of molecular orientation imparted during the melt spinning process. However, the push is more for orientation in bulk structures, such as in injection molded parts, rather than incorporating fibers to enhance the properties of bulk materials. Unfortunately, injection molding of liquid crystalline materials leads to a highly oriented outer skin with a relatively unoriented inner core (Hey93). The enhancement in mechanical properties is much less than if bulk orientation were possible.

Magnetic field processing is a promising new technique used to impart this kind of orientation. Magnetic field processing of polymeric materials to obtain bulk orientation has been the focus of a great deal of research in the recent past (Liu97, Kos97, Ass97, Shi97a). Magnetic fields have one basic advantage over extensional flow in that the orientational effects do not decrease in the center of the material. The material typically used for such processing techniques are liquid crystalline thermoset (LCT) materials. LCT materials possess the cooperative molecular motion that is required for orientation

to occur, plus they posses an initial low viscosity which allows them to reorient easily. Finally, because they are thermosets, the orientation obtained becomes locked into the network as the cure reaction proceeds past the gel point.

Liquid crystalline thermosets (LCTs) are a specific class of LC materials that offer the advantages of liquid crystals as well as the high performance of thermosets. LCTs are simply rigid rod molecules with crosslinking endgroups attached. They are reacting systems which can be crosslinked in a variety of ways including thermal curing. These systems also possess an initial low viscosity upon melting making them useful for filling intricate mold cavities or penetrating fiber weaves or mats for composite construction. Once crosslinked these materials offer the outstanding mechanical properties commonly associated with thermoset materials. As discussed earlier this initial low viscosity becomes critical in magnetic field processing. The low viscosity allows the molecules to orient in the magnetic field, and then the crosslinking reaction locks the orientation in place leaving a highly oriented bulk structure.

To make magnetic field processing a practical technique to use for mass production of high strength materials a balance needs to be achieved between performance and cost. Producing a magnetic field large enough for production purposes is no small nor inexpensive task. As the field strength increases so does cost, but performance cannot be sacrificed either. Thus a process needs to be developed in which a significant amount of orientation can be obtained in a practical manner with respect to cost.

The purpose of this study is to probe the effects that the processing variables have on the reorientation process and measure the amount of control that exist over the

final material properties. The magnetic field strength, time in the field, and amount of B-staging, or precuring, were determined to be the most important and most easily controllable variables which affect the final properties of the material. To accomplish this a statistical experimental design was employed to test the interaction effects of these three process variables and determine the amount of control there exists over the final properties of the material.

The resin system used in this study consisted of a liquid crystalline di-epoxy coupled with a tetrafunctional crosslinking agent. The system, 4, 4'-diglicidyloxy-α-methylstilbene (DOMS)--sulfanilamide (SAA), was formulated and poured into aluminum molds and then B-staged and cured under the influence of a magnetic field. The response variable chosen to be measured was the second moment of the orientation function which is a measure of the amount of macromolecular orientation in the material. The orientation parameter, as it is also called, is determined through the use of wide angle x-ray scattering (WAXS).

Dynamic mechanical spectroscopy (DMS) analyses were also carried out on the samples to determine if the reorientation process had any effect on the mechanical properties of the material or on the viscoelastic response of the material. Multi-frequency experiments were performed in order to determine the apparent activation energies of each of the major relaxations of the material. This was accomplished to observe any trends in the activation energies that may result as the magnetic field strength is increased.

CHAPTER 2
BACKGROUND

Overview of Liquid Crystalline Thermosets

Liquid crystalline thermosets (LCTs) have been the subject of much research recently. Specifically, liquid crystalline acrylates and methacrylates (Hik91, Lit93, Zen85); maleimides, nadimides, and the like (Ben92, Hoy90a); acetylenes (Ben92, Mel94); vinyl ethers (Hik93); glycidyls (Bar92a, Car93, Car94a, Car94b, Car94d, Car94e, Gia95, Liu97); and crosslinkable copolyesters (Eic96) have come under intense study. LCTs are promising new materials which may offer the high strength, high temperature capabilities sought after for many applications.

Unfortunately, there have been only a few studies that have looked at the mechanical properties of LCTs. Some work has been accomplished using dynamic mechanical analysis in which dynamic storage moduli of about 4.5-4.8 GPa at room temperature have been reported (Mel94). Other studies have looked at the static mechanical properties of LCTs in which elastic moduli of 3-4 GPa, improvable up to 8 GPa through processing, have also been reported (Ben98, Smi96). A strong correlation between the elastic modulus and the degree of orientation has also been reported (Ben98).

Not only are LCTs attractive because of their mechanical properties, but also because of their various other unusual properties. They possess the ability to flow like

liquids which allows them to fill intricate mold cavities for processing purposes or thoroughly penetrate fiber weaves or mats for construction of fiber composites. Their molecular architecture also allows them to be easily aligned to form anisotropic structures. Photopolymerizable LCTs can be processed at very low temperatures but still exhibit very high glass transitions temperatures (Mel94, Lit93). They have little shrinkage upon cure, which prevents stressing of the interfacial bond in fiber composites (Lit93). In particular, acetylenes have been shown to produce void free laminates (Adm78), have good batch to batch homogeneity (Rat80), and possess high T_g's (Her80). And because they have a thermally initiated cure, it has been implied that they possess a long shelf life (Mel94). It has also been shown that LCTs yield a high degree of conversion due to their crystalline order (Lit93), which may lead to the improved mechanical properties discussed earlier. Hikmet et al. also found that aligned networks lose very little of their degree of orientation with temperature owing to the stability of the network (Hik93).

Liquid crystalline thermosets often fall into the category of thermotropic liquid crystals, meaning they may possess several different mesophases that change with thermal energy, also known as polymorphism. The phases a thermotropic liquid crystal can possess are: isotropic, nematic, cholesteric, and smectic. The isotropic phase is characterized by the display of no long-range positional order. The nematic, cholesteric, and smectic phases are differentiated between primarily based upon their symmetry. Nematic ordering is the simplest of the three phases characterized by long range directional order but lack of long range correlation between the centers of mass of the molecules. The cholesteric phase is characterized by nematic ordering of molecules within

layers that are ordered in a helical manner. Cholesteric phases are typically found in cholesterols, hence the name. Smectic liquid crystals are the most highly ordered of the phases and possess several degrees of ordering. Smectic liquid crystals are characterized by long range directional order as well as positional, or layered, ordering. Figure 2-1 shows the four types of mesophases found in liquid crystals including the smectic A and smectic C structures.

Certain liquid crystalline thermoset molecules lend themselves to either nematic or smectic structures. Molecules which do not differentiate between right and left, or those which are symmetrical, can form either nematic or smectic phases. Amphiphilic molecules, or molecules which possess groups that tend to segregate, tend to form smectic structures. The most common of such molecules are those with rigid, aromatic mesogens with aliphatic end-groups. It has been found that liquid crystalline order can be sustained over the crosslinking reaction of some epoxies when the reaction is carried out in the thermal stability region of that particular liquid crystalline phase even though the system may possess other mesophases (Car93).

Liquid crystalline epoxies (LCEs) are a subclass of LCTs which have the potential to fill the need for high strength, high temperature structural materials. LCEs combine the two distinct, advantageous properties of liquid crystalline and thermoset materials. They possess the high performance of thermoset epoxies yet have the unusual properties of liquid crystalline materials (Car93). Through the combination of these properties LCEs possess a reduced brittleness when compared to other epoxies. As Carfagna et al. found the fracture toughness of a particular liquid crystalline epoxy can be improved well over

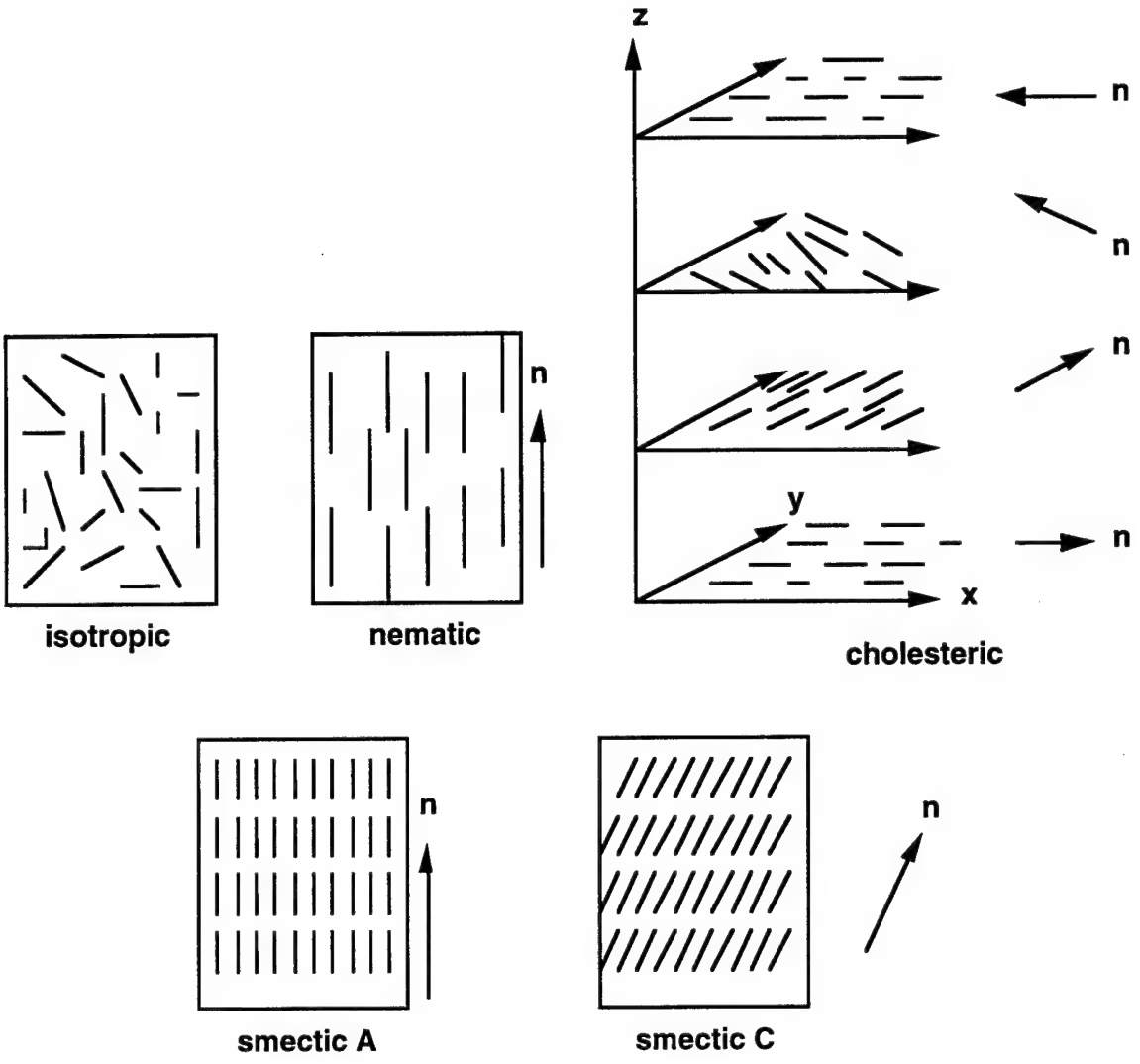

Figure 2-1. Different types of liquid crystalline mesophases.

50% over its isotropic counterpart (Car94a, Car94c). These outstanding properties have made LCEs prime candidates for applications such as matrices in composites and waveguides in nonlinear optics.

One particular liquid crystalline epoxy, which has been the focus of much research recently, is the diglycidyl ether of 4, 4'-dihydroxy-α-methylstilbene, or 4, 4'-diglycidyloxy-α-methylstilbene (DOMS) (Bar92, Car93, Liu97). The DOMS liquid crystalline molecule is attractive to researchers because of several different reasons. Researchers have shown the crosslinking rates to be readily controllable (Bar92). Authors have shown that controlling the crosslinking rates reveals a marked difference in final product properties (Lin97). Finally, because it is isotropic, the final structure of the DOMS epoxy system can be controlled through the curing profile. Lin et al. found that DOMS initially melts into an isotropic phase, but upon further cure displays liquid crystalline order (Lin94)

The structure can also be controlled, to some degree, with the use of a particular curing agent. For example, researchers have found that the use of a difunctional amine, the aniline adduct of 4, 4' dihydroxy-α-methylstilbene, as the crosslinking agent gives rise to nematic liquid crystalline order. Whereas, the use of a tetrafunctional amine, sulfanilamide (SAA), gives rise to a smectic liquid crystalline structure (Lin97). But as Shiota and Ober found, crosslinking is not necessarily required to form a smectic structure (Shi97c). The use of different crosslinking agents can alter not only the final crystalline structure but the kinetics of the formation of liquid crystalline domains.

In particular the SAA crosslinking agent has a profound effect on the formation of the network. The amine group was found to react much quicker than the sulfonamide group which gives rise initially to the formation of linear polymer sections. The lower reactivity of the sulfonamide group allows time for liquid crystalline organization to occur at the elevated cure temperatures leading to the formation of a smectic structure. Upon further curing the material crosslinks and eventually vitrifies with liquid crystalline order.

Processing

Most of the techniques used in processing liquid crystalline materials deal with alignment of the molecules in some sort of field mainly because, as Dreher et al. found, of a synergy between orientation and physical properties (Dre98). The nature of the molecule lends itself to two primary techniques. The first is molecular alignment in an external field. Magnetic and ac/dc electric fields are generally used. These techniques exploit the initial low viscosity of the system, which allows the molecules to rotate and align themselves in the melt. The second is mechanical orientation through use of shear forces which occur in processing applications such as injection molding, extrusion, pultrusion, etc.

Mechanical

The most common techniques researchers have used to mechanically orient liquid crystalline materials is with the application of a tensile strain at a temperature above the T_g. This is done by either melt-drawing (Han96), melt-spinning (Moo96), stretching heated films uniaxially or biaxially (Bar92, Eck96, Kos97), extrusion (Yos96), and

injection molding (Dre98, Eng94, Hey93). Dynamic shear conditions have also been studied (Alt95).

For many of the mechanical orientation techniques it has been found that the alignment depends greatly on the mesophases present and the shear conditions. Alt et al. found that for nematic-like liquid crystals little orientation occurs under oscillatory shear, but high degrees of orientation are obtained under large steady shears; whereas, smectic-like liquid crystals form highly aligned structures under dynamic shear with very small strain amplitudes (Alt95). Differences in behavior also arise depending on whether or not the liquid crystal is in the backbone or attached as a side chain. Zhao et al. found that mechanically stretching a side chain liquid crystalline polymer (SCLCP) with smectic ordering produces macroscopic orientation perpendicular to the stretching direction, and a nematic SCLCP displays the opposite result (Zha96).

Not only have studies been conducted on orientation of pure liquid crystalline materials but also on blends of liquid crystalline materials and thermoplastics. The addition of liquid crystalline materials to thermoplastics has several advantages: the melt viscosity of the blend is lowered thus lowering the processing temperature (Dut90); there is a marked increase in the degree of crystallinity in the material (Yos96), and the machinery is worn less and contamination is low as opposed to when chopped fibers are used (Kis87). The processing times are also shorter due to the fact that conventional thermoplastics need to be stretched after processing to impart significant orientation, whereas the LCP-thermoplastic blends do not (Moo96).

One major drawback to mechanical alignment of these materials is, as Sawyer and Jaffe found, that the final structure is a highly oriented skin with an unoriented inner core (Hey93, Saw86). The orientation in the skin is most likely due to high shear on the material, and the randomness in the core may be due to the "log rolling" effect described by Marrucci and Grizzuti. (Mar91). This is typically not as prominent in fiber drawn structures as in injection molded, and the like, structures. Another possible disadvantage of mechanical processing is the anisotropy in shrinkage caused from the orientation which is difficult to predict in complicated geometries (Hey93). However, some work has been done on fluid particle tracking to predict director orientation for flow induced orientation in simple geometry injection molded parts (Cha94).

The effect of conducting mechanical orientation of these materials is an enhancement of their various physical properties. It has been reported that a three-fold increase in the tensile modulus of a liquid crystalline polymer can be obtained through mechanical orientation means (Kos97). A change in the coefficient of thermal expansion (CTE) for such materials has also been reported (Kos97). The CTE of the material in the direction parallel to the machine direction decreases drastically, while that in the transverse direction increases. Eckert and Finklemann have also reported the possible birth of a new class of materials based on the improved piezoelectric properties obtained from mechanically orienting these materials (Eck96).

Electric Fields

Although not as popular processing technique as mechanical or magnetic orientation processes for obtaining high strength materials for structural applications,

some researchers have still managed to tackle the problem of conducting orientation in electric fields with some amount of success (Iiz85, Li96, Shi97b).

Processing using ac/dc electric fields requires a coupling between the field and the dielectric and conductive coefficients of the molecules. Once coupled a dielectric torque drives the molecules to reorient in the field. This reorientation causes elastic deformations in the material for which there is some amount of force working against rotation of the molecules. Therefore, there exists a threshold value of the electric field strength before any reorientation of the molecules will occur. This threshold field strength is given by (Tal93):

$$U_o = \pi\sqrt{4\pi K_{ii} / \Delta\varepsilon}$$

where K_{ii} are elasticity constants of the material, and $\Delta\varepsilon$ is the anisotropy of the dielectric constant of the material. When the U_o is equal to the return of the elastic forces reorientation will occur.

Several factors help to dictate the reorientation process when using electric fields. When the anisotropy of the dielectric constant is greater then zero, $\Delta\varepsilon > 0$, the molecular axis tends to line up parallel to the electric field direction, and when $\Delta\varepsilon < 0$ the molecular axis tends to line up perpendicular to the field direction. In ac electric fields Kishore et al. found that as the strength of the electric field increases the molecules approach a parallel alignment with the field, and as the frequency is increased the threshold field strength increases up to a certain frequency and then remains constant above that value (Kis78). They concluded that low frequency fields (conduction regime) are more effective in

reorienting the molecules than high frequency fields (dielectric regime). The mesophase present and the type of electric field also have a significant effect on the orientation process. Carr found that nematics tend to align parallel to dc and ac electric fields, while smectics tend to align parallel to ac fields and perpendicular to dc fields (Car70). Shiota and Ober also found that the frequency of the ac fields had an interesting effect on the orientation process (Shi97b). They found that below 10 kHz the nematic-like molecules aligned parallel to the field, while above 20 kHz the molecules aligned perpendicular to the field. They attributed this effect to the relationship between the stability of the field and various system parameters including the viscosity, anisotropic conductivity, anisotropy of the dielectric constant, and anisotropy of the diamagnetic susceptibility.

In conducting orientation experiments using electric fields researchers have found that a resulting enhancement of the mechanical properties occurs. As with the mechanical field processing Shiota and Ober found a higher elastic modulus for oriented versus unoriented materials (Shi97b). They also reported similar changes in the CTEs of the materials as was found for materials oriented mechanically. Kozak et al. found that the extent of alignment, and hence the enhancement of the mechanical properties, for materials processed in a dc electric field were not as great as those processed in an ac electric field (Koz89).

Magnetic Fields

Although much research has been conducted on both techniques of field orientation and mechanical orientation, this paper will focus mainly on magnetic field orientation techniques. Researchers have conducted magnetic orientation on a number of

different types of molecules including polyesters and copolyesters (Anw91, Hud90, Kos97, Mar82, Shi97a), polypeptides (Avi76, Iiz85), and other types of liquid crystalline polymers and copolymers (Anw93, Gul72, Moo85, Shi97b). Specific interest has arisen in the magnetic processing of LCTs because of their unique properties (Ass97, Bar92, Liu97, 5060). In their liquid state LCT molecules will orient quickly and easily due to their initial low viscosity. However, after time, as the curing reaction proceeds, the material gels and the oriented structure becomes locked in place. Upon further curing and, eventually, vitrification the material can become a solid with liquid crystalline order at room temperature.

Magnetic field orientation draws on the anisotropy of the diamagnetic susceptibility, $\Delta\chi$, of the molecule for success. Again, as with the electric field orientation process, there exists a threshold magnetic field strength value below which no reorientation will occur due to the return of the elastic forces acting on the molecules. This threshold value is given by (Tal93):

$$H_o = \frac{\pi}{d}\sqrt{4\pi K_{ii} / \Delta\chi}$$

where K_{ii} are, again, elasticity constants of the material, and $\Delta\chi$ is the anisotropy of the diamagnetic susceptibility.

Liquid crystalline molecules are often aromatic containing compounds. The anisotropy of the diamagnetic susceptibility arises from differences in the diamagnetic susceptibility in the plane of the aromatic ring and perpendicular to the plane of the aromatic ring. When subject to an external magnetic field perpendicular to the plane of the

ring a current is created in the ring. The current reduces the flux of magnetic fields lines passing through it. The energy of the system is then increased and a magnetic torque is induced on the molecule by the magnetic field. From de Gennes (deG93) the free energy per cm^3 is given as:

$$F = F_d - \frac{1}{2}\chi_\perp H^2 - \frac{1}{2}\chi_a(\mathbf{n} \bullet \mathbf{H})^2$$

where F is the free energy of the molecule, F_d is the distortion energy, $\chi_\perp$ is the diamagnetic susceptibility perpendicular to the plane of the molecule, H is the magnetic field strength, and χa is the anisotropy of the diamagnetic susceptibility. It can be seen that the free energy F is minimized when **n**, the optical or molecular axis, is collinear with **H**, the magnetic field direction. Thus, the molecule aligns itself with the magnetic field direction to reduce the free energy of the system.

Another important point in the orientation process in liquid crystalline materials is the fact that one molecule alone will not align itself in the magnetic field. There needs to be a cooperative motion between many molecules for any substantial alignment to occur. The coupling energy between a single molecule and the magnetic field, $(\mu H)2/E$, has been shown to be very small when compared to k_BT, the thermal energy (deG93). Where μ is the Bohr magneton, H is the field strength, E is an electronic excitation energy, k_B is Boltzman's constant, and T is the temperature. Thus, a molecule would not align itself because it alone cannot overcome the thermal vibration energy it possesses. However, if the number of molecules is on the order of, for example, 10^{22}, the coupling

energy becomes N(μH)2/E, where N is the number of molecules. This energy is now much larger than k_BT and the sample will align itself with the magnetic field.

Several factors affect the orientation process: melt viscosity, rate of reaction, field strength, time in the field, and diamagnetic susceptibility of the molecule. Moore and Stupp developed a basic equation to try to incorporate some of these constraints to try to understand the orientation process better (Moo87). The equation to describe the time dependence of the director orientation is

$$\tan\theta_o = \tan\theta_o' \exp\left[-(t/\tau)\right]$$

where θ_o is the angle the director makes with the magnetic field direction, and θ_o' is some initial value for this angle, and τ is a characteristic orientation time which is equal to $\gamma/(\Delta\chi)B^2$, where γ is the material viscosity, $\Delta\chi$ is the anisotropy of the diamagnetic susceptibility, and B is the magnetic field strength. One particular disadvantage of this model is that it does not take into account the viscosity increase of the material as the cure reaction proceeds. Another disadvantage is that it models only a single domain although they have applied it to polydomain samples. Assender and Windle have also tried to describe the limits of orientation imposed by neighboring domains for polydomain samples (Ass97).

As with the previous two techniques for molecular orientation, magnetic field processing acts to improve the physical properties of the material, and the morphology is a good indicator of this improvement. Anwer and Windle reported a fibrillar structure for samples with a high degree of orientation (Anw93). Further, Kossikhina showed that

even after the removal of the outer skin, the material displays this fibrillar structure revealing the bulk orientation obtained in the magnetic field (Kos97).

Through further testing researchers have shown that the mechanical properties are, in fact, enhanced from the processing. Smith et al. reported a three-fold increase in the elastic modulus for oriented versus unoriented material (Smi96). The changes in CTE, as with mechanical aligned techniques, are also prevalent (Shi97b, Smi96).

Although all three techniques are useful in orienting molecules in a material, there are advantages and disadvantages to each. A major drawback to ac electric field processing as opposed to magnetic field processing is that it takes much more energy to align molecules in an ac electric field than to do the same in a static magnetic field. Tensile strengths for mechanical versus magnetic alignment techniques often show higher values for the mechanical technique (Kos97, Shi97a); however, these values are for thin films. As discussed before the mechanical alignment technique typically produces a highly oriented outer skin with a relatively randomly oriented inner core for thicker structures (Hey93, Saw86). Shimoda et al. found that for blended materials the mechanical alignment process seems to be better than the magnetic field alignment process because the long thermal history of the material when processed in the magnetic field cause segregation of the material and a reduction in the tensile properties; with the mechanical orientation process this segregation does not occur (Shi97a). It was also found that for magnetic field processing, and consequently electric field processing, that there exists a limited maximum in the degree of orientation attainable dictated by the size of the domains (Anw97).

Similarly, the degree of orientation obtainable with the mechanical drawing technique is limited by the molecular weight of the material (Anw97).

Characterization

Researchers have employed many ways in which to study the reorientation process in liquid crystalline materials. Among them are studies of the electrooptical properties of materials dealing with the Frederiks transition, a phase transition possessing a critical field strength H_c at which the conformation of the domains will become distorted; flexoelectric distortion, the polarization induced in a liquid crystalline material due to distortion of the material (bending); and ferroelectric switching, switching of the director with the application of a magnetic field; (Bli97) as well as electrohydrodynamic instabilities (Rao76) and field induced domain patterns (Kra76). Some more common techniques researchers have used to describe the reorientation process are those which provide a way in which to measure the degree of ordering in a material. These techniques provided researchers with a way to describe the amount or degree of orientation in a material with a single number to make them easier to compare. These numbers are typically referred to as the moments of orientation. The average orientational distribution function is given by (Col97):

$$f(\theta) = S_0P_0(\cos\theta) + S_2P_2(\cos\theta) + S_4P_4(\cos\theta) + S_6P_6(\cos\theta) + \ldots$$

where P_n is the moment of orientation, θ is the angle between the molecular axis and the director, and S_n is a coefficient describing the orientation distribution function (some authors use a normalized S parameter to describe the orientation in a material). Only the

even powers of the moment of orientation can be calculated since the director can only be defined by one of two opposite directions, +n or -n.

Two techniques, NMR (deG93) and Raman (Jen73, Miy78) spectroscopy, have been used to determine the fourth moment of the orientation distribution. Birefringence (Bee96), ESR line shape analysis (Han96), diffuse reflectance infrared spectroscopy (DRIFT) (Bee96), and attenuated total reflection IR (Moo96) have also been used to determine ordering but only give the second moment of the orientation distribution. Scattering methods such as SANS, SAXS, and WAXS have also been employed to probe the materials at different length scales (Ben98).

Optical Microscopy

Under cross-polarized light the birefringent nature of liquid crystalline materials allows for the observation of textures in the material. Textures are nothing more than pictures of thin layers of liquid crystalline material caused by the existence of different kinds of defects (Dem80). There are a number of different defects visible in liquid crystals: Frenkel defects, point singularities, translational dislocations, twin boundaries, inversion walls, stacking faults, etc. Some of these are visible in both solid and liquid states, but others, e.g. disclinations, are visible only in the liquid state (Dem80).

Defects in liquid crystals have stronger distortions which correspond to much larger defects. This is why liquid crystal textures are visible at low magnifications in an optical microscope, whereas, solid state crystals are submicroscopic cannot be seen (Dem80). Defects are also in much higher concentrations in liquid crystals due to the high mobility of the molecules. Violent disturbances due to streaming, electrical or magnetic

fields, temperature gradients, or mechanical stress cause these defects to be seen during all growth processes of liquid crystals. This allows for the determination of transition and clearing temperatures.

Nematic liquid crystals typically display what is knows as a Schlieren texture. Schlieren textures are characterized by displays of dark brushes, also called black stripes or schlieren, with irregular curved shapes. The formation of these brushes correspond to extinction positions in the nematic liquid. Each of these extinction positions is designated by s=-1, -½, . . ., 1 depending on the number of brushes and the angular distributions of the director.

Smectic textures appear in a variety of ways, but the two main categories are planar and non-planar. Planar textures appear when layers are parallel to the glass slide indicating that the light is parallel to the optic axis of the molecules. This is known as homeotropic or pseudoisotropic because the light is nearly extinguished completely. Small bright ribbons may appear near the edges of the specimen or near the edges of bubbles in the specimen. Non--planar textures appear when the layers are at some angle to the glass slide and the light is traveling at some angle to the optic axis of the molecules. These typically appear as polygonal, fan--shaped textures or some variations of them. The appearance of any of these textures is very dependent upon the specimen preparation and preparation of the glass slide. Certain chemicals may cause one texture to appear versus another, and rubbing the slide will obviously change the structure.

Finally, as mentioned above measuring the birefringence of a liquid crystalline material is a helpful way to determine the amount of orientation in the material. This is

most easily done by measuring the birefringence of the material twice. This is accomplished by measuring the parallel absorption spectrum (electric vector is in the Z direction) and the perpendicular absorption spectrum (electric vector is perpendicular to Z or in the Y direction), and then comparing these differences to calculate the moment of orientation distribution (Mic86). In particular the second moment of orientation can be calculated for a nematic liquid as shown by Beekmans and Posthuma de Boer by taking the ratio of the birefringence, Δn, and the maximum birefringence, Δn_{max}, determined from the method described above (Bee96):

$$\frac{\Delta n}{\Delta n_{max}} = \langle P_2 \rangle = \frac{1}{2}\left(3\langle \cos^2 \alpha \rangle - 1\right)$$

where $\langle P_2 \rangle$ is the second moment of the orientation function and α is the angle between the molecular optic axis and the machine direction.

Wide Angle X-ray Scattering

As mentioned above scattering techniques have the ability to probe the materials at different length scales. Wide angle x-ray scattering (WAXS) is commonly used because of its ability to probe the small spacing between oriented molecules. WAXS is also an attractive technique because the second moment of the orientation distribution can be determined directly from the diffraction data. WAXS can also render orientation distributions where many other techniques cannot, and it provides absolute orientation parameters where other techniques such as DRIFT can only provide trends in orientation (Bee96).

Diffraction patterns such as those depicted in figure 2-2 are the result of the wide angle x-ray scattering (WAXS) experiments of solid LCTs with nematic or smectic A liquid crystalline ordering. The inner ring is indicative of the layer spacing characteristic of the smectic ordering, and the outer ring is indicative of the intermolecular correlation, not to be confused with an amorphous halo for amorphous materials. Nematic ordering produces only the outer ring.

For the DOMS-SAA system the appearance of the inner ring at approximately $2\theta = 4.0°$ corresponds to a layer thickness of 22.1Å. Lin et al. found that this distance corresponds to the length of the DOMS molecule disregarding any contribution from the SAA molecule as a branching side-group (Lin97). Benicewicz et al. also found that the appearance of a diffuse ring at a d-spacing of 6Å corresponds well with the length of a sulfanilamide molecule (Ben98). This good agreement between the information obtained from the x-ray diffraction data and the molecular structure indicates a smectic A structure as shown in figure 2-2 versus a smectic C structure which would produce a diffuse outer ring at some angle to the layer normals.

As discussed earlier the data obtained from WAXS is used to derive the second moment of the orientation distribution, which is also known as the Herman's Orientation parameter (Cre92). The parameter is calculated using the following equations:

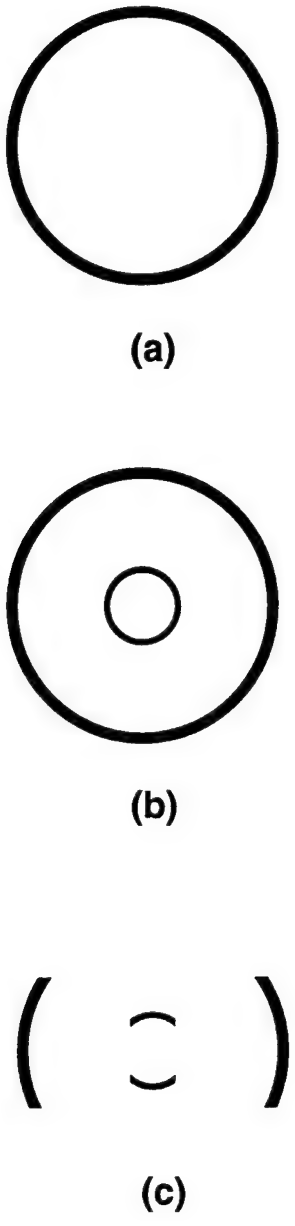

Figure 2-2. WAXS patterns for (a) nematic, (b) smectic, and (c) oriented smectic liquid crystalline materials.

$$\left\langle \cos^2 \alpha \right\rangle = \frac{\int_0^{\pi/2} I(\alpha)\left(\sin\alpha \cos^2 \alpha\right) d\alpha}{\int_0^{\pi/2} I(\alpha)(\sin\alpha) d\alpha}$$

$$\left\langle P_2 \right\rangle = \frac{1}{2}\left(3\left\langle \cos^2 \alpha \right\rangle - 1\right)$$

For a randomly oriented sample and, consequently, a sample in which $\alpha = 54.7°$ $\langle P_2 \rangle$ = 0, and for a sample perfectly oriented in the magnetic field direction $\langle P_2 \rangle = 1$. Perfect orientation in the transverse direction to the magnetic field direction gives $\langle P_2 \rangle = -0.5$.

Dynamic Mechanical Spectroscopy

Most of the epoxies discussed thus far have been or are being considered for structural applications. As a result their viscoelastic behavior must be thoroughly investigated for these types of applications. Epoxy and polyester resins typically undergo structural rearrangements at temperatures well below their T_g. These structural rearrangements are significant enough to cause a change in the materials' mechanical properties. Several factors can help to bring about these changes including preparation method (Mik87), stoichiometry (Bel90), water sorption (Car95), crosslink density (Gup85), and cure schedule (Arr72).

A common way researchers have used to characterize LCTs (Lin97) and other epoxy materials (Gri91, Kee79, Och85, Pog70, San95, Sas91) is by dynamic mechanical thermal analysis (DMTA). DMTA provides a wealth of information regarding these materials mechanical properties and the transitions that affect them.

The transitions that occur in these materials are typically found to be thermally activated. This thermal activation can typically be described by the Arrhenius equation which, shown here, is the temperature dependence of the mean relaxation time, τ (Fer97):

$$\tau(T) = \tau_0 \exp(\Delta E / RT)$$

where τ_o is an exponential prefactor representing the reciprocal of a test frequency and ΔE is the activation energy. A plot of $\ln(\tau_o)$ versus 1/T gives a line with slope ($\Delta E/RT$), thus the activation energy can be calculated. This activation energy can disclose a good deal of information about the molecular packing in thermoset networks. Networks tightly packed may require a higher amount of energy to relax than a loosely packed network, and so on.

Researchers have found that liquid crystalline and non-liquid crystalline bisphenol based epoxies generally undergo three distinct transitions. From the schematic shown in figure 2-3 the three major transitions or relaxations are typically denoted γ, β, and α, in order of increasing temperature. However, there is much disagreement on the source of these relaxations.

The γ transition, with a transition temperature in the range of -80 to -55°C, has been associated with a number of motions in the network. Pogany associated the relaxation to the wriggle motion of the aromatic ring (Pog70), contrary to others' claims that rotation of the aromatic ring is responsible for the relaxation (Lin97). In DOMS

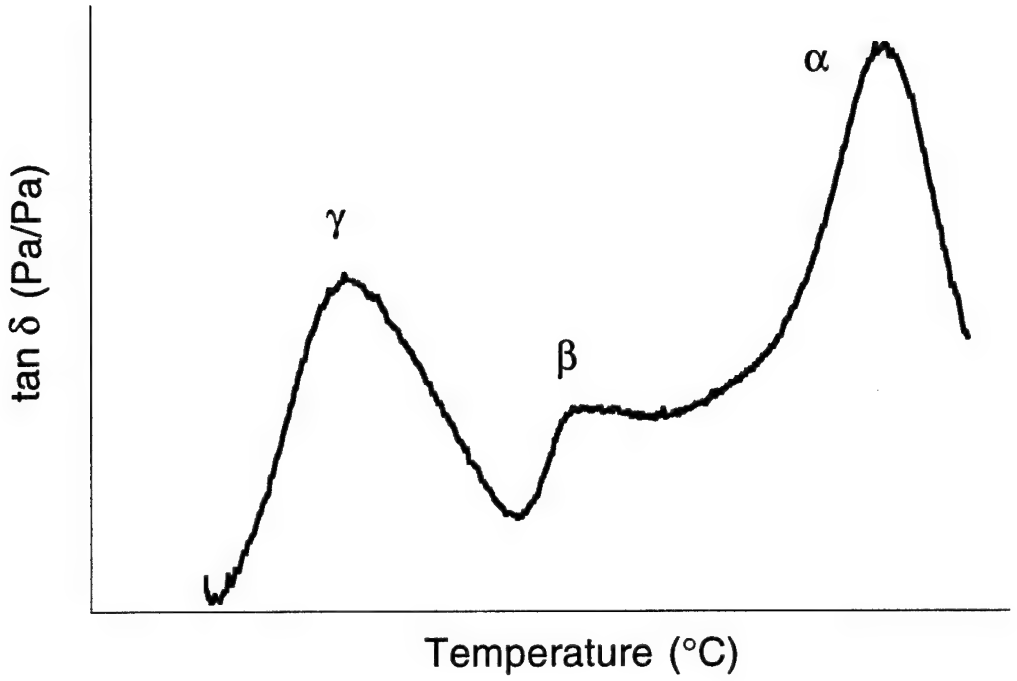

Figure 2-3. Schematic of a typical tan δ curve for an epoxy showing the three major transitions γ, β, and α.

specifically Lin et al. concluded that the rotation of the mesogenic unit about the para ether linkage leads to little or no disturbance of the neighboring units and does not change the length of the chain. Lin et al. also showed that the γ peak does not shift with differences in curing conditions, which suggest the motion is due to mesogenic rotation and not to molecular motion of the segments (Lin97). Other authors have associated the relaxation with the crankshaft type motion within the mesogenic unit (Kee79, San95)

The β transition is a much smaller transition that appears at around 50°C. Some authors have attributed the relaxation to the motion of unreacted species in the network or inhomogeneities in the sample due to difference in crosslinking densities (Kee79, San95). Other authors claim it is due to structural relaxation of the entire network but hesitate to identify it positively (Lin97). However, Sasuga et al. claim the motion of unreacted species is not reasonable and that the relaxation should be assigned to local motion of those chains which are heavily restricted by crosslink points (Sas91). Yet others have associated the relaxation with motion of the para-substituted phenylene groups (Och85).

The α transition is the result of segmental motion of the molecular network, i.e. glass transition. The α transition is the final transition to appear, but its relaxation temperature as well as its activation energy have been found to vary greatly depending on the type of epoxy and curing conditions. The temperature at which this transition occurs depends on several factors. The first is chemical (crosslinks) constraints. Some authors have found that an increase in crosslinking density increase the glass transition temperature (Bar92, Hik91). The second is the physical (entanglements) constraints.

Finally the packing density of the segments also affects the glass transition temperature. Grillet et al. found that the activation energy of the relaxation decreases as the molecular weight between crosslinks increases (Gri91). Others have found that unreacted species cause a plasticization effect in the network and lower the glass transition temperature (Kee79).

Perspective

This literature background attempts to provide a general summary of some of the work that has been accomplished using liquid crystalline thermosets. The major focus was on the orientation of the molecules to produce anisotropic properties in the final product. The question remains on how much control there exists over the orientation processes. The work here was done to answer that question for magnetic field processing of a liquid crystalline epoxy and provide insight into the largest effectors of the process. The background given for the different characterization techniques was provided to familiarize the reader with the techniques that were used to characterize the materials in this study.

The work here will help to determine the feasibility of obtaining these anisotropic properties at reasonable operating conditions. Much of the work in the past was accomplished only to display the orientation properties of the materials. This work attempts to put a real-world prospective on the process of orienting liquid crystalline materials and its use in mass-producing structural parts for use in everyday applications.

CHAPTER 3
MATERIALS AND METHODS

Experimental Design

A statistical experimental design was employed in this study to examine the effects of the time in the field, the magnetic field strength, and the extent of B-staging on the orientation parameter of the final product. The CARD® (Computer Aided Research and Development) software by S-Matrix® was used to generate and analyze the design. The design chosen was a standard process variable screening design. The design resembles a fractional factorial design modified to reduce the total number of samples but still include enough replicates to perform an error analysis.

The three variables thought to be the largest effectors of the reorientation process are the time in the magnetic field, the magnetic field strength, and the B-staging time. All three were continuous variables ranging from 5 to 75 minutes, 0.5 to 12 Tesla, and 0 to 180 minutes, respectively. Table 3-1 lists the samples generated for design and analysis. The first 11 samples were generated specifically for this design. The remaining samples were included from preliminary work and to help increase the sample size for more degrees of freedom in the model. Samples Stat2-Stat7, Stat3-Stat9, Stat5-Stat6, Stat12-Stat13, Stat15-Stat16, and Stat18-Stat19 are the replicate pairs in the design for

experimental error analysis. Each of the samples were made and characterized as follows in this chapter.

Table 3-1. Statistical experimental design samples.

Sample	Time in field (min)	Field strength (Tesla)	B-staging time (min)
Stat1	58	3.4	45
Stat2	75	12	0
Stat3	5	0.5	0
Stat4	75	0.5	180
Stat5	40	6.3	90
Stat6	40	6.3	90
Stat7	75	12	0
Stat8	75	12	180
Stat9	5	0.5	0
Stat10	58	3.4	140
Stat11	5	12	180
Stat12	60	3	0
Stat13	60	3	0
Stat14	60	4.5	0
Stat15	60	6	0
Stat16	60	6	0
Stat17	60	7.5	0
Stat18	60	9	0
Stat19	60	9	0
Stat20	60	12	0
Stat21	60	3	120
Stat22	60	6	120
Stat23	60	9	120
Stat24	60	12	120
Stat25	45	6	30
Stat26	45	6	60
Stat27	45	6	90
Stat28	45	6	150
Stat29	30	6	0
Stat30	45	6	0
Stat31	75	6	0

After analysis of the data the optimization function in the software was used to calculate the various values of the time in the field, the magnetic field strength, and the B-staging time for a particular desired orientation parameter value to test the model obtained from data analysis. The optimization function requires starting points for each of the three variables to be input by the user. It then calculates, using the regression model results, the value of each of the variables to obtain a desired response (orientation parameter), while keeping the output values as close to the starting points as possible. In this case the starting points for each of the variables chosen were 40 minutes time in the field, 6 Tesla field strength, and 90 minutes B-staging time. The desired orientation parameter values and the process variable values obtained from the optimization output are listed in table 3-2. The maximum orientation parameter value obtained for the

Table 3-2. Optimization outputs from regression model

Desired orientation parameter	Time in field (min)	Field strength (Tesla)	B-staging time (min)
Max. (1.4791[a])	5.0	12.0	8.4
0.95	40.0	10.0	90.0
0.90	40.0	9.4	90.0
0.85	40.0	8.8	90.0

[a]Maximum value given from model.

orientation parameter from the optimization function is 1.4791.

Materials

Liquid Crystalline Epoxy System

The liquid crystalline epoxy monomer, 4, 4'-diglycidyloxy-α-methylstilbene (DOMS), was obtained from The Dow Chemical Company (Midland, MI) [Lot# KE300180B1] and used without further purification. The epoxy equivalent weight (EEW) given by Dow was 175. The sulfanilamide (SAA), 99%, crosslinking agent was purchased from Aldrich Chemical Company, Inc. (Milwaukee, WI) and used without further purification. The F-2 organophosphonium catalyst used was also acquired from The Dow Chemical Company. The F-2 catalyst contained 40% solids in methanol, reference no. 54647-28. Figure 3-1 shows schematic of the DOMS and SAA molecules.

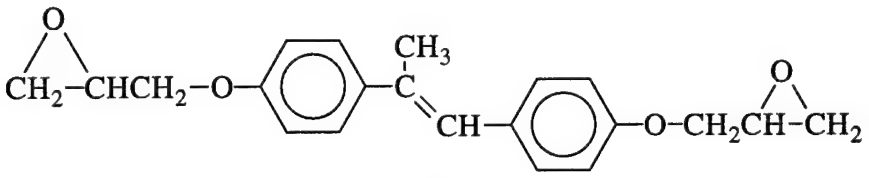

DOMS

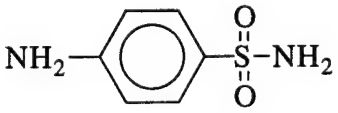

SAA

Figure 3-1. Resin system used in this study: 4, 4'-diglycidyloxy-α-methylstilbene (DOMS) and sulfanilamide (SAA).

Sample Molds

The sample molds were constructed of two aluminum plates and a thin Teflon® sheet. Figure 3-3 shows a diagram of the molds. Each aluminum piece had two holes drilled to hold cartridge heaters, and one side had a hole drilled down the center to hold a thermocouple wire. The two aluminum pieces were separated by a U-shaped piece of 1.5 mm thick Teflon® sheet. Each mold also had holes drilled through the faces near the top corners for a thin steel wire to pass through so the molds could be lowered into the magnet bore. The sample size was about 30 mm wide by 100 mm long by 3 mm thick.

The molds were sanded to a 600 grit finish with silicon carbide sandpaper, cleaned with acetone, and sprayed with Crown® #6075 Dry Film Lubricant and Mold Release Agent (TFE) purchased from Fisher Scientific. The molds were then put together and held in place by 5/8 inch steel binder clip.

Sample Preparation

Sample Formulation

A weighed amount of DOMS was placed in a 60mL Qorpak® sample bottle. The amount of resin used depended upon the number of molds to fill. One mold used about 10 g of formulated resin. The bottle was placed in a convection oven at 170°C to induce melting. Once melting had begun the temperature was reduced to 150°C. After complete melting a stoichiometric amount of sulfanilamide was added to the melt given by:

$$\text{Equivalent wt. of SAA} = 43.05 \div \text{EEW of DOMS} \times \text{Wt. of DOMS used}$$

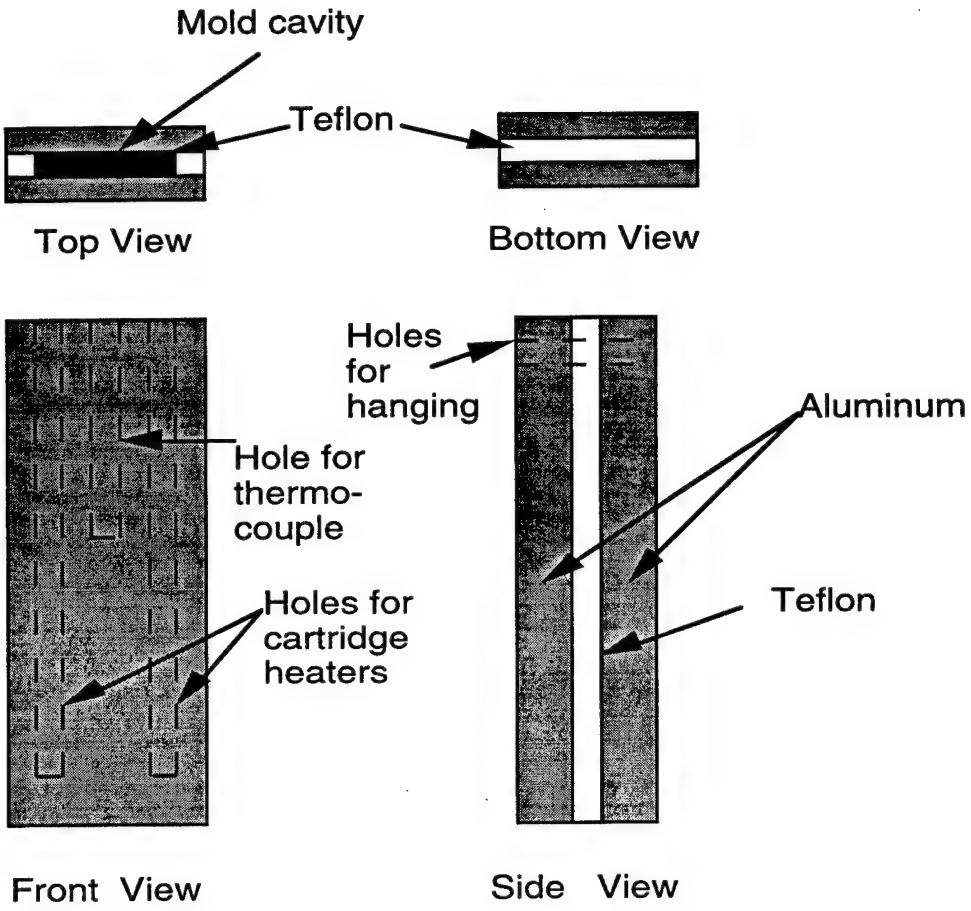

Figure 3-3. Aluminum molds for sample preparation.

The SAA was allowed to dissolve into the melted resin with occasional stirring with a spatula. This typically took about 20-30 minutes. Once dissolved the solution was allowed to sit at 150°C for 4-5 minutes. The solution was then removed from the oven and allowed to cool for 1-2 minutes. Two milliequivalents of the F-2 catalyst were then added to the solution based on the number of grams of DOMS used:

Milliliters of F-2 = Weight of DOMS ÷ EEW of DOMS x 482.49 x 0.002 ÷ 0.4

The catalyst was slowly added with a syringe while stirring with the spatula. Once all the catalyst was added and the solution stirred completely the mixture was outgassed for 1-2 minutes or until no more gas bubbles could be seen escaping the solution.

Following outgassing the solution was poured into molds that had been prepared previously and heated to the formulation temperature to prevent fast cooling of the resin and void formation. Filled molds were stored in a freezer until ready for use or ready for transport to the magnet laboratory, for which they were put under dry ice. Samples that had to be B-staged were placed in the oven at 120°C for the desired length of time, cooled to room temperature and then stored in the freezer until ready for use or transport.

Sample Processing and Preparation for Characterization

The molds were taken to the National High Magnetic Field Laboratory in Tallahassee, FL for processing. The magnets used were a 50 mm bore, variable field resistive magnet or a 61 mm bore superconducting magnet with a room temperature bore. The mold was hung with steel wire and lowered to the center of the magnetic field in the magnet bore. Once in place the magnet was adjusted to the desired field strength and the sample was heated up to 150°C at about 35°/minute and held for the desired amount of

time. Temperature was controlled by an Omega® CN3251-R Temperature/Process Controller purchased from Omega Engineering, Inc. using a type J thermocouple wire purchased from Cole-Parmer Instrument Co. Heat was provided from CSS series 3/16" x 4" cartridge heaters also purchased from Omega Engineering, Inc. At the end of the allotted time for processing in the magnet the samples were allowed to cool at bore temperature to 100°C and then removed from the field.

Once processing in the magnet was complete the molds were cooled to and stored at room temperature until curing could be completed. The entire cure cycle is shown in figure 3-3. The time indicated includes the time spent in the magnetic field. The ramp rates in the oven during the final cure are indicated. The ramp rate in the magnet was approximately 31°C/min. The cool down rate in the magnet was approximately 5°C/min.

Once cured the samples were removed from the molds and labeled appropriately. A diamond saw blade purchased from Web Industries was used to cut the samples into 10mm x 45mm samples for dynamic mechanical spectroscopy tests. The samples were sanded lightly to remove any surface blemishes that may have formed. A small portion of the leftover sample was sanded to about 1mm thickness for characterization using x-ray diffraction.

Sample Testing

Polarized Optical Microscopy

Polarized optical microscopy experiments were carried out using a Nikon Fluophot microscope and a Linkham Scientific Instruments HFS91 hot stage controlled

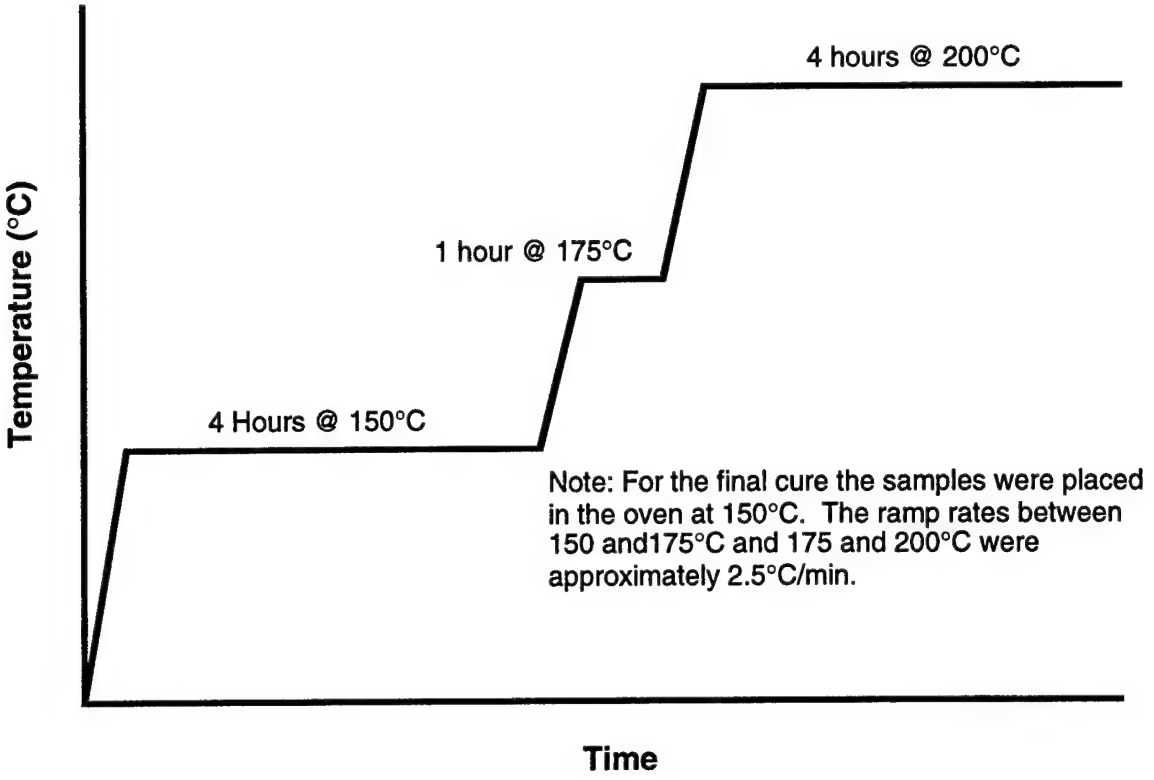

Figure 3-3. Cure cycle for DOMS-SAA system used in this study.

by a TMS 91 temperature controller. A small amount of the sample to be studied was placed between two microscope cover slips. The temperature was ramped up at a rate of 120°C/minute to the desired temperature. The time from melting to liquid crystalline appearance was recorded for each sample tested.

Rheology Measurements

Rheology measurements were conducted using the Parr Physica UDS 200 Universal Dynamic Spectrometer. Experiments were conducted in the parallel plate configuration operating in oscillation mode at 1 Hz and 5% strain using aluminum plates at a 1mm gap spacing. The measurements were taken every 30 seconds during isothermal

cure at 150°C under an air atmosphere. The tests were terminated once the gel point for that particular material was reached.

The measurements were conducted on formulated, uncured resin with no B-staging and 30, 60, 90, 120, 150, and 180 minutes of B-staging at 120°C. The material used was taken from storage in the freezer and allowed to warm to room temperature before being tested. The plates were heated to 150°C and a small amount of resin, about 1g, was placed on the lower plate and allowed to melt. The upper plate was lowered into position and the test was commenced.

Dynamic Mechanical Spectroscopy (DMS)

DMS measurements were conducted using the Seiko SDM/5600 DMS 110 thermomechanical analyzer interfaced with a Seiko SDM/5600H Rheostation for data collection and analysis. The DMS 110 uses a double-cantilever testing apparatus in flexure. The distance between load points is 10mm. Testing was done with rectangular samples with dimensions of 45mm by 10mm and 1 to 1.5mm thick. Samples were clamped in the flexure fixture with a torque wrench using 9.4 kgf/cm, which was sufficient to prevent slippage of the sample during testing

The sample chamber was purged with nitrogen gas at the rate of 200 ml/min. The temperature range was -100 to 250°C to capture all three major relaxations of the material. The temperature was ramped at 0.75°C/min to ensure that all five frequency tests occurred at the same temperature for each data point. The samples were tested at five different frequencies, 0.1, 0.5, 1, 5, and 10 Hz.

The activation energies for two of the relaxations, γ and α, were calculated using an Arrhenius relationship and the tan δ curve. The equation used was:

$$\ln(f) = \ln(A) + \frac{E_A}{RT}$$

where f is the test frequency, A is some pre--exponential factor, T is the relaxation temperature, R is the gas constant equal to 8.31451×10^{-3} kJ/mol-K, and E_A is the activation energy in kJ/mol. The activation energies were calculated from the slope of a plot of ln(f) versus 1/T.

Wide Angle X-ray Scattering (WAXS)

WAXS diffraction patterns were collected using a Siemens General Area Detector Diffraction System (GADDS®) V3.323 equipped with the Siemens HI-STAR Detector System. The sample was mounted between the x-ray generator and detector about 1 cm from a long, fine-focus collimating tube with cross-coupled Göble mirror monochromator with 500 μm collimation and 10cm from the detector with the magnetic field direction perpendicular to the beam direction. The sample holder provided an additional point collimation of 300 μm using a pinhole situated flush with the sample to reduce edge scattering noise. Monochromatic Cu-K_α x-ray radiation was provided by a Kristalloflex 760 2.2 kW generator operating at 50 kV and 35 mA. Each sample was subject to x-ray irradiation for 30 to 60 minutes. A 4° beam stop was mounted 40 mm behind the sample.

The data was processed using the GADDS® software. The data was unwarped to correct for inhomogeneities in the data collection of the detector. This correction also

allowed the pattern collected in three-dimensional space to be represented on a two-dimensional surface A background was also collected under the same conditions to correct for air scattering.

After unwarping the data a series of corrections were conducted. The first and second corrections were a combined function of the software correction, called the Lorentz-polarization corrections, correct for differences in the scattering process due to variations in the experimental conditions and polarization of the x-rays, respectively (Bal89).

The third correction is the plate correction which corrects for absorption of the x-rays by the sample. The correction as done by the GADDS software is:

$$A = \frac{e^{-\frac{\mu t}{\cos(b)}} - e^{-\frac{\mu t}{\cos(a)}}}{(\mu x)\cos(a)}$$

where

$$x = \frac{1}{\cos(a)} - \frac{1}{\cos(b)}$$

and A is the x-ray absorption, t is the sample or plate thickness, a is the incident beam angle with the sample normal, b is the diffracted beam angle with the sample normal, and μ is the linear absorption coefficient. The value used for the linear absorption coefficient for the DOMS-SAA system samples was 10.91 cm^{-1} and was calculated using

$$\mu = \left[\sum_i w_i \left(\frac{\mu}{\rho}\right)_i\right]\rho$$

where w_i is the weight fraction of atom i, $\left(\frac{\mu}{\rho}\right)_i$ is the mass absorption coefficient of component i, and ρ is the density of the DOMS-SAA system samples calculated using the Archimedes method. The density of the material was calculated using a series of samples with no B-staging and a series of samples with 120 minute B-staging, both at varying field strengths. The density obtained from the Archimedes method was 1.2545 g/cm^3. The w_i's were calculated based upon the stoichiometric additions of 2 mol DOMS and 1 mol SAA. The w_i's calculated were 0.0613, 0.6792, 0.0330, 0.1887, and 0.0377 for hydrogen, carbon, nitrogen, oxygen, and sulfur, respectively. The mass absorption coefficients used were 0.3912, 4.219, 7.412, 11.03, and 92.53 for the hydrogen, carbon, nitrogen, oxygen, and sulfur, respectively.

The azimuthal intensity distribution of the inner ring was determined from radial integration through the entire ring in step sizes of $\phi = 0.1$ degrees. The integrations took place at $2\theta = 3.5°$ to 4.7°. Integrations to correct for amorphous scattering were also taken at $2\theta = 3.0°$ to 3.4° and $2\theta = 4.8°$ to 5.2°. Their averaged intensities were then subtracted from the previous integration results. A linear baseline was assumed due to the sharpness of the peak intensities.

The data from the integration was transferred to a spreadsheet program for further analysis. The data were plotted and the two peaks appearing from the ring were averaged and the beam stop shadow was removed. The data were then shifted so that maximum

intensity occurred at exactly ϕ=0°. The intensity distribution in the sample I(α) was then determined from the intensity distribution of the diffraction pattern I(ϕ) by:

$$\cos(\alpha) = \cos(\phi)\cos(\theta)$$

where θ is the Bragg angle and α is the angle between the layer normals and the magnetic field direction.

From the intensity distribution in the sample I(α) the second moment of the orientation function was calculated using:

$$\langle P_2 \rangle = \frac{1}{2}\left(3\langle \cos^2 \alpha \rangle - 1\right)$$

where $\langle \cos^2 \alpha \rangle$ is the average angle with respect to the field direction determined by:

$$\langle \cos^2 \alpha \rangle = \frac{\int_0^{\pi/2} I(\alpha)(\sin\alpha)\left(\cos^2 \alpha\right)d\alpha}{\int_0^{\pi/2} I(\alpha)(\sin\alpha)d\alpha}$$

Additional Crosslinking Agents

The DOMS-SAA system is well known to cure with smectic liquid crystalline order (Lin94, Liu97). Other epoxy--sulfanilamide systems are also know to cure with smectic liquid crystalline order (Shi96, Shi97c, Shi98). An important comparison to make is between that system and one that cures with nematic liquid crystalline order. One may favor reorientation over the other, and thus higher orientation degrees could be obtained.

The first step in conducting this comparison is to develop a crosslinking agent which favors the formation of nematic liquid crystalline order.

The crosslinking agents used in this study were benzenesulfonamide (BSA); 1, 3-benzenedisulfonamide (BDSA); 4, 4'-methylenebis(benzenedisulfonamide) (MB-BDSA), 4, 4'-biphenyldisulfonamide (BPDSA); 1, 4-phenylenediamine (PD); 4, 4'-methylenedianiline (MDA) (Note: methylenedianiline is a highly toxic cancer suspect agent). A schematic of these amines is shown in figure 3-2. The method used in replacing the chlorine with an amine in some of the following procedures was adapted from the procedure for making sulfanilamide by Pavia et al. (Pav88).

BSA Formulation

The BSA used was purchased from Aldrich Chemical Company, Inc. and used without further purification. The BSA was mixed mechanically via mortar and pestle with SAA for use in the formulation. The two were mixed in stoichiometric amounts with respect to the DOMS resin. Three mixtures were accomplished including 5, 30, and 50 mol% BSA. The samples were formulated in stoichiometric amounts according to the procedures for the DOMS-SAA system formulation. After formulation was complete a small amount of each mixture was placed on a glass microscope cover slip and cured according to the cure cycle for the DOMS-SAA system. An x-ray analysis was then performed on each of the slides.

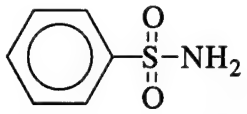

benzenesulfonamide (BSA)

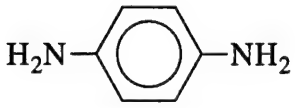

phenylenediamine (PD)

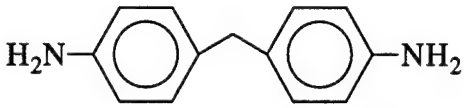

methylenedianiline (MDA)

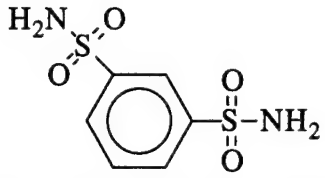

1,3-benzenedisulfonamide (BDSA)

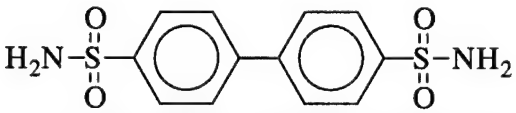

4, 4'-biphenyldisulfonamide (BBPDSA)

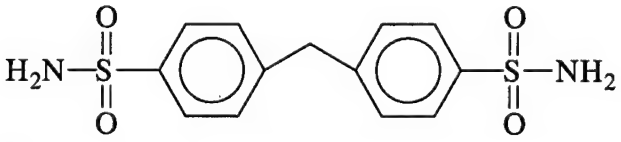

4, 4'-methylenebis(benzenedisulfonamide) (MB-BDSA)

Figure 3-2. Additional amines used as hardeners in this study.

BDSA Synthesis and Formulation

The BDSA was synthesized by first placing 6g of 1, 3-benzenedisulfonyl chloride, purchased from Aldrich Chemical Company, Inc. and used without further purification, in a round bottom flask under argon. To this 30mL of concentrated NH_4OH was added slowly at room temperature. The solution was stirred and heated at 100°C oil bath. Once the base was added the mixture began bubbling immediately. The reaction was allowed to continue for 15 minutes upon which the flask was removed from the oil bath and allowed to cool at room temperature for 5 minutes and then allowed to cool completely in an ice bath. Once cool concentrated HCl was added to the solution until just acidic to litmus. The white precipitate that had formed was then filtered and washed with distilled water. Synthesis of BDSA was confirmed using NMR and elemental analysis.

The BDSA was then added in a stoichiometric amount to molten DOMS resin according to the formulation procedure given for the DOMS-SAA system. Following formulation a small amount of the mixture was placed on a glass microscope cover slip and cured according to the cure cycle given for the DOMS-SAA system. An x-ray analysis was then conducted on the cure samples.

MB-BDSA Synthesis and Formulation

The synthesis of MB-BDSA was accomplished by first adding 2mL concentrated NH_4OH to approximately 1g 4, 4'-methylenebis(benzenedisulfonyl chloride), purchased from Aldrich Chemical Co. and used without further purification. The mixture

immediately began to bubble while being stirred. After approximately 10 minute the reaction vessel was lowered into a silicon oil bath at 100°C. The reaction was allowed to continue for an additional 15 minutes. At the end of this time the vessel was removed from the heat and allowed to cool in air for 5 minutes and then placed in an ice bath to cool completely. When completely cool, concentrated HCl was added to the pasty white mixture while stirring until just acidic to litmus. The solid was then filtered and washed with deionized water and vacuum dried at 30°C for 24 hours.

Once dry the solid was formulated with the DOMS resin according to the procedure for the DOMS-SAA formulation. Unfortunately, a subsequent elemental analysis and NMR of the sample revealed that the reaction did not occur and only the starting material, the 4, 4'-methylenebis(benzenedisulfonyl chloride), was obtained from the reaction.

BPDSA Synthesis and Formulation

The BPDSA was synthesized by first refluxing 2.51 g of 4, 4'-biphenyldisulfonyl chloride, purchased from Aldrich Chemical Company, Inc. and used without further purification, with excess oxalyl chloride (5mL) and benzene (30mL) at 75°C for 3 hours with constant stirring. After refluxing approximately half of the solution was removed to rid of any excess oxalyl chloride. To the remaining solution 30mL of hexane were added and left under an argon atmosphere for approximately 12 hours. A white solid precipitated out of the hexane solution. This solid was filtered and washed with hexane. The solid was then placed under a vacuum to removed as much hexane as possible. After approximately 1 hour the solid was put under argon and 20mL of concentrated NH_4OH

was added to the flask. The mixture immediately began bubbling. The reaction was allowed to carry on for approximately 15 minutes at 100°C. The mixture was then cooled at room temperature for 5 minutes and then placed in an ice bath until completely cool. While stirring, concentrated HCl was added until the solution was just acidic to litmus. The solid was then filtered and washed using distilled water and dried in a vacuum over at 60°C.

Once dry, the solid was added in stoichiometric amount to molten DOMS resin. The BPDSA did not completely dissolve into the molten DOMS although it was left in for approximately the same time it took for SAA to dissolve into the melted DOMS resin. The cooled mixture was then cured in a convection oven according to the cure cycle for the DOMS-SAA system, and a small portion of the uncured resin was studied using cross polarized microscopy.

PD and MDA Formulation

The PD flakes and MDA pellets were purchased from Aldrich Chemical Company, Inc. (Milwaukee, WI) and used without further purification. However, they were both crushed in a mortar and pestle to a fine powder for easier and more accurate weighing.

Both the PD and MDA agents were mixed individually in stoichiometric amounts with the DOMS resin and dissolved completely in chloroform. Excess chloroform was removed under vacuum at room temperature. Once dry, a small portion of each of the mixtures was placed on a microscope cover slip and cured according to the cure cycle

given for the DOMS-SAA system. Optical microscopy tests were also performed on each of the mixtures.

An additional cure was performed with the DOMS-MDA system in which the mixture was heated to 120°C until all of the solid was melted and then the temperature was lowered to 80°C and cured for 5 hours until the temperature was raised to 140°C for an additional 10 hours.

CHAPTER 4
RESULTS AND DISCUSSION

Orientation Parameters from X-ray Analysis

Figure 4-1 shows typical WAXS patterns collected for the 0 minute B-staged samples and the 120 minute B-staged samples. The two patterns on the left are patterns indicative of samples with a low degree of orientation because of the presence of the entire inner and outer rings. The two patterns on the right are patterns indicative of more highly oriented samples because of the presence of only arcs for the inner and outer reflections.

Figure 4-2 shows a plot of orientation parameter versus field strength for (a) the 0 minute B-staged samples and (b) the 120 minute B-staged samples cured for 60 minutes in the field. As would be expected each plot shows an increasing orientation parameter for increasing field strength. The plot in (a) shows the possible existence of some plateau or maximum value of the orientation parameter obtainable for that material. This may be attributed to the size of the domains as Anwer and Windle found affects the amount of orientation achievable (Anw93). Larger domains lead to less orientation as they hinder each others rotation during the reorientation process. The plot in (b) shows the possible existence of some threshold value of the field strength for significant orientation to occur, which will be dealt with later in this chapter.

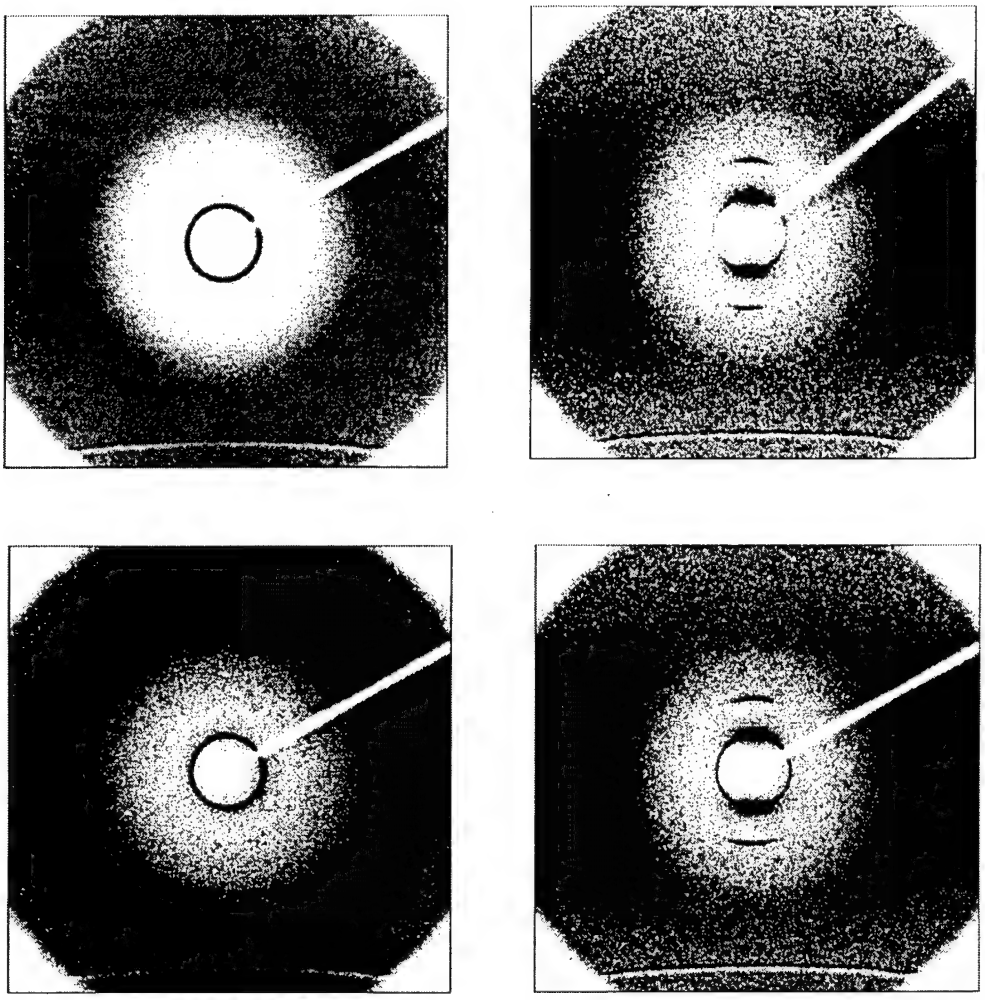

Figure 4-1. WAXS patterns for the (clockwise from top left): 0 minute B-staged/0 Tesla; 0 minute B-staged/12 Tesla; 120 minute B-staged/12 Tesla; and 120 minute B-staged/0 Tesla samples.

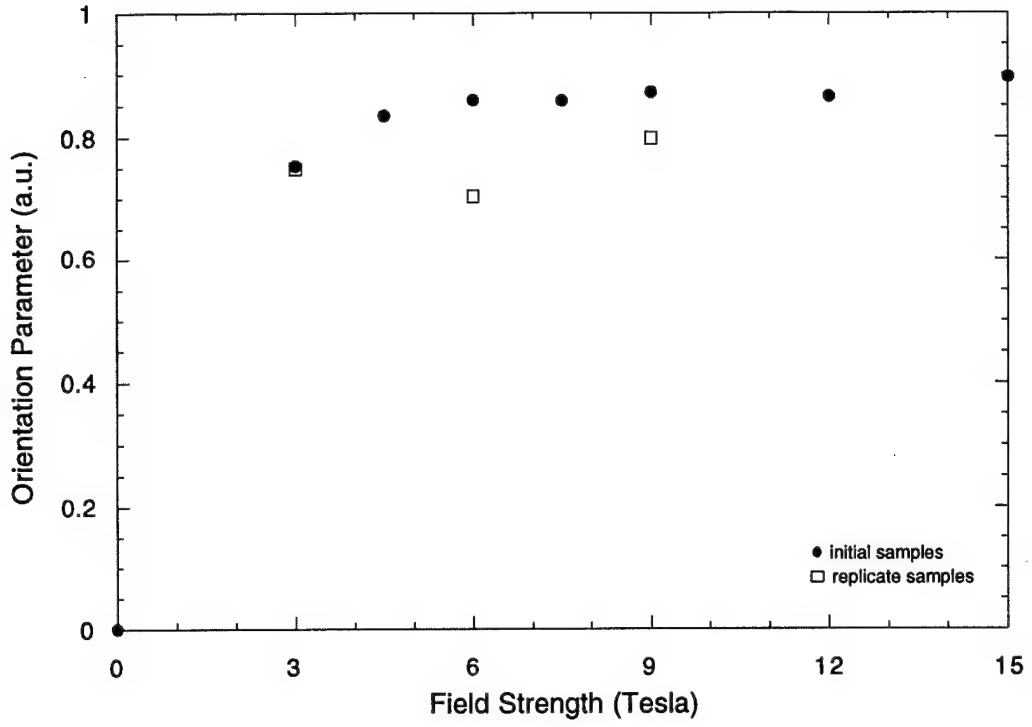

(a)

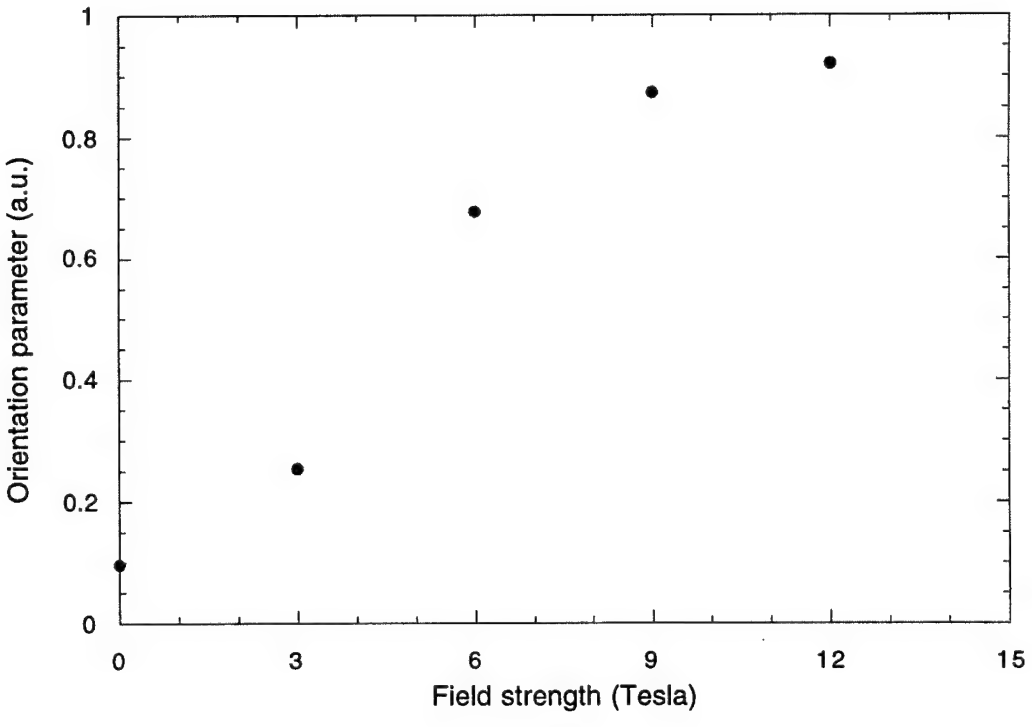

(b)

Figure 4-2. Orientation parameter as a function of field strength for (a) 0 minute B-staged samples and (b) 120 minute B-staged samples.

Rheology and Optical Microscopy

The results of the rheology and optical microscopy tests are listed in table 4-1. Included are the gel time, complex viscosity at the gel point, dynamic storage modulus, all determined from the rheology experiments; and the time to liquid crystalline appearance, determined by optical microscopy. The first item of interest is the time to liquid crystalline appearance. This time is measured as the time from melting to the beginning of the isotropic-liquid crystalline phase transition. These results display a decreasing length of time from melt to the transition as the amount of B-staging increases. At 0 minutes B-staging the material melts into an isotropic phase; whereas, at 120 minutes B-staging the material melts into a liquid crystalline phase. This is due to the difference in the reactivities of the two amine groups on the sulfanilamide molecule. The amine substituted directly on to the benzene ring reacts much quicker than the other amine. This gives rise to the formation of a linear prepolymer at the beginning of cure. This linear prepolymer increases the aspect ration of the molecule, which supports the formation of liquid crystalline phases. Thus, these two materials were used as a direct comparison for this study.

The cooperative motion of the molecules allows orientation to take place only in the liquid crystalline phase. If the material initially melts into a liquid crystalline phase reorientation can begin immediately. On the other hand if the material melts into an isotropic phase, reorientation cannot begin until the material becomes liquid crystalline. It would then be expected that the 120 minute B-staged material would orient

Table 4-1. Rheology and optical microscopy data for the 0 minute B-staged and the 120 minute B-staged series.

B-stage time (min)	Gel time (min)	Complex viscosity at gel point (Pa-s)	Dynamic modulus at gel point (Pa)	Time to liquid crystalline appearance (min)
0	38.7	1604.5	7214	19
30	26.9	3458.9	15520	12
60	24.7	11973.5	54101	9
90	19	13168.2	58688	5
120	15.4	26171.57	78029	LC upon melting
150	7.6	20547.11	91836	Incomplete melting
180	8.3	56436.28	205000	[a]

[a]sample not accomplished in optical microscopy due to incomplete melting at 150 minutes B-staging time.

quicker and easier, because it is liquid crystalline upon melting, than the 0 minute B-staged material, because it is not liquid crystalline upon melting.

However, working against the reorientation process in the 120 minute B-staged material is the increased viscosity. Figure 4-3 shows the complex viscosity curves for the two samples. The 120 minute B-staged material exhibits a sixteen times increase in the viscosity over the 0 minute B-staged material at the gel point. The short gel time for the 120 minute B-staged material, 15.4 minutes, also works against orientation of the material. The short gel time indicates less time for the material to be oriented in the magnetic field.

In the model given by Moore and Stupp (Moo87):

$$\tan\theta_o = \tan\theta_o' \exp[-(t/\tau)]$$

where $\tau = \gamma/\Delta\chi B^2$, this increase in viscosity and associated decrease in gel time should decrease the amount of orientation obtained under the same processing conditions for the

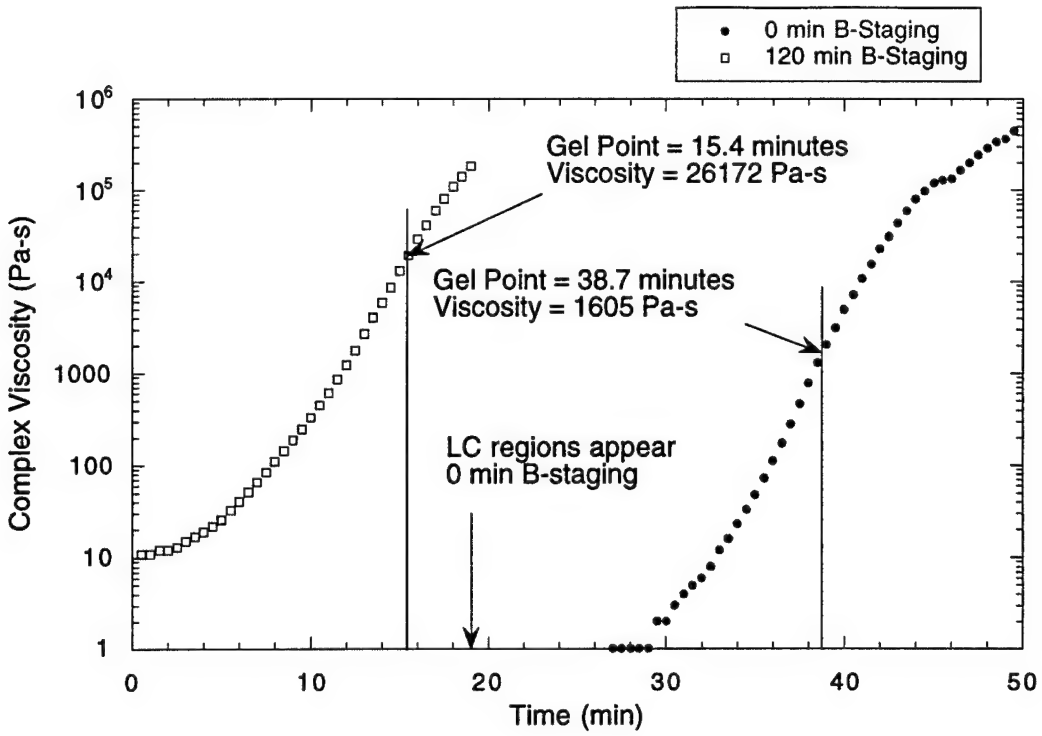

Figure 4-3. Complex viscosity curve comparison between 0 minute B-staged material and 120 minute B-staged material.

B-staged versus the non B-staged material. However, the orientation parameter results shown in figure 4-2 from x-ray analysis of the samples show that this is not the case.

Although the 120 minute B-staged samples display a lower orientation parameter at lower field strengths, < 9 Tesla, orientation parameters comparable to those for the 0 minute B-staged material are seen at higher field strengths, ≥ 9 Tesla. The lower orientation parameters at lower field strengths for the B-staged samples may be a result of some threshold value of the field strength required to overcome the increased viscosity of the material. It would be expected that this trend of lower orientation parameters would continue at high field strengths because of the increased viscosity. Again, looking at figure 4-2 this is not the case.

The threshold is a point at which the $\Delta\chi B^2$ term simply overwhelms the viscosity of the material. At low field strengths this term is small and the increasing viscosity of the B-staged material dominates the exponential term, τ. Thus, orientation is substantially hindered. As the field strength increases the $\Delta\chi B^2$ becomes the dominating factor in τ. Significant orientation is, thus, achieved at the higher field strengths.

Dynamic Mechanical Spectroscopy Analysis

Figure 4-4, 4-5, 4-6, and 4-7 show typical tan δ and loss and storage modulus curves obtained for the 0 minute and 120 minute B-staged samples at low and high orientations. The tan δ and loss modulus curves clearly show the presence of the three major transitions typical of epoxies. The γ transitions appear in the temperature range of -35 to -50°C, the β transitions in the range of 50 to 60°C, and the α transitions in the range of 190 to 200°C.

The dynamic storage moduli curves show the gradual decrease in magnitude typical of many epoxies (Kee79, San95, Van68). However, the presence of the liquid crystalline nature of the material is apparent as well. The dynamic storage moduli are largely unaffected by the relaxations the material undergoes, and, as Melissaris et al. found, the moduli change little as the material transitions from a glassy to a rubbery state indicative of the high crosslink density of liquid crystalline materials (Mel95). This is also due, in part, to the stiffness of the molecules which sterically hinder the network from large motions during the relaxations.

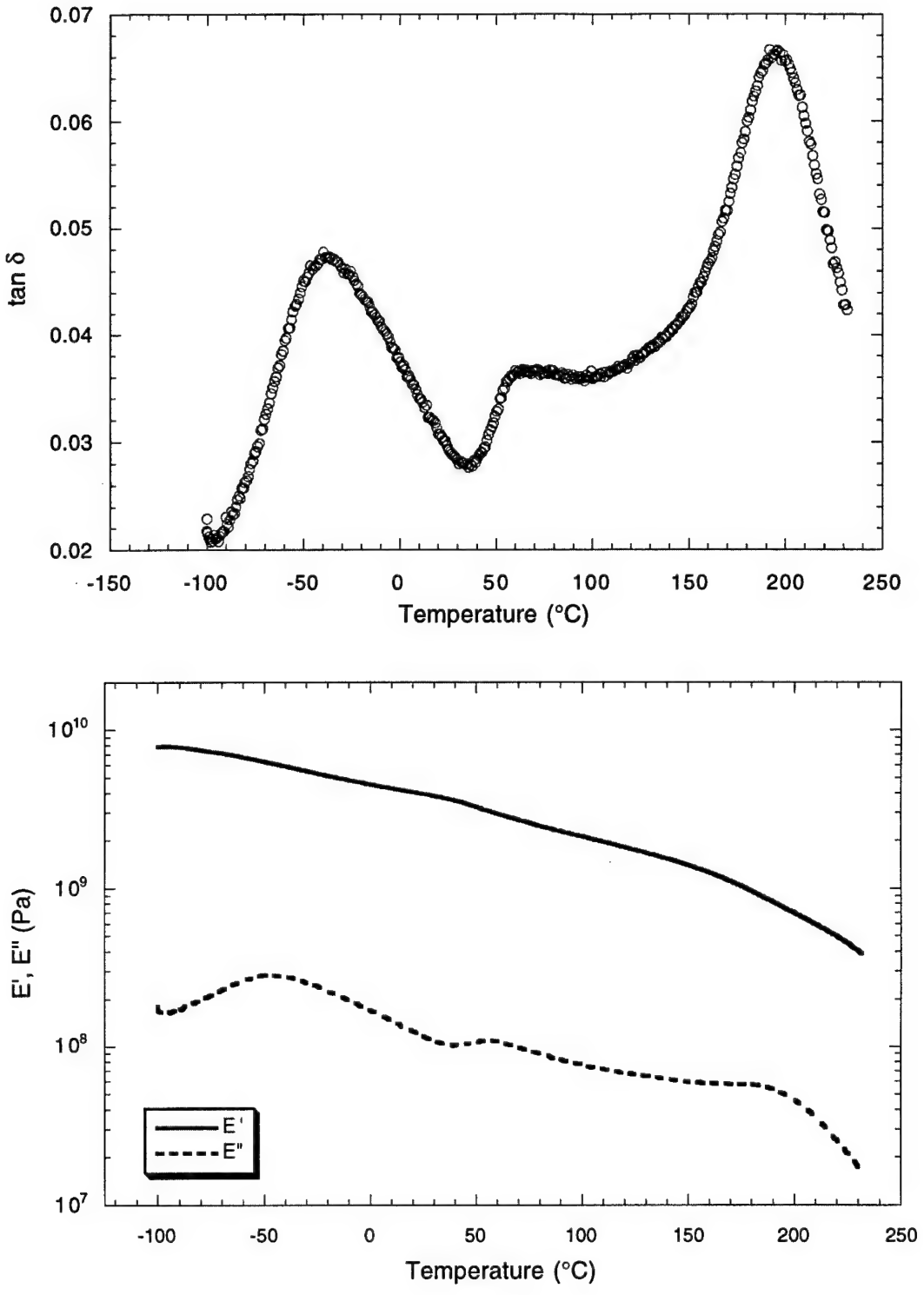

Figure 4-4. The tan δ and the dynamic loss and storage modulus curves for the 0 minute B-staged, 0 Tesla sample.

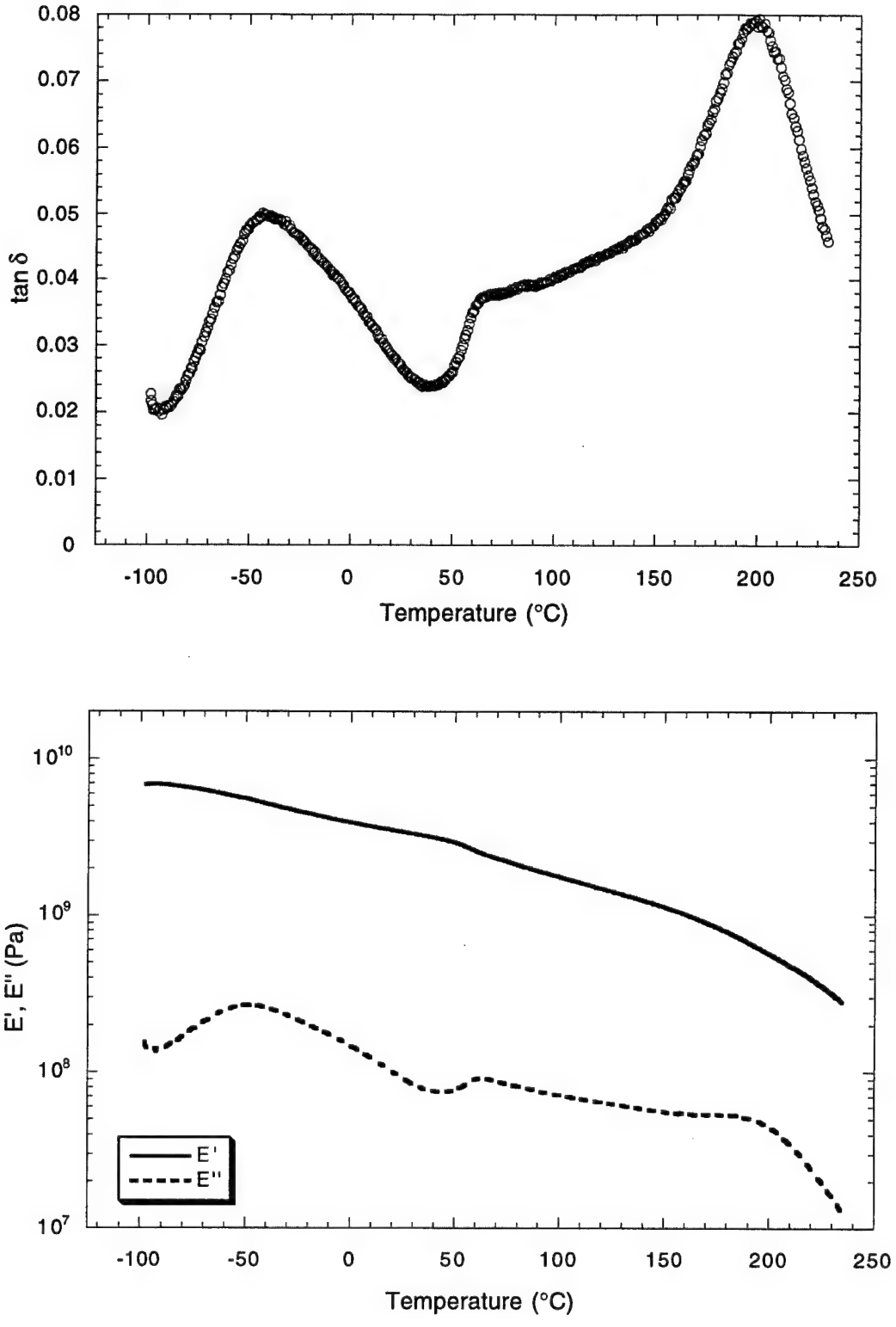

Figure 4-5. The tan δ and the dynamic loss and storage modulus curves for the 120 minute B-staged, 0 Tesla sample.

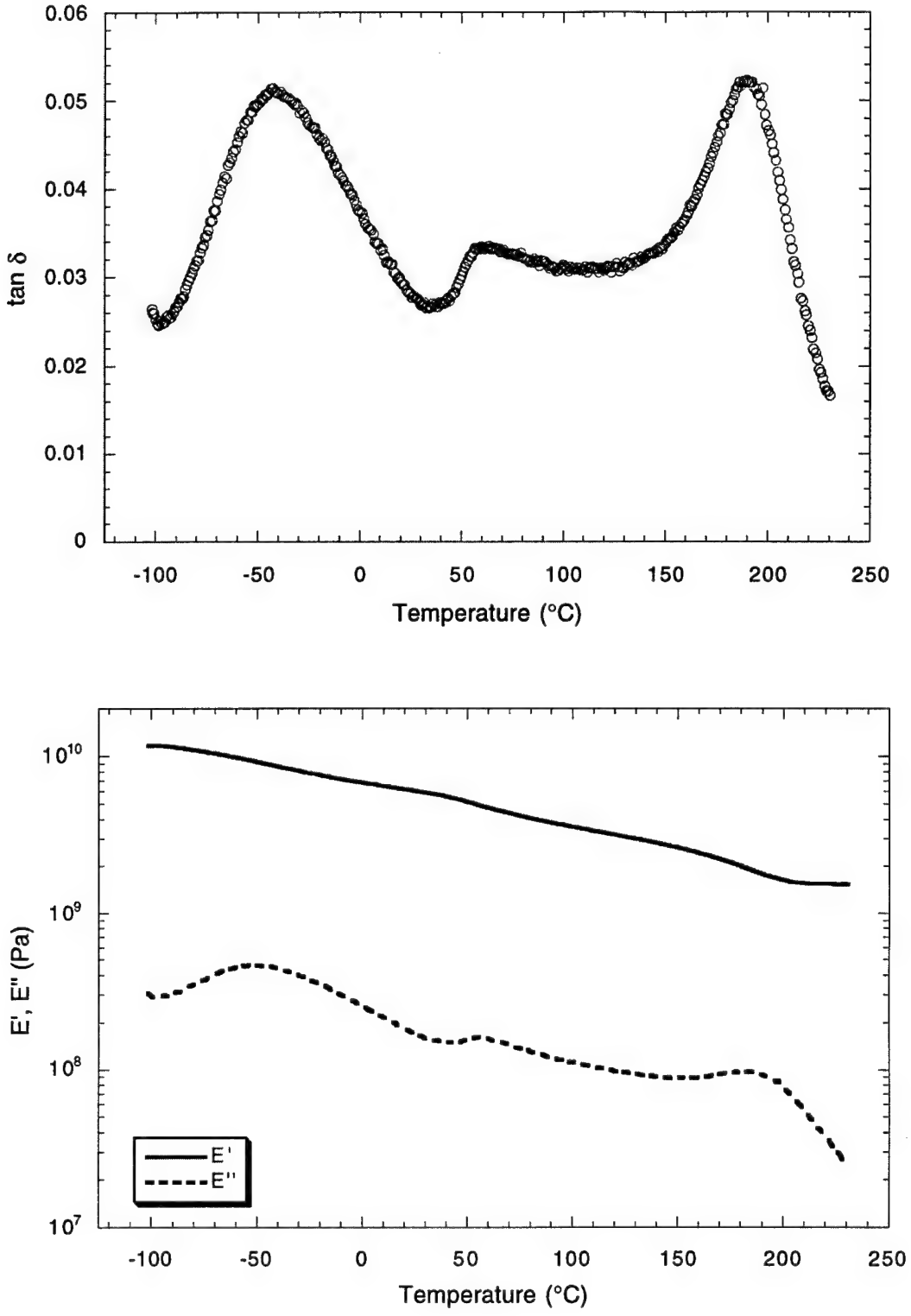

Figure 4-6. The tan δ and the dynamic loss and storage modulus curves for the 0 minute B-staged, 12 Tesla sample.

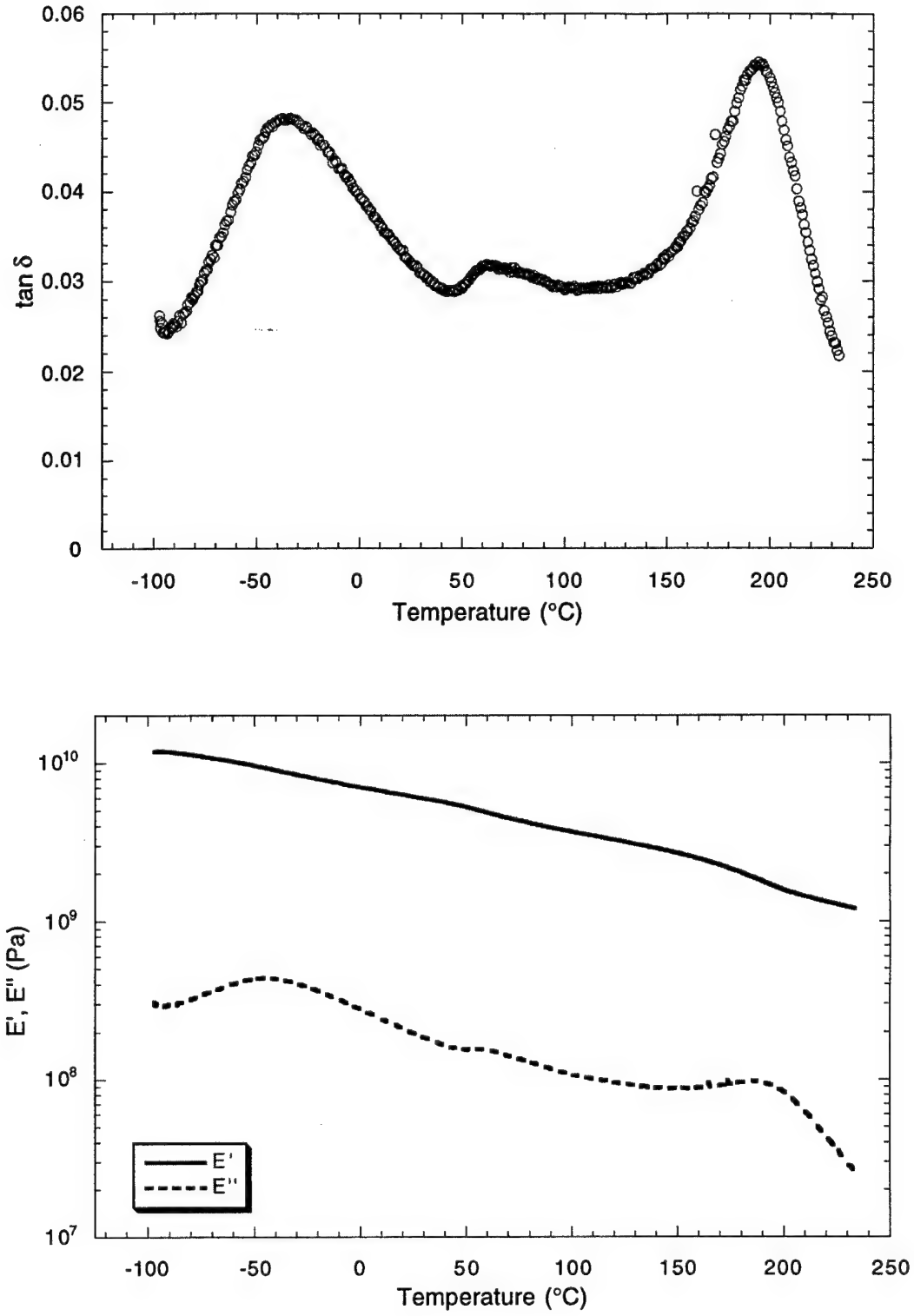

Figure 4-7. The tan δ and the dynamic loss and storage modulus curves for the 120 minute B-staged, 12 Tesla sample.

Figure 4-8 shows a plot of dynamic storage moduli versus field strength at 1 Hz for both (a) the 0 minute B-staged material and (b) the 120 minute B-staged material. With the 0 minute B-staged material an increase of nearly 60% in the dynamic storage modulus was obtained with the application of the magnetic field. Similarly, an increase in the dynamic storage modulus of nearly 80% was obtained for the 120 minute B-staged material. However, the maximum moduli obtained for both materials is nearly the same.

Table 4-2 lists the results from the dynamic mechanical spectroscopy test conducted on the 0 minute B-staged samples and the 120 minute B-staged samples. The transition temperatures and apparent activation energies for the α and γ peaks are included. The β peak does not display any Arrhenius type behavior and is, therefore, not included.

It was first believed that reorientation of the molecules under the influence of magnetic fields may have some effect on the packing efficiency of the molecules. Because the molecules are being aligned in the material a better packing would result. The results in table 4-2 confirm this belief. For the 0 minute B-staged series significant orientation occurs in the sample processed at 3 Tesla, and the activation energy for the α peak displays a corresponding jump in magnitude between the sample at 0 Tesla (random orientation) and 3 Tesla (high orientation). However, this trend does not continue as the field strength is increased, but the orientation parameter in not increased significantly either.

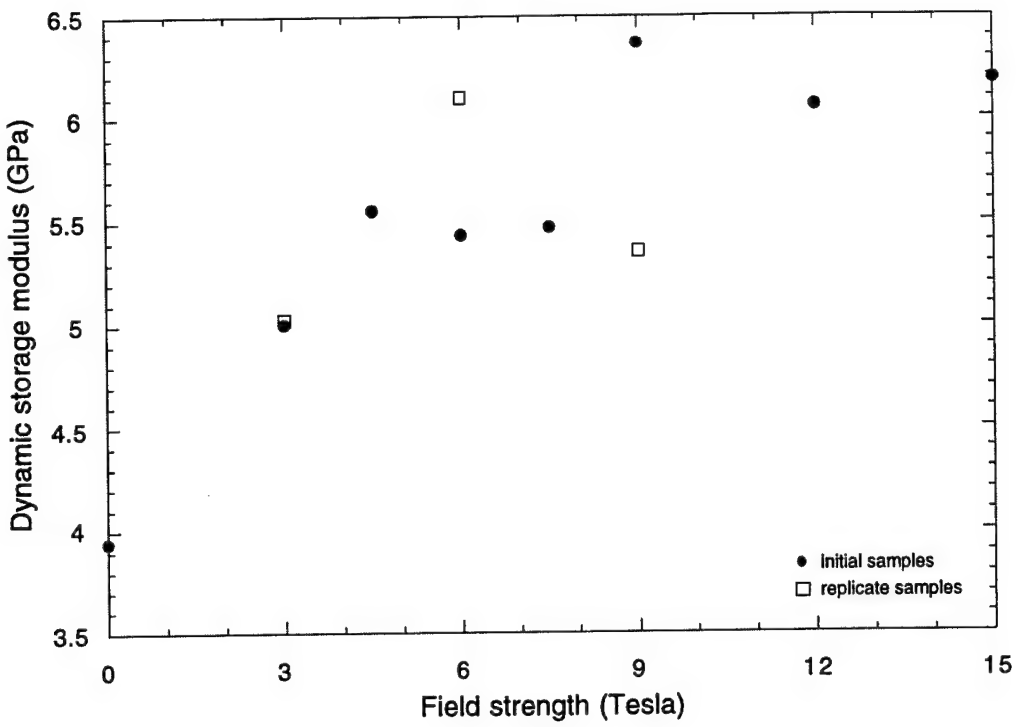

(a)

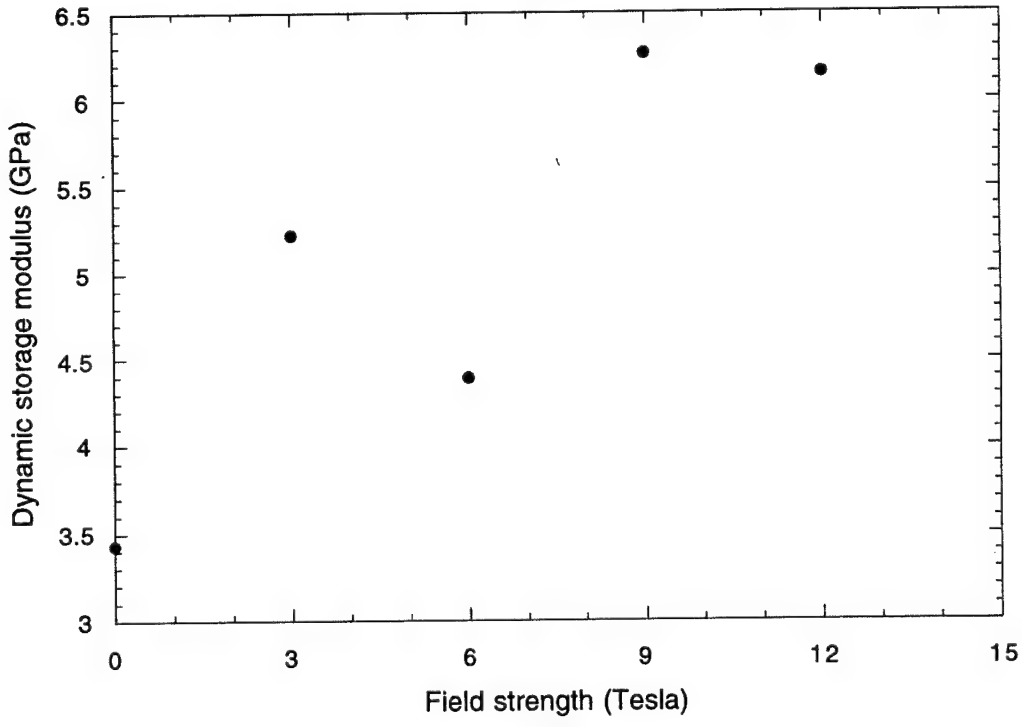

(b)

Figure 4-8. Dynamic storage moduli as a function of field strength for (a) the 0 minute B-staged samples and (b) the 120 minute B-staged samples at 1 Hz and 25°C.

Table 4-2. Dynamic mechanical spectroscopy results for the 0-minute B-staged and 120 minute B-staged series.

Sample	Field strength (Tesla)	B-staging time (min)	Activation energy (kJ/mol) [α peak]	Relaxation temperature (°C) @ 1 Hz	Activation energy (kJ/mol) [γ peak]	Relaxation temperature (°C) @ 1 Hz
1	0	0	341.5 ± 9.9	196.0	76.5 ± 1.5	-37.9
2	3	0	440.6 ± 25.8	189.5	73.9 ± 2.0	-46.7
2b[a]	3	0	430.3 ± 8.6	192.4	80.4 ± 2.2	-41.1
3	4.5	0	466.9 ± 19.5	189.9	69.6 ± 3.1	-47.5
4	6	0	502.2 ± 21.6	189.2	63.8 ± 1.7	-50.0
4b[a]	6	0	485.3 ± 28.5	190.8	67.8 ± 0.7	-41.6
5	7.5	0	483.5 ± 27.2	189.8	66.0 ± 1.7	-48.6
6	9	0	522.7 ± 31.8	188.0	67.2 ± 1.6	-45.6
6b[a]	9	0	458.9 ± 9.1	192.6	75.9 ± 1.7	-38.5
7	12	0	502.4 ± 31.1	189.9	78.2 ± 2.1	-41.9
8	15	0	471.6 ± 14.3	189.2	75.1 ± 1.3	-39.7
9	0	120	353.1 ± 12.0	198.6	67.1 ± 1.3	-42.5
10	3	120	487.2 ± 34.5	196.7	75.2 ± 1.0	-35.1
11	6	120	534.0 ± 41.7	195.1	81.6 ± 2.4	-36.1
12	9	120	542.6 ± 35.3	194.7	78.3 ± 2.6	-36.6
13	12	120	530.7 ± 24.3	195.2	71.3 ± 4.1	-36.4

[a]replicate samples

Again, looking at table 4-2 and the B-staged samples series a jump in the activation energy occurs between the 0 Tesla sample (random orientation) and the 3 Tesla sample (higher orientation). However, for this series the trend continues, but significant orientation is also obtained between samples as the field strength is increased up to 9 Tesla. So, it does seem that there is some effect on the packing density of the material due to orientation in the magnetic field. As the molecules and domains are aligned within the network they must reduce the amount of free volume and pack together more tightly giving rise to the increased activation energy for the glass transition.

The same trends and jumps are not seen in the activation energies for the γ peak. This is expected due to the origin of the γ transition. Better packing of the molecules and domains in the material should have no effect on the rotation of the mesogen in the network and no effect on the activation energy of the transition.

One item of particular interest from the data in table 4-2 is the increased glass transition temperature for the B-staged material versus the non B-staged material. As described earlier it is possible that due to the different reactivities of the amines on the sulfanilamide molecule that a linear prepolymer is formed during B-staging. As also seen with cross polarized optical microscopy the 120 B-staged material is liquid crystalline upon melting. The 120 minute B-staged material is already in a liquid crystalline form when it begins to crosslink after melting; whereas, the non B-staged material begins crosslinking after melting in an isotropic phase. As Litt et al. found liquid crystalline materials typically have a higher degree of conversion than isotropic materials due to the

higher degree of molecular order prior to crosslinking (Lit93). Thus the increased T_g may arise form the fact that the B-staged material, which is liquid crystalline upon melting, obtained a higher degree of crosslinking than the non B-staged material, which is not liquid crystalline upon melting.

Statistical Experimental Design

The statistical experimental design used for this study was designed using CARD® (Computer Aided Research and Development) software by S-Matrix®. The experiments are based on a fractional factorial design modified to reduce the total number of samples required for analysis but still include replicate samples for experimental error analysis. A process variable screening design matrix was chosen for this study. The variables used were time in field, field strength, and B-staging time and the response variable was the orientation parameter. Table 4-4 lists the orientation parameter response values for the samples contained in the design matrix. Samples Stat1 through Stat11 were generated specifically for this design. The remaining samples were obtained from the preliminary work discussed earlier in this chapter.

A preliminary experimental error analysis of the data revealed that the variance for the Stat2 and Stat7 replicate pair was significantly different (>95% confidence) from the pooled variance of all the replicate pairs. Therefore, this pair was removed and the experimental error analysis was completed. Analysis of the remaining five replicate pairs revealed an experimental error percent of 5.82%. This means that 5.82% of the variability in sample response can be attributed to experimental error. The remaining 94.18% of the

Table 4-4. Orientation parameter responses for the samples included in the statistical experimental design.

Sample	Actual	Predicted
Stat1	0.6301	0.7424
Stat2	0.8609	a
Stat3	0.3882	0.3757
Stat4	-0.0172	-0.0886
Stat5	0.8863	0.6537
Stat6	0.7884	0.6537
Stat7	0.5660	a
Stat8	0.5863	0.6123
Stat9	0.4056	0.3757
Stat10	0.7863	a
Stat11	0.2173	0.2119
Stat12	0.7532	0.7081
Stat13	0.7486	0.7081
Stat14	0.8341	0.7353
Stat15	0.8587	0.7625
Stat16	0.7035	0.7625
Stat17	0.8579	0.7897
Stat18	0.8711	0.8169
Stat19	0.7978	0.8169
Stat20	0.8651	0.8713
Stat21	0.2536	0.4042
Stat22	0.6772	0.5865
Stat23	0.8735	0.7689
Stat24	0.9205	0.9512
Stat25	0.7911	0.8310
Stat26	0.5998	0.7839
Stat27	0.6429	0.6594
Stat28	0.0109	0.1781
Stat29	0.7718	0.8386
Stat30	0.6661	0.8006
Stat31	0.6532	0.7245

[a]Samples not included in the model

variability in sample response can be attributed to variations in the time in the field, field strength , and B-staging time. This error percent translates into an error in the orientation parameter response of ± 0.0627.

The data was analyzed in a stepwise regression at a 95% confidence level. No data transformations were required to be performed on the data in order for the model to be generated. An upper limit of 1 and a lower limit of -0.5 were used according to the theoretical value limits the orientation parameter can have. The ranges used for the three variables was 5 to 40 minutes time in the field, 0.5 to 6 Tesla field strength, and 0 to 180 minutes B-staging time. The first order terms (i.e. X_n, etc.) retained these ranges of values when included in the model. The ranges were scaled from -1 to 1 for use in the second order terms (i.e. Xn^2, X_nX_m, etc.) in the model. This is done to normalize the three variable ranges to prevent fabricated interaction effects due to the different range limits.

A quadratic model was chosen for the data analysis to include all variable effects and complex (higher order) interaction effects. The model included the following terms:

$$y = \beta_o + \beta_1X_1 + \beta_2X_2 + \beta_3X_3 + \beta_4X_1^2 + \beta_5X_2^2 + \beta_6X_3^2 + \beta_7X_1X_2 + \beta_8X_1X_3 + \beta_9X_2X_3$$

where β_n are the model coefficients, X_1 is the time in field, X_2 is the field strength, and X_3 is the B-staging time. Preliminary analysis revealed sample Stat10 to be an outlier, so it was removed and the data reanalyzed. The final analysis of the data revealed the X_3, X_2, X_1X_3, X_1X_2, X_1, X_2X_3, and X_3^2 terms to be the statistically significant variable-effect terms, in order from strongest to weakest effector of the orientation parameter, with a >95% confidence level. The model coefficients acquired from the data analysis and

regression were $\beta_0 = 0.4651$, $\beta_1 = 0.0055$, $\beta_2 = 0.0783$, $\beta_3 = -0.0058$, $\beta_6 = -0.3485$, $\beta_7 = -0.2837$, $\beta_8 = 0.2925$, and $\beta_9 = 0.1839$. The remaining model parameters were excluded due to lack of confidence in their fit (<95%). The coefficient of determination, R^2, for this model is 0.8577, meaning that 85.77% of the variability in the orientation parameter response is accounted for by the X terms in the model.

As determined form the model the B-staging time is the largest effector of the orientation parameter. This result is expected as seen from the preliminary work in which the B-staged material displayed a marked decrease in the orientation parameters at lower field strengths. Surprisingly, the amount of B-staging also has a positive effect on the orientation process as well as determined by the model. The maximum orientation parameters can only be obtained at some degree of B-staging. The levels of B-staging with a positive impact on the orientation process must allow orientation to occur despite the increased viscosity but also resist relaxation of the molecules/domains back to a randomly oriented state.

Figures 4-9, 4-10, and 4-11 show surface and contour plots to display the orientation responses for the samples based upon the regression model calculated from the data. Figure 4-9 plots the predicted orientation parameter as a function of the B-staging time and field strength (the largest two effectors of the response variable) for a constant time in the field of 40 minutes. The plot predicts a maximum obtainable value of the orientation parameter of 1.3, which exceeds the maximum theoretical value of 1. The model also predicts negative orientation parameters values lower than -0.5, the theoretical

minimum value of the orientation parameter. This is a rsult of the analytical solution given by the software, which cannot account for the upper and lower limits of the orientation parameter without severly distorting the model. Essentially, the orientation parameter would be maximized at 1 and minimized at zero. These plots also show the large effect of the B-staging as it shows the maximum predicted orientation parameter values can only be obtained for some non-zero values of B-staging.

Figure 4-10 plots the predicted orientation parameter as a function of the B-staging and the time in the field (the next two largest effectors of the response variable) for a constant field strength of 6 Tesla. As expected this plot displays a decrease in the orientation parameter as the amount of B-staging increases and time in the field decreases.An interesting effect seen at low B-stage times (<20 minutes) and high times (>45 minutes) is that the orientation parameter decreases. A possible explanation for this is that the low amount of B-staging results in a lower viscosity in the material, and a good deal of mobility for the domains remains. Orientation occurs early on in the process, but as the material nears the gel point and, eventually vitrifies, the domains begin to crosslink with one another which disrupts orientation which was previously obtained causing the drop in the orientation parameter. This does not occur at higher B-staging times because the mobility of the domains is severely limited by the increase in viscosity due to B-staging. Again, the model also predicts high negative orientation parameters (< -0.5) at high B-staging times and low times in the field. These again are essentially zero.

Finally, figure 4-11 plots the predicted orientation parameter as a function of the field strength and the time in the field for a constant B-staging time of 90 minutes. The

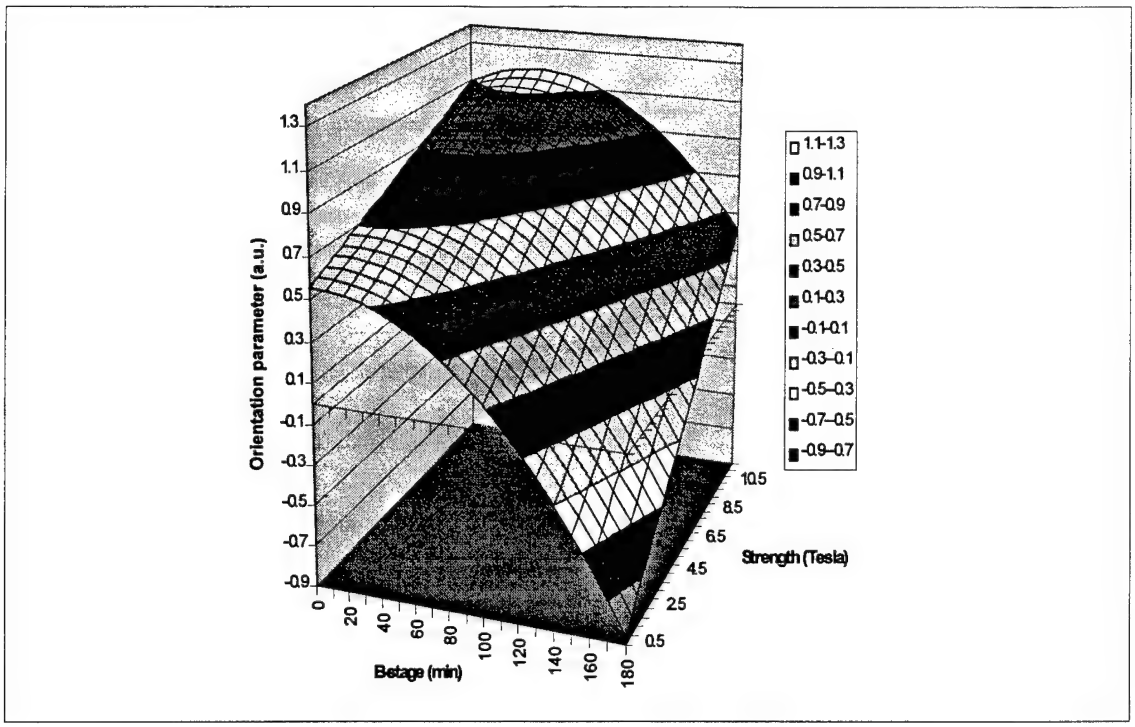

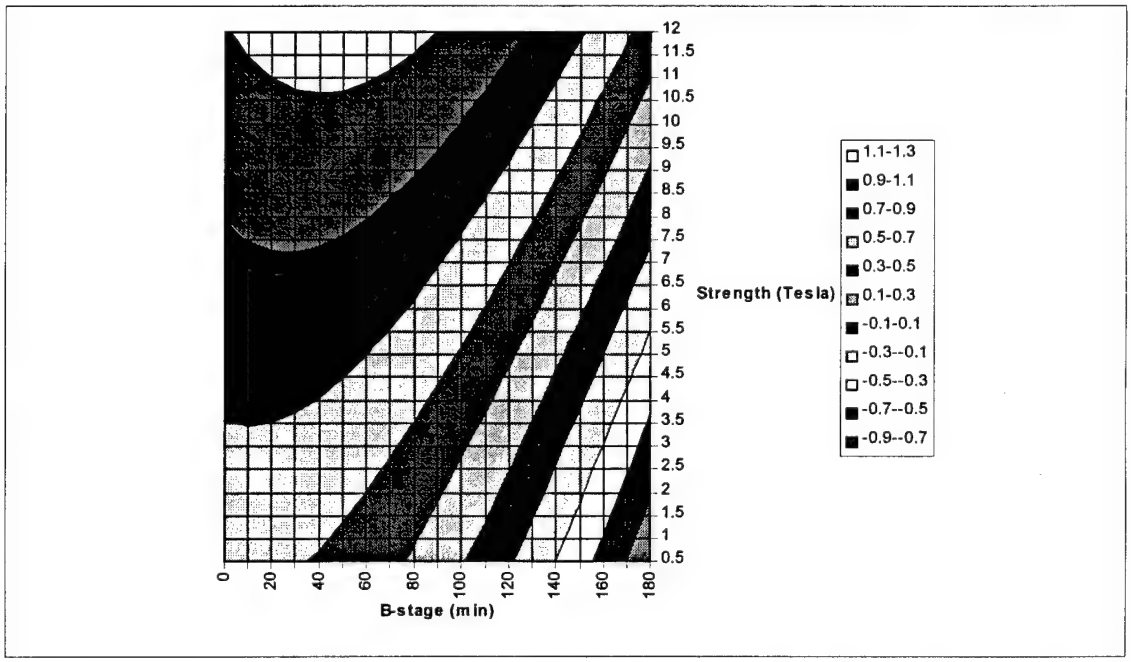

Figure 4-9. Surface and contour plots of the predicted orientation parameter response variable as a function of the B-staging time and the field strength for a constant time in the field of 40 minutes.

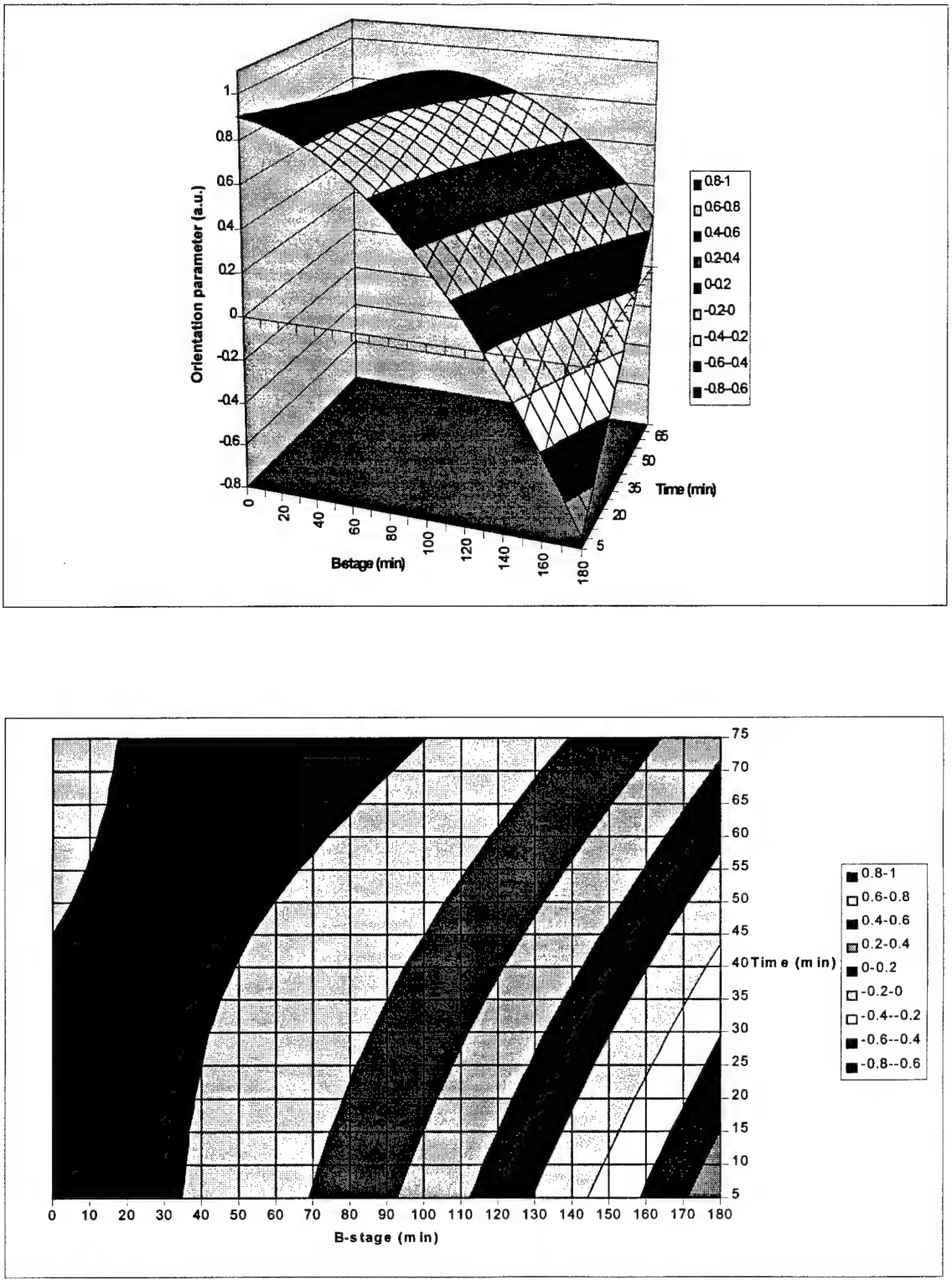

Figure 4-10. Surface and contour plots of the predicted orientation parameter response variable as a function of the B-staging time and the time in the field for a constant field strength of 6 Tesla.

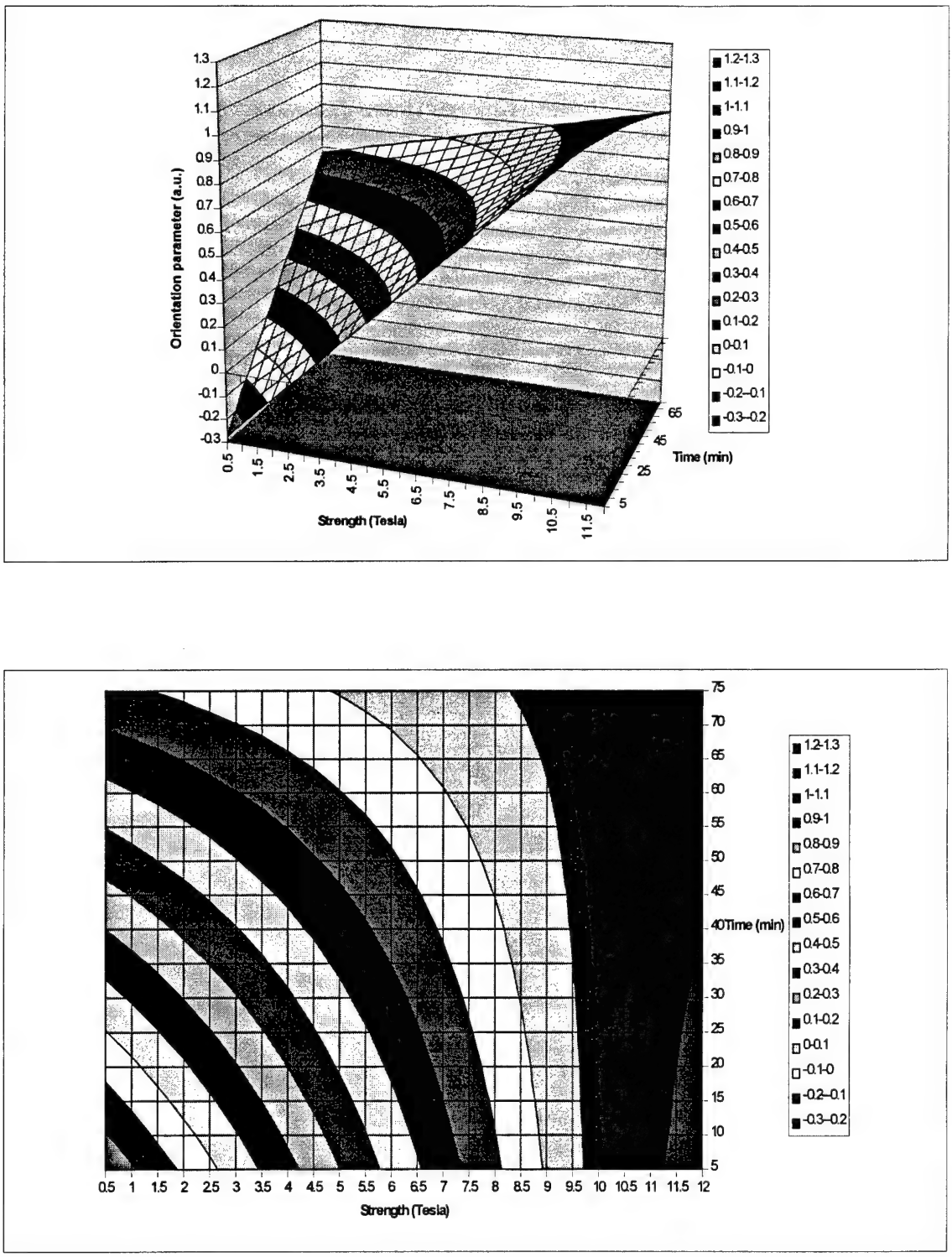

Figure 4-11. Surface and contour plots of the predicted orientation parameter response variable as a function of the field strength and time in the field for a constant B-staging time of 90 minutes.

plot predicts a maximum orientation parameter of 1.3, which is essentially 1. As expected the model predicts an increasing orientation parameter for increasing field strength and increasing time. However, as the last plot showed a decrease in the orientation parameter is seen at high field strengths (>11.5 Tesla) and high times (>45 minutes). Again, this may be due to disruption in the orientation as domains crosslink near the gel point before vitrification.

The orientation parameter results obtained for the samples from the optimization portion of this study are listed in table 4-5. The input variables were obtained from the optimization function in the software by entering the desired (predicted) orientation parameters and allowing the software to calculate their values. The first sample represent the maximum orientation parameter values given by the model. The value of the orientation parameter for last three samples are all within the 95% confidence limits of

Table 4-5. Orientation parameter responses from the optimization.

Time in field (min)	Field strength (Tesla)	B-staging time (min)	Predicted orientation parameter	Experimental orientation parameter
5	12	8.4	1.48	0.5714
40	10	90	0.95	0.8859
40	9.4	90	0.90	0.9221
40	8.8	90	0.85	0.9196

$\pm$ 0.2378, model error, given by the optimization function. The first sample is well outside these limits. This may due to the fact that the model could not account for the upper and lower limits of 1 and -0.5 without being severly distorted.

The three samples that fall within the experimental error limits indicate a high degree of control over the orientation parameter using the model obtained from the data analysis. Again, their values are also very close to one another indicating the presence of some plateau value of the orientation parameter. This plateau could emerge as an effect of the size of the domains as discussed earlier in this chapter.

Nematic LC Attempts

The purpose of conducting a search for a crosslinking agent the cures with the DOMS resin to form a nematic liquid crystalline order is to determine if a nematic phase may favor orientation in the magnetic field. Nematic phases possess one less degree of order, positional order, than smectics. They may, therefore, orient easier in the magnetic field due to less constraints on the ordering. Easier ordering may lead to lower field strengths and less processing time and possibly even higher degrees of orientation.

The search in this study focused mainly on finding crosslinking agents with similar reactivities to that of the sulfanilamide molecule so as to give a straight up comparison of the two systems and their orientation. There are many amines available, but the ones chosen here were determined to potentially have a similar reactivity to that of the SAA.

The first attempt at producing a cured sample with nematic liquid crystalline order with the benzenesulfonamide (BSA) failed. None of the BSA-SAA/DOMS formulations worked to produce a material with liaqiud crystalline order. The system was formulated and cured under the same conditions as the DOMS-SAA resin system. A possible explanation for this behavior is that the system is thermotropic and the cure at 150°C

falls within the temperature region in which the isotropic phase is stable. Another possible explanation for the structure of the material is that the phenyl side-group that is generate from the reaction acts as a bulky side-group large enough to disrupt any possibility of liquid crystalline order in the network. This result is consistent with Liu et al. who also found no liquid crystalline structure present for the DOMS-BSA system.

The attempt using 1, 3-benzenedisulfonamide as the crosslinking agent also failed. Again the cure temperature of 150°C may fell within the temperature range in which the isotropic phase is most stable. However, a more probable explanation is the fact that the molecule is kinked to the point in which disrupts any possibility of liquid crystalline order. This is consistent with results by Carfagna et al. who found that for their particular system kinked crosslinking agents produced isotropic samples while more linear crosslinking agents would produce samples with liquid crystalline order (Car94a).

Synthesis of the 4, 4'-methylenebis(benzenedisulfonamide) failed as determined by NMR and elemental analysis. This may have been due, in part, to the air sensitive nature of the starting material, 4, 4'-methylenebis(benzenedisulfonyl chloride). The material may have hydrolyzed prior to reaction with the concentrated NH_4OH giving the reaction no chance to take place. Because of this possibility, the synthesis of the 4, 4'-biphenyldisulfonamide (BPDSA) included a chlorination step to ensure the material would react with the NH_4OH.

Synthesis of the BPDSA was confirmed by NMR. However, the formulation and cure still did not produce a liquid crystalline structure as seen by the glassy appearance,

to the eye, of the cured material. This may due to a thermotropic nature of the system in which the cure at 150°C falls within the isotropic phase temperature stability range.

Finally, for the phenylenediamine (PD) system it was found that the DOMS-PD system did in fact cure with cure with a liquid crystalline structure at 150°C. However, from x-ray analysis it was found that this structure was with smectic ordering. For the system containing methylenedianiline the DOMS-MDA cured without liquid crystalline order at 150°C.

However, it has been reported by Barclay et al. that the DOMS-MDA system will, in fact, cure with nematic liquid crystalline structure when heated to 115°C to melt the material, then lowered to 80°C and cured for 5 hours, and then raised to 140°C and cured for 10 hours (Bar92a). This lower cure temperature allows the liquid crystalline domains to form before crosslinking occurs. This cure cycle was accomplished and it was found that the cured sample possessed a highly mottled appearance resembling a solid suspended in a glassy matrix. Under optical microscopy using the hot stage it was observed that the uncured material seemed to undergo two distinct meltings, which was most likely the melting of the MDA at 90°C and then melting of the DOMS resin at a temperature of about 125°C. Upon cooling to 80°C needle-like crystals formed and grew until they filled the viewing area. The material was allowed to cure in the microscope until the gel point was reached, as determined with a rheometer, at around 60 minutes. X-ray diffraction analysis using a powder diffractometer revealed a broad diffraction peak at $2\theta = 20°$, which is indicative of a nematic structure, but can also be easily confused with

isotropic scattering. Therefore, it is difficult to conclude that the material does, in fact, cure with nematic liquid crystalline structure given the conflicting data from optical microscopy and x-ray diffraction.

Of particular note in both cases of the DOMS-PD and DOMS-MDA systems, as the mixtures aged either at room temperature or at freezer temperature both changed colors over a period of time. The DOMS-PD mixture changed from a cream color to a bluish tinted color. The DOMS-MDA mixture turned from a cream color to a greenish tinted color. Due to the high reactivity of the system it may be that both systems have a diffusion controlled room temperature cure capability. The formation of very small domains may be the cause of the color change. However, it was also found that the phenylene diamine also changed colors even more rapidly under the intense microscope light, implying that a photopolymerization reaction may be taking place since the intense microscope light caused the color change more rapidly than daylight.

CHAPTER 5
CONCLUSIONS

The preliminary work accomplished in this study showed that the field strength does have an effect on the orientation process as expected. Significant orientation can be obtained for non B-staged material even at low field strengths of 3 Tesla. It was also demonstrated that the field strength affect the mechanical properties of the material by increasing the dynamic storage modulus by almost 60% with the application of a magnetic field at 15 Tesla. It is also apparent that the packing efficiency of the material is affected by the orientation as shown by the large increase in the apparent activation energy for the glass-rubber transition.

It was also demonstrated that the amount of B-staging had an affect on the orientation process. Rheology experiments showed that the viscosity of the material at the gel point increased drastically at 120 minutes B-staging time. This increased viscosity was seen to hinder the orientation of the material at low field strengths, <9 Tesla. Fortunately, this trend did not continue for field strengths >9 Tesla as orientation parameters comparable to the non B-staged material were obtained. It is apparent that the increased viscosity becomes overwhelmed at high field strengths and significant orientation occurs.

Results from the statistical experimental design to probe the effects of the process variables confirmed that the amount of B-staging and the filed strength are large effectors

of the orientation process. The model constructed fit the orientation parameter response data with an R^2 value of 0.8577, which is a very good fit for this type of model. The experimental error percent was also shown to be very good at only 5.82% variability in the sample response due to experimental error.

The optimization portion of the study revealed that the model predicts the input values for a given orientation parameter well. Three of the four samples tested fell within the 95% confidence limits of the model. One possible drawback of this particular model is that it does not account for the upper and lower theoretical limits of 1 and -0.5 for the orientation parameter. This may lead to false predictions in certain arears of the model. The model does, however, predict the values of the input variables well within the orientation parameter limits.

Unfortunately, the attempts to produce a system that cures with nematic liquid crystalline order all failed. It may be that this particular monomer will only cure with smectic liquid crystalline order, or that at the temperatures it was cured at lie within the smectic liquid crystalline phase temperature stability range. Curing agents may exist that will cure with DOMS with nematic liquid crystalline order but with very different curing kinetics, which does not offer a good comparison of the orientation characteristic with the smectic system.

CHAPTER 6
FUTURE WORKS

A logical next step in this research is to further characterize the mechanical properties of this material. As seen from the DMS work the modulus seems to increase, but to what extent it can still needs to be determine. It has been found that high degrees of conversion for many epoxies lead to an anomalous behavior in the material in that the modulus, as well as other properties, actually decreases at high degrees of conversion (Enn83, Ven95a, Ven95b). This material being liquid crystalline already has a high degree of conversion. The question needs to be answered of whether this is working to the detriment of the material.

A further probe into the effects of the amount of B-staging also needs to be done. It was seen that the B-staging does affect the orientation process both negatively and positively. If the exact source of this effect can be identified modifications may be made to the molecular architecture or the process to make this process a reality for mass production of structurally sound parts. Studies on the characteristic relaxation time, τ, as a function of time would be of great help in further describing the effects of B-staging on the orientation process.

Another obvious next step in continuing this research is to try this process in some real-world applications. Even a high degree of control over the process may not

lead to the desired results in some applications. For example, the complicated geometries of some parts may not be conducive to this process because orientation in one direction may severely weaken the part at a critical point. The techniques used in the fabrication fiber composites may work against the orientation process, for example pultrusion of fiber composites. The mechanical flow direction parallel to the fiber direction may disrupt any orientation obtained in the matrix perpendicular to the pulling direction. This is not to say that this process cannot be used, but modifications to existing techniques may have to be made to incorporate this process into the overall fabrication process.

The search needs to continue for materials that melt into liquid crystalline phases to possibly reduce the need for B-staging and reduce the time required to obtain significant orientation. The search also needs to continue for materials that cure in a nematic liquid crystalline phase. The possibility still remains that nematic liquid crystalline materials may be more favorable to orientation than smectic liquid crystalline materials.

Finally, other LCTs need to be investigated. Changing the molecular architecture, reactivity, or network formation process may have a profound effect on the ability of the material to 1) be oriented and 2) retain that orientation. There is much research going on currently with many different types of LCT materials including acrylates and methacrylates, maleimides and nadimides, acetylene, vinyl ethers, other glycidyls, and crosslinkable polyesters any of which may be ideal for processing in a magnetic field.

APPENDIX A
WAXS PATTERNS

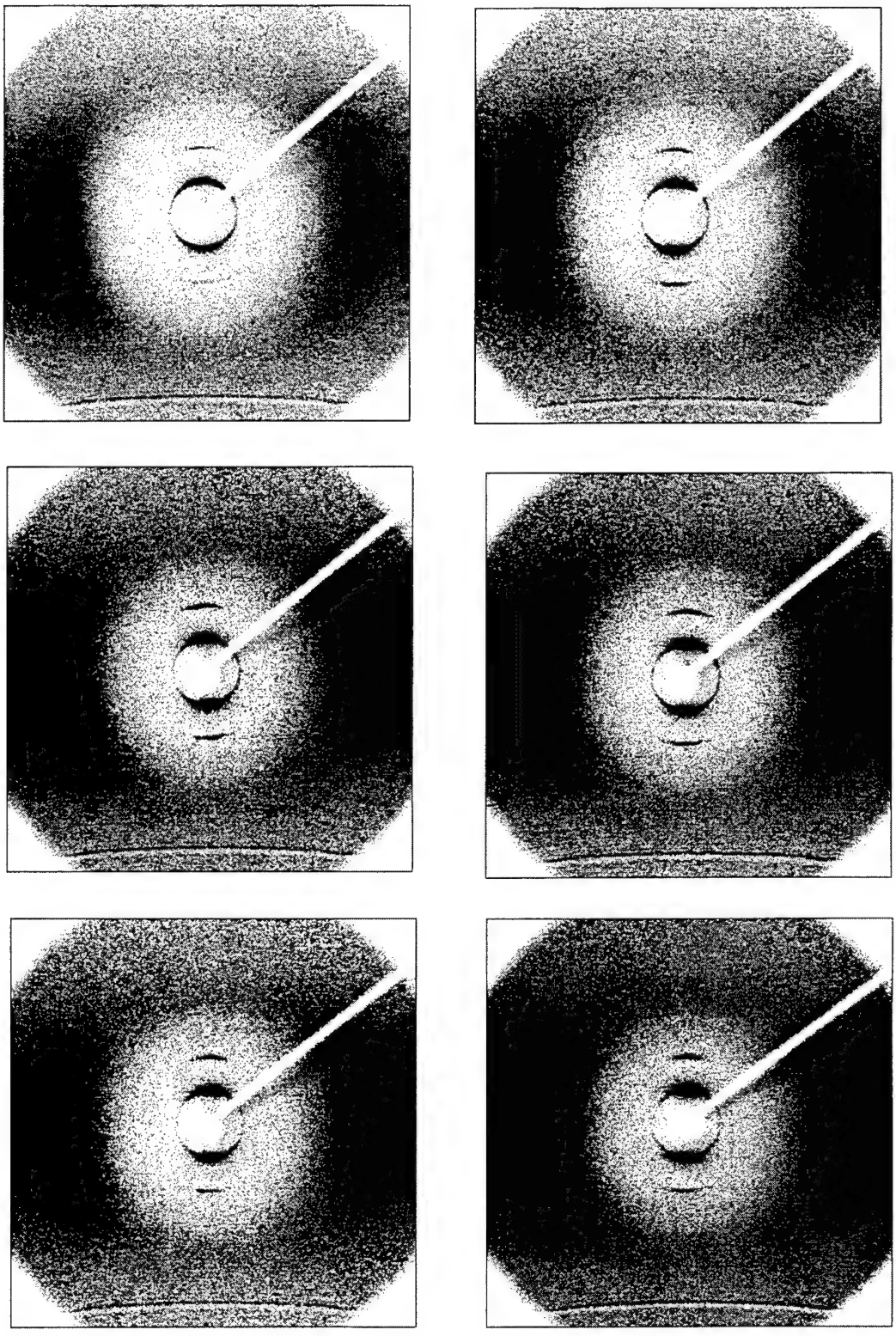

WAXS patterns for remaining 0 minute B-staged samples (by row left to right): 3 Tesla, 4.5 Tesla, 6 Tesla, 7.5 Tesla, 9 Tesla , and 15 Tesla.

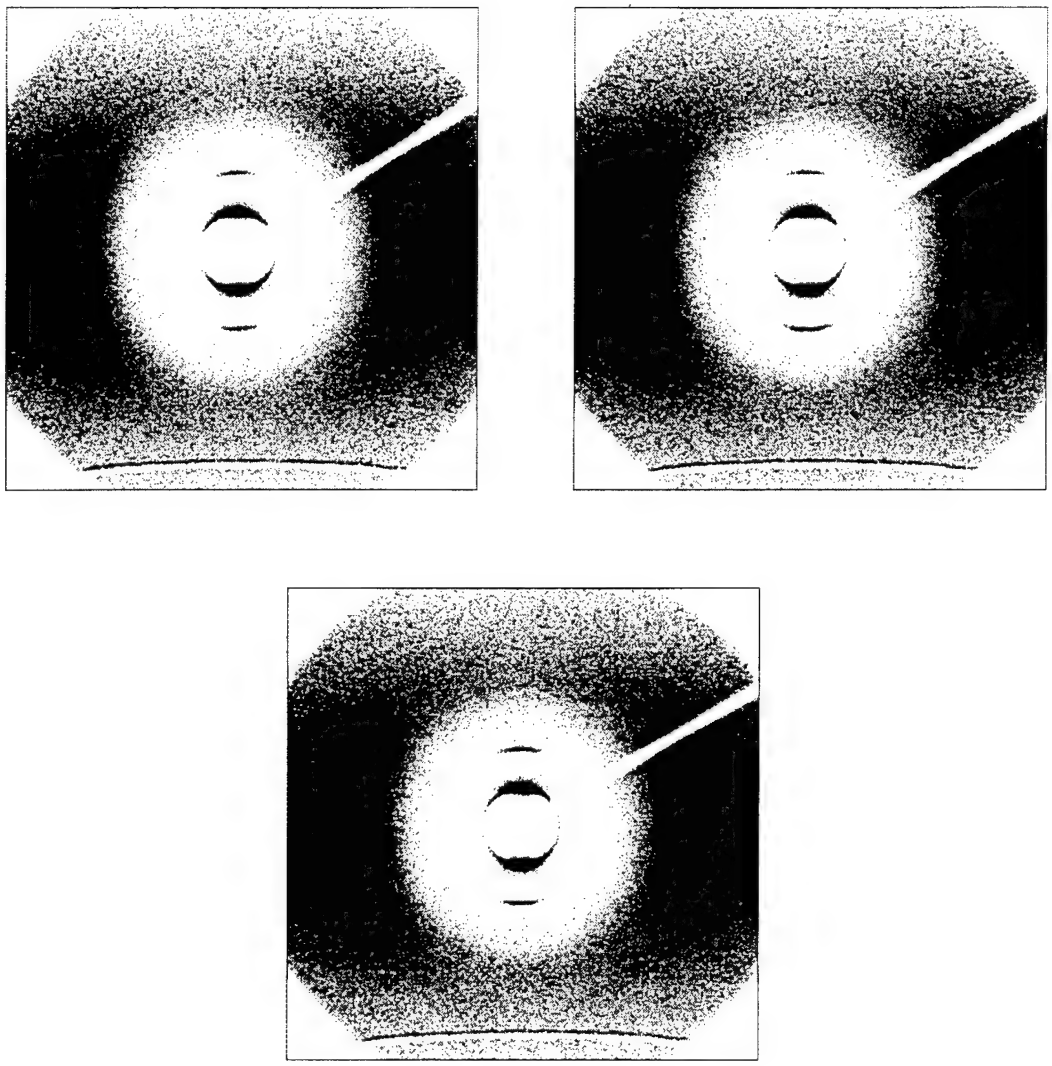

WAXS patterns for remaining 120 minute B-staged samples (clockwise from top left): 3 Tesla, 6 Tesla, and 9 Tesla.

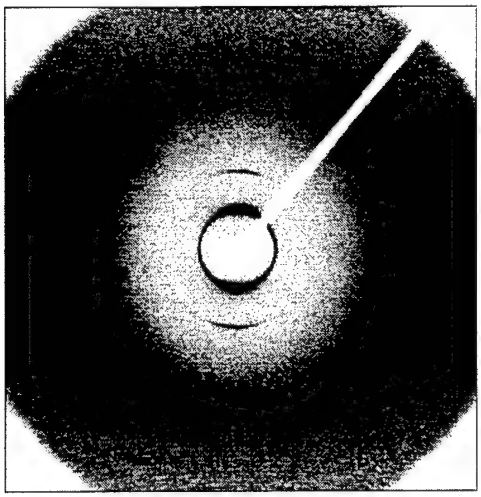

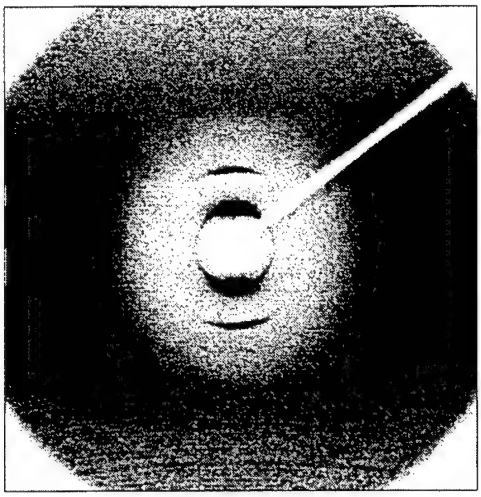

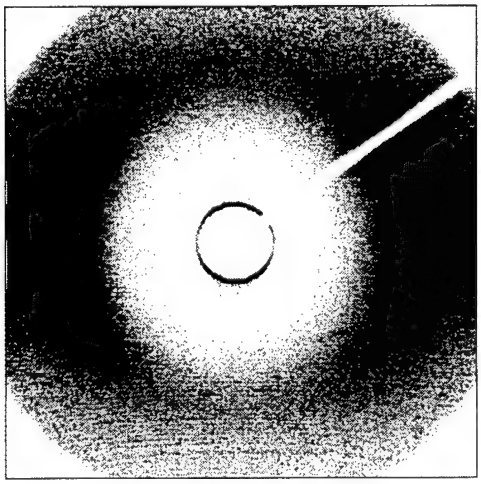

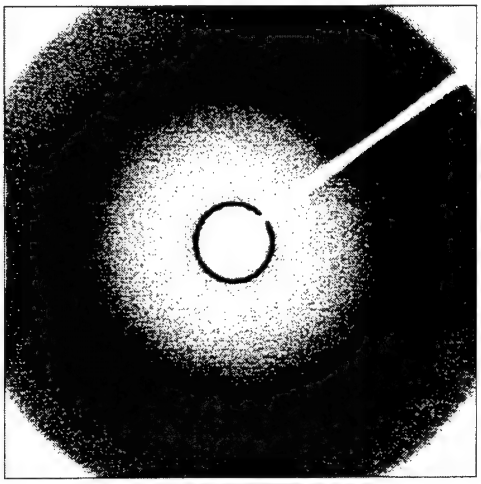

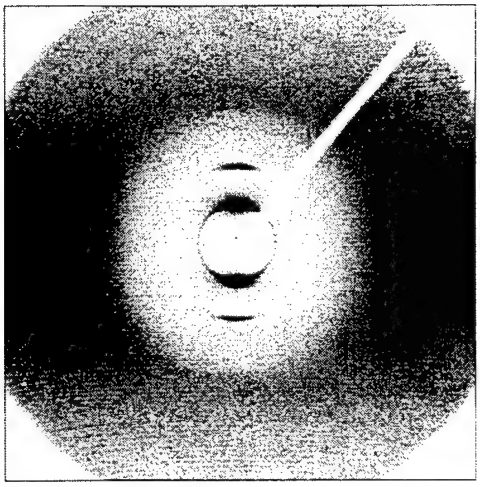

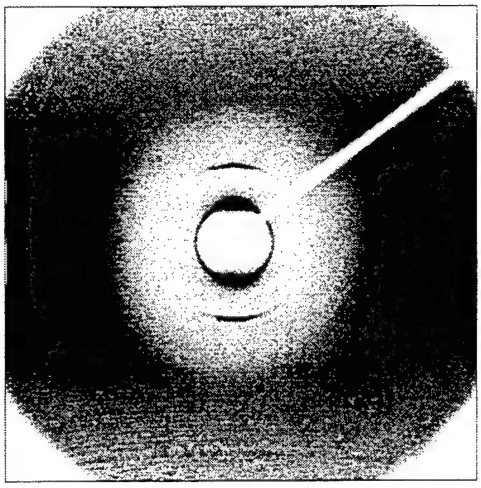

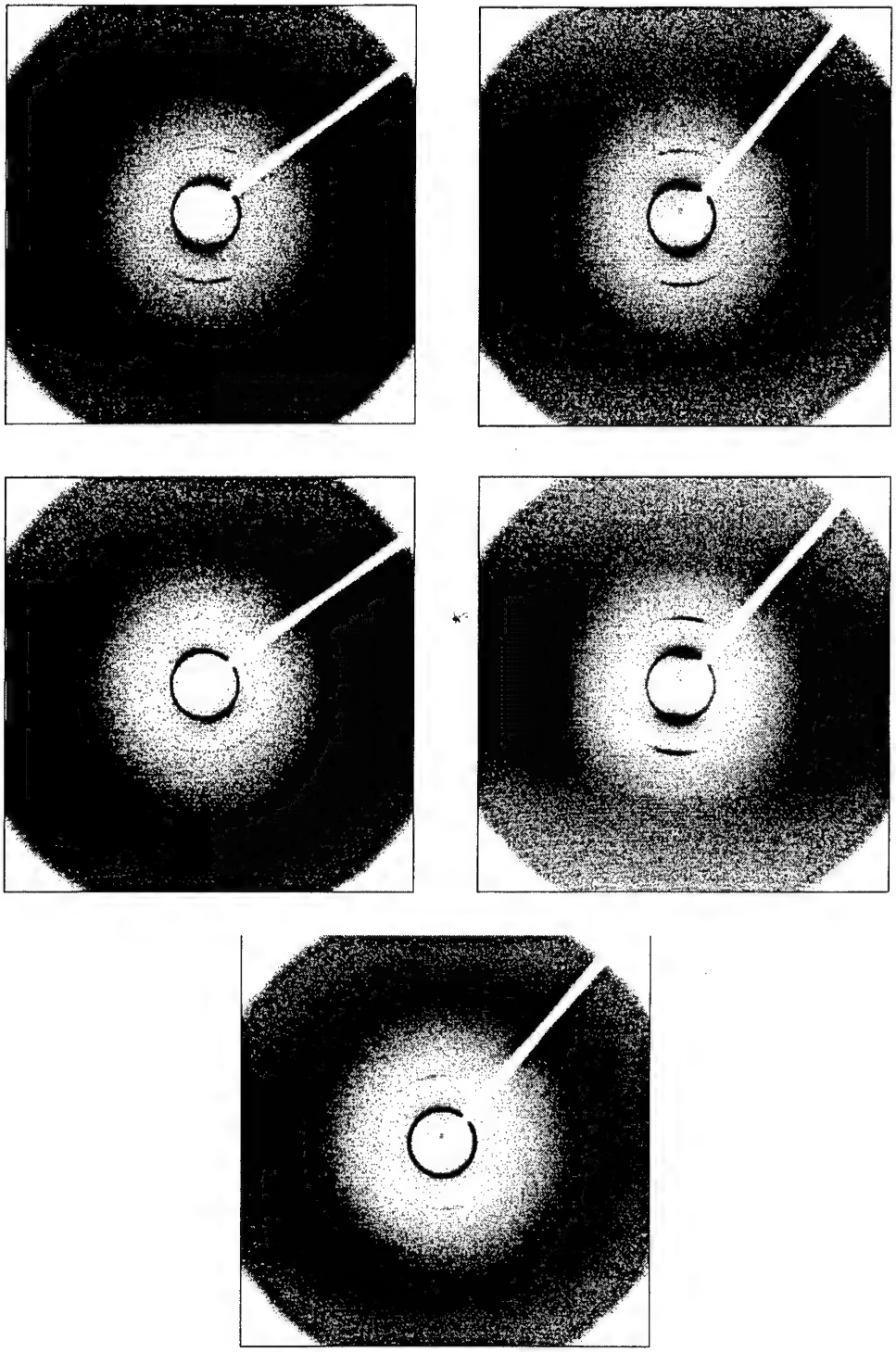

WAXS patterns for statistical design samples (by row left to right): Stat1, Stat2, Stat3, Stat4, Stat5, and Stat6.

APPENDIX B
TAN δ, DYNAMIC LOSS AND STORAGE MODULUS CURVES

Tan δ, dynamic loss and storage modulus curves for the 0 minute b-staged, 3 Tesla sample.

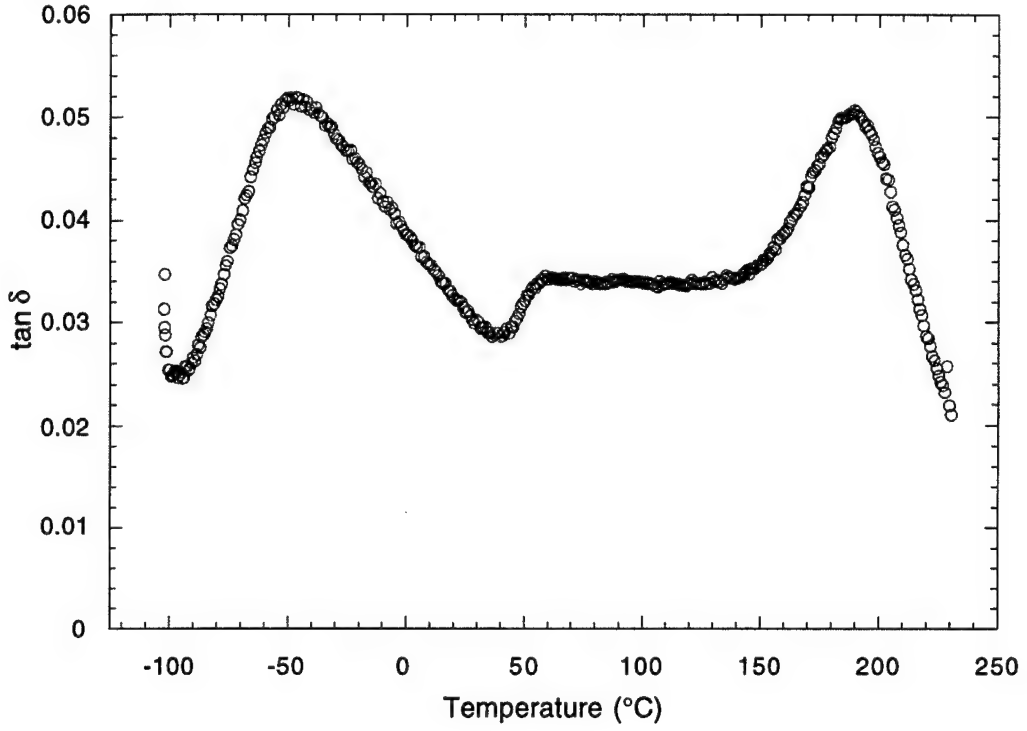

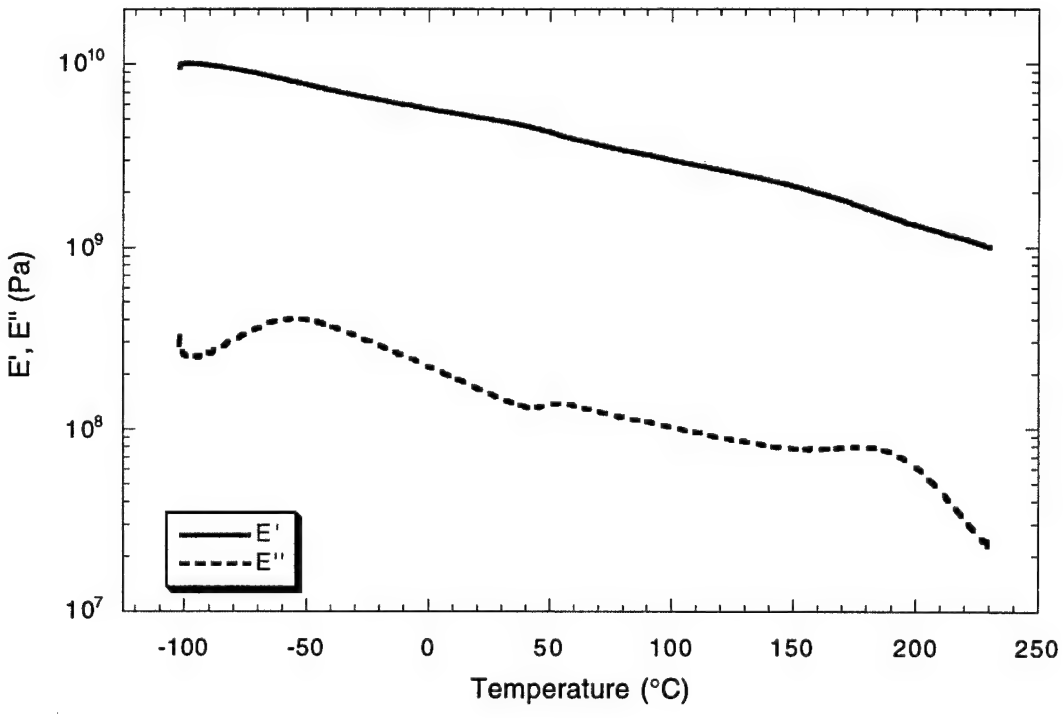

Tan δ, dynamic loss and storage modulus curves for the 0 minute b-staged, 3 Tesla replicate sample.

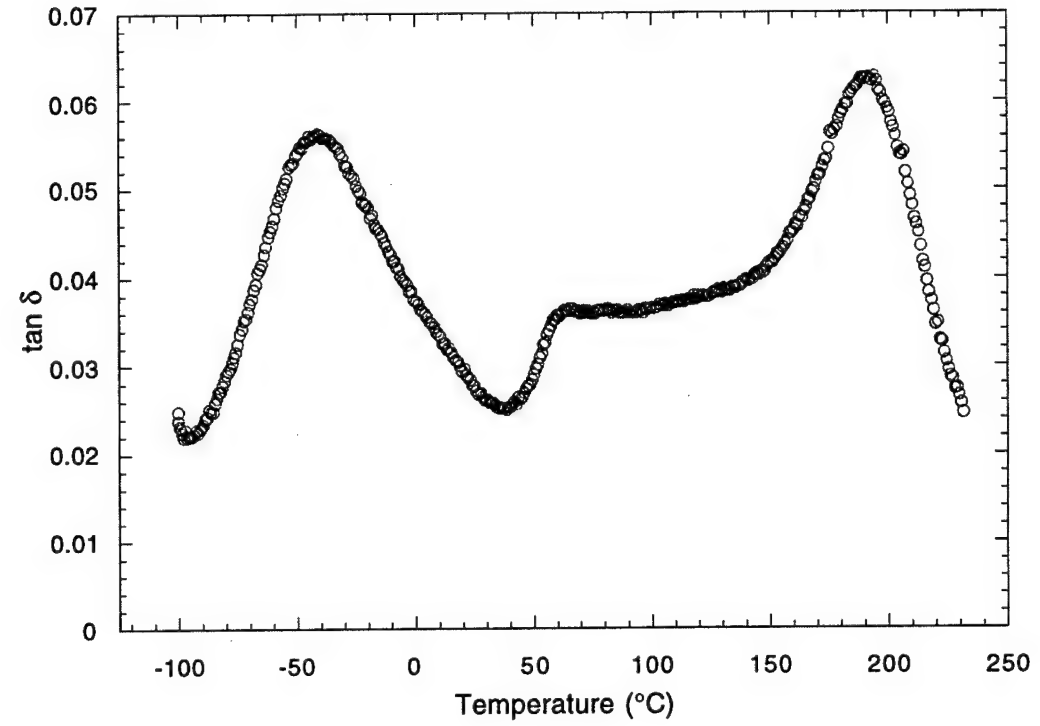

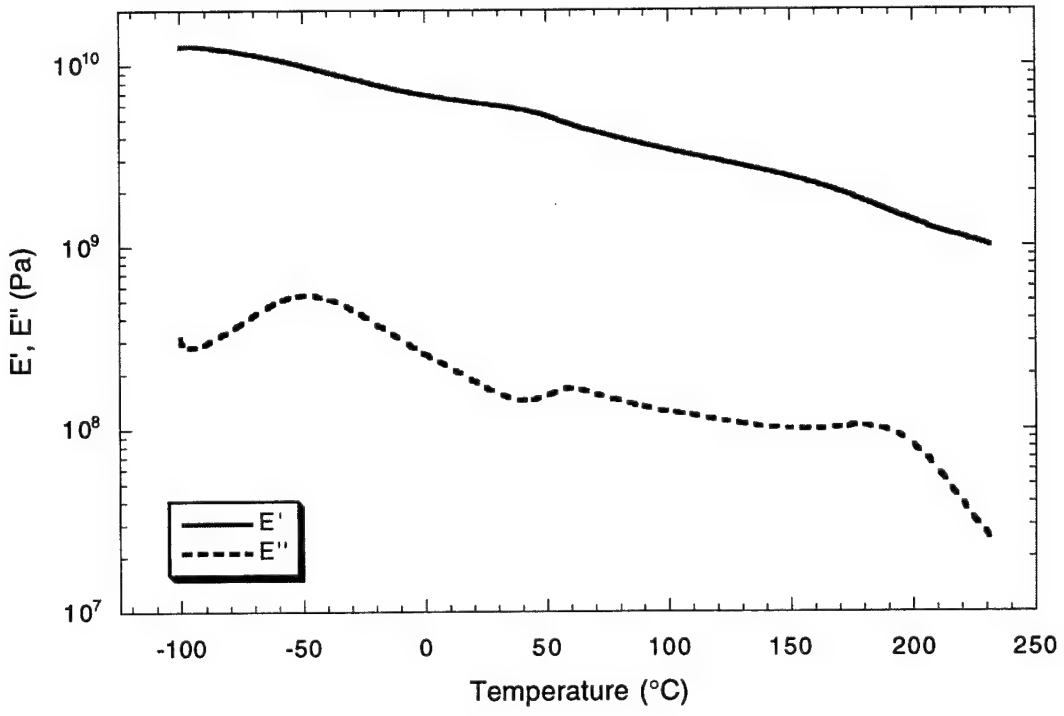

Tan δ, dynamic loss and storage modulus curves for the 0 minute b-staged, 4.5 Tesla sample.

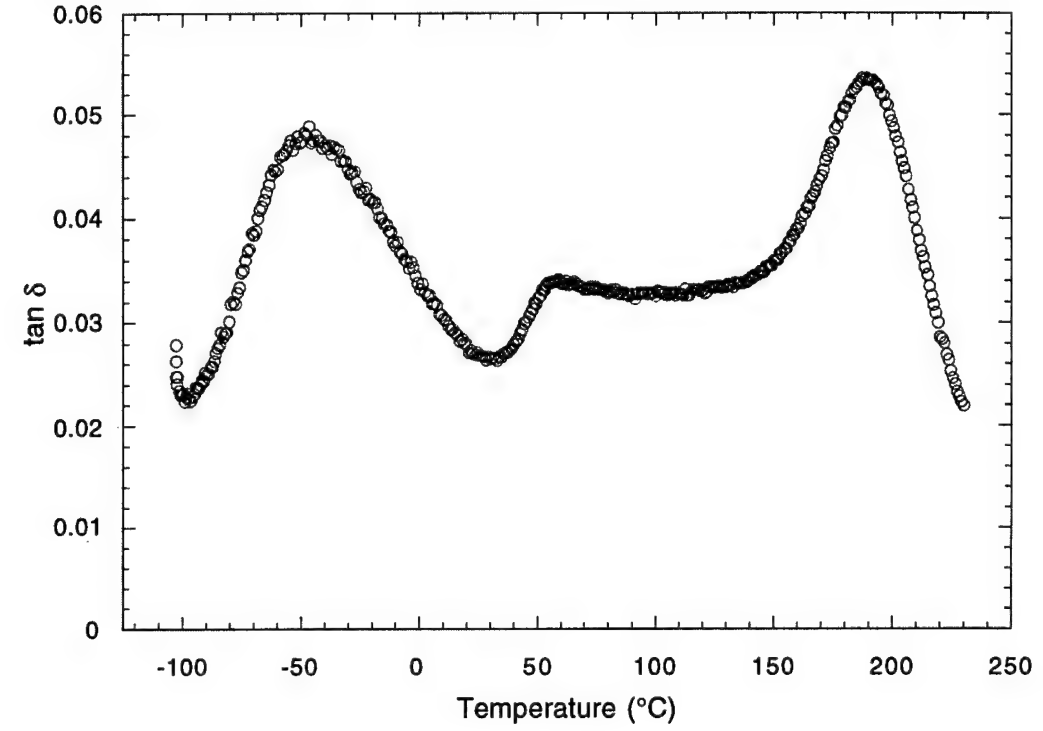

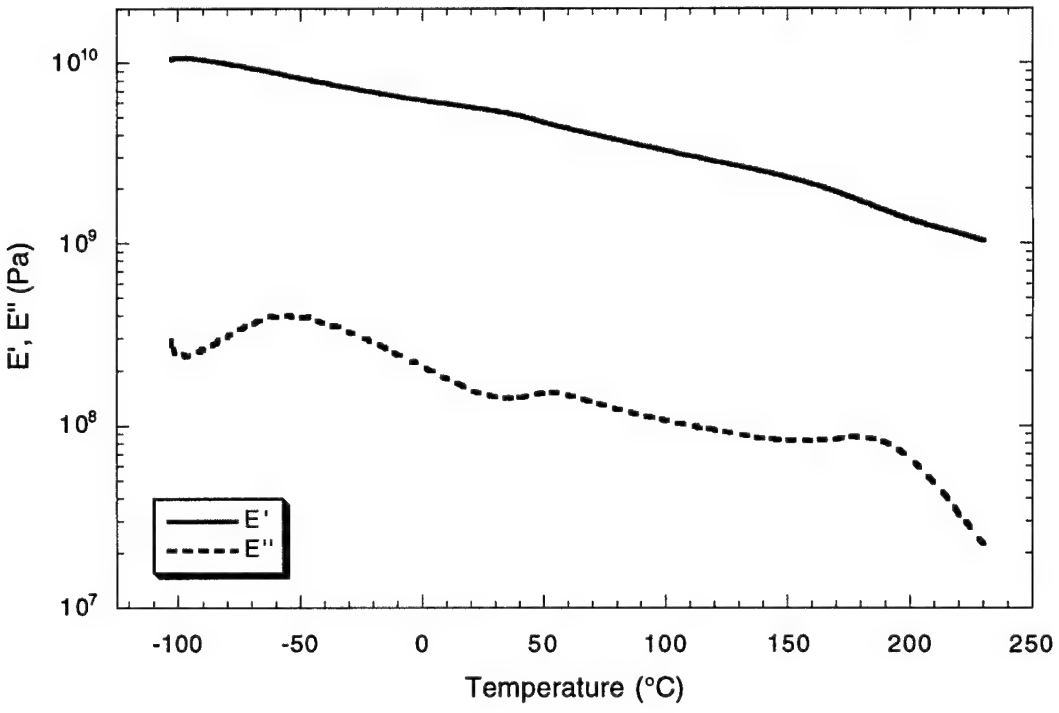

Tan δ, dynamic loss and storage modulus curves for the 0 minute b-staged, 6 Tesla sample.

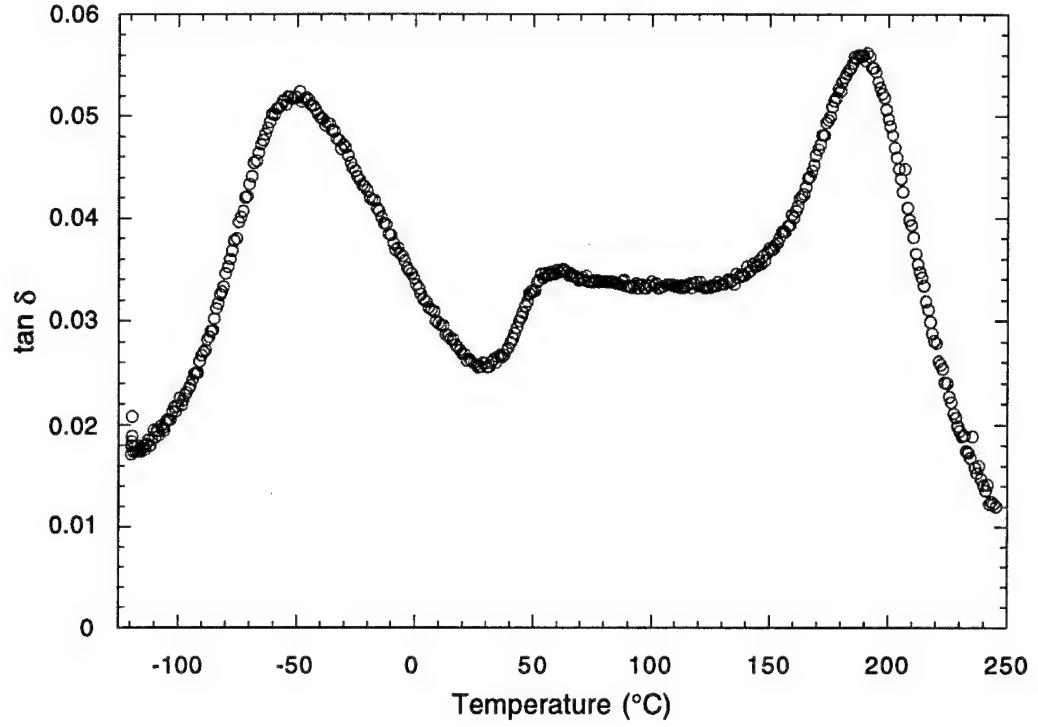

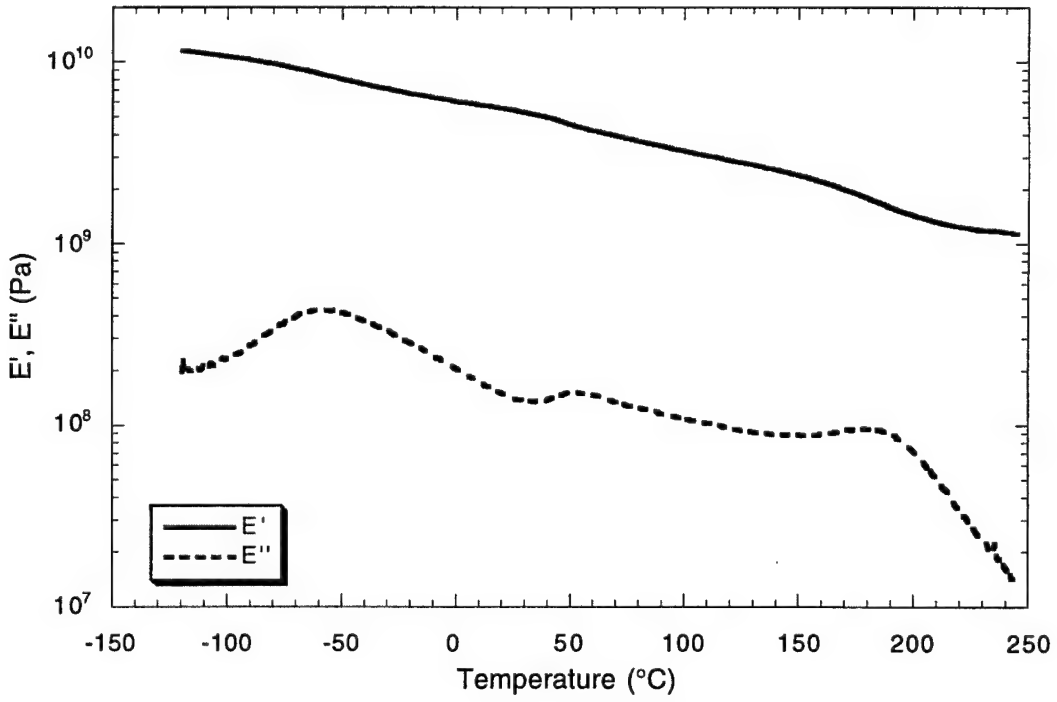

Tan δ, dynamic loss and storage modulus curves for the 0 minute b-staged, 6 Tesla replicate sample.

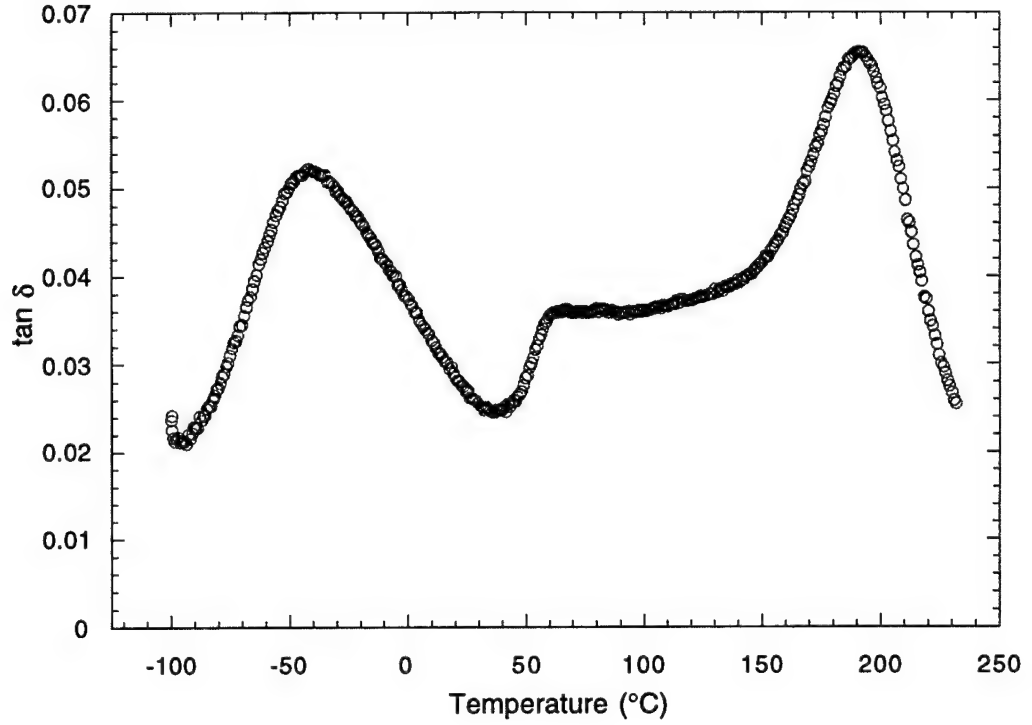

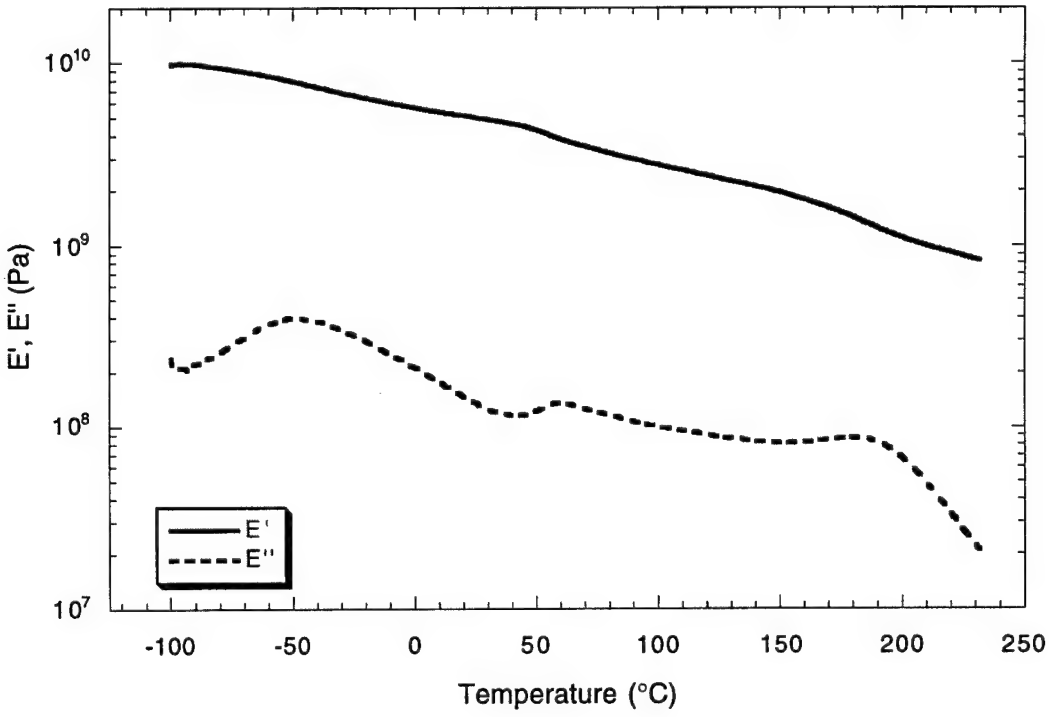

Tan δ, dynamic loss and storage modulus curves for the 0 minute b-staged, 7.5 Tesla sample.

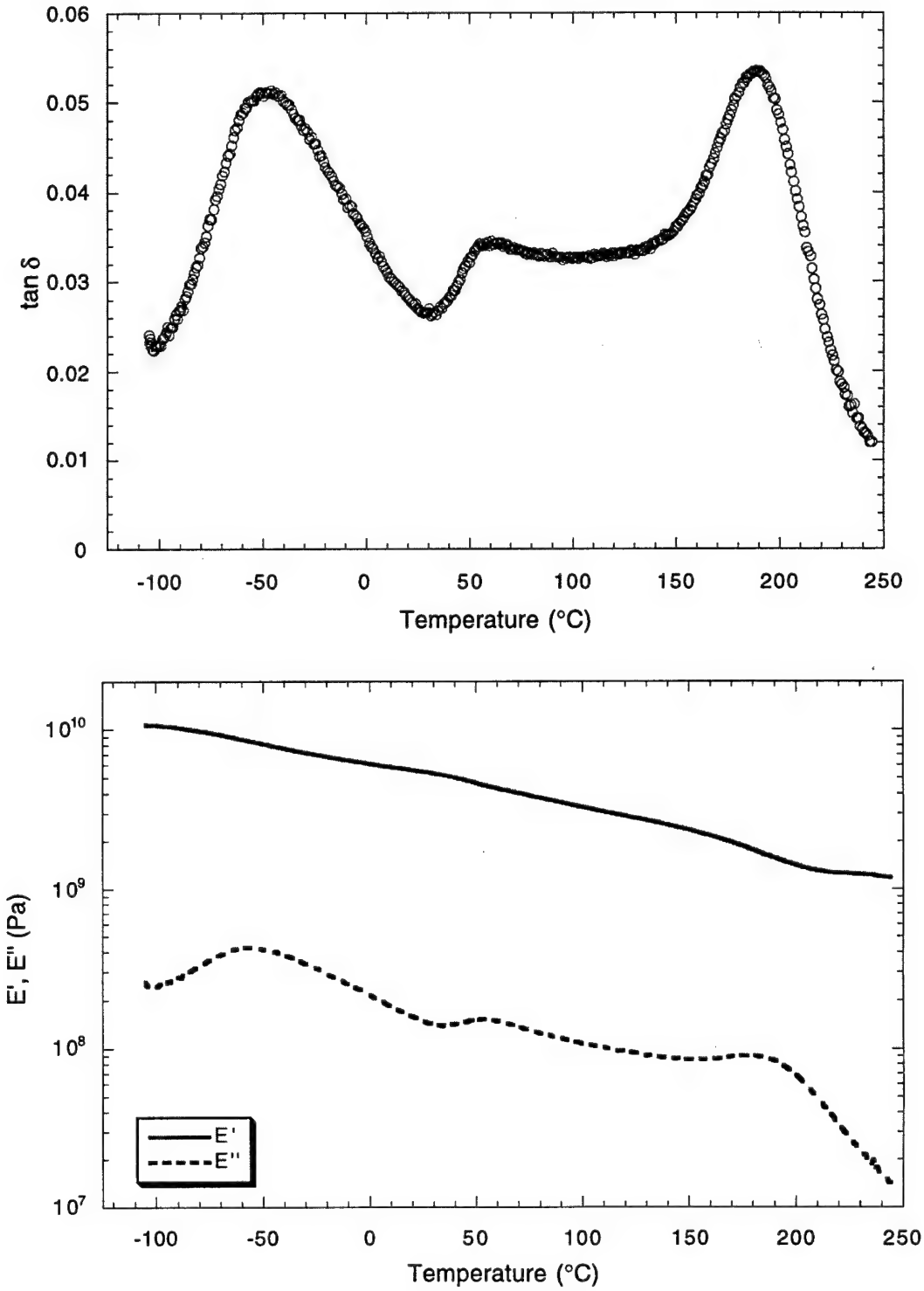

Tan δ, dynamic loss and storage modulus curves for the 0 minute b-staged, 9 Tesla sample.

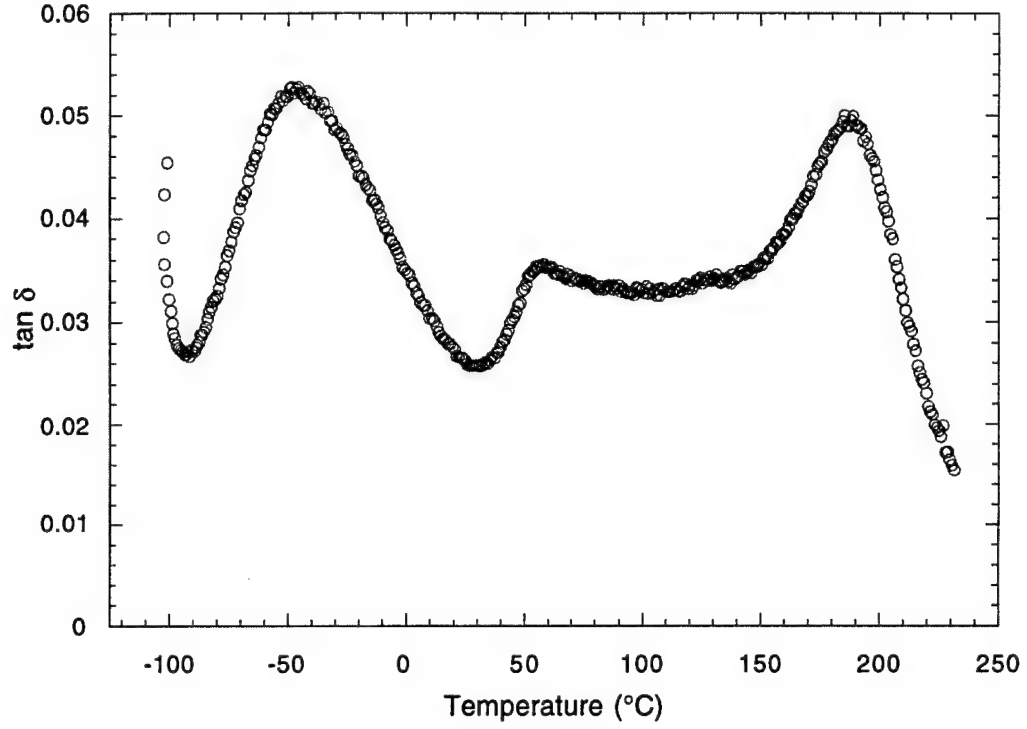

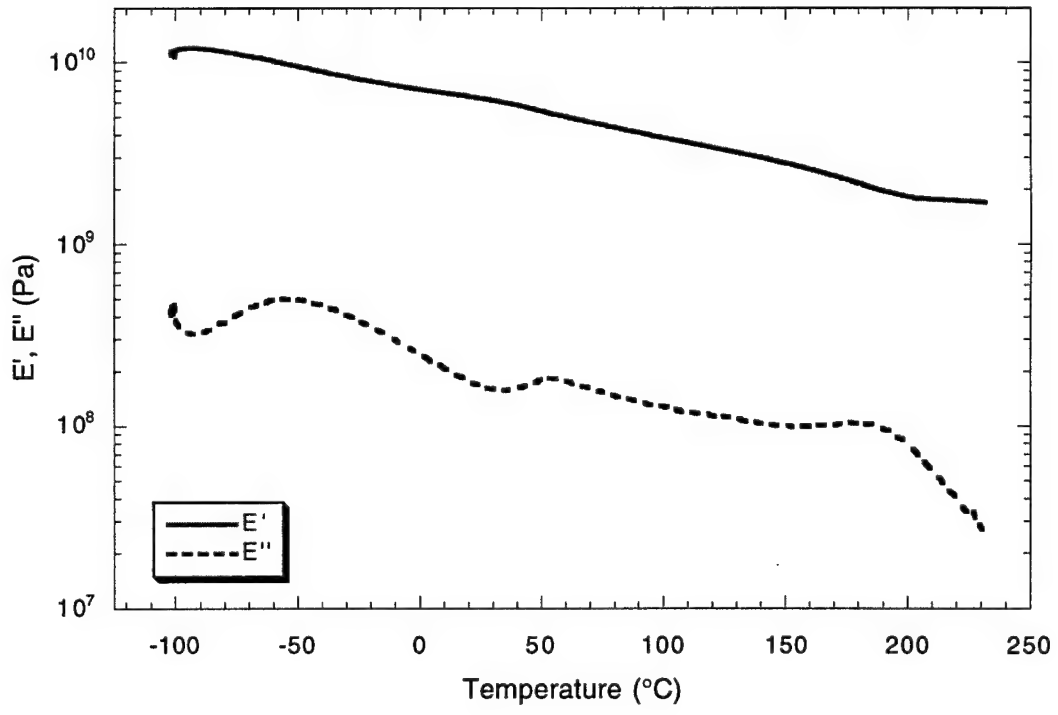

Tan δ, dynamic loss and storage modulus curves for the 0 minute b-staged, 9 Tesla replicate sample.

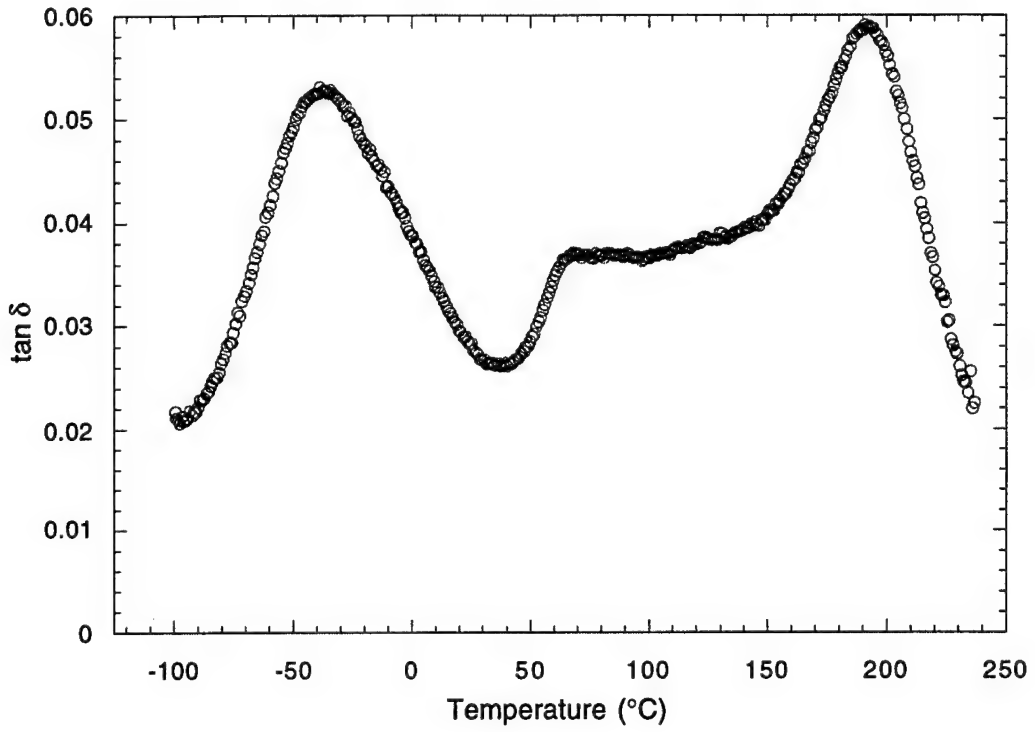

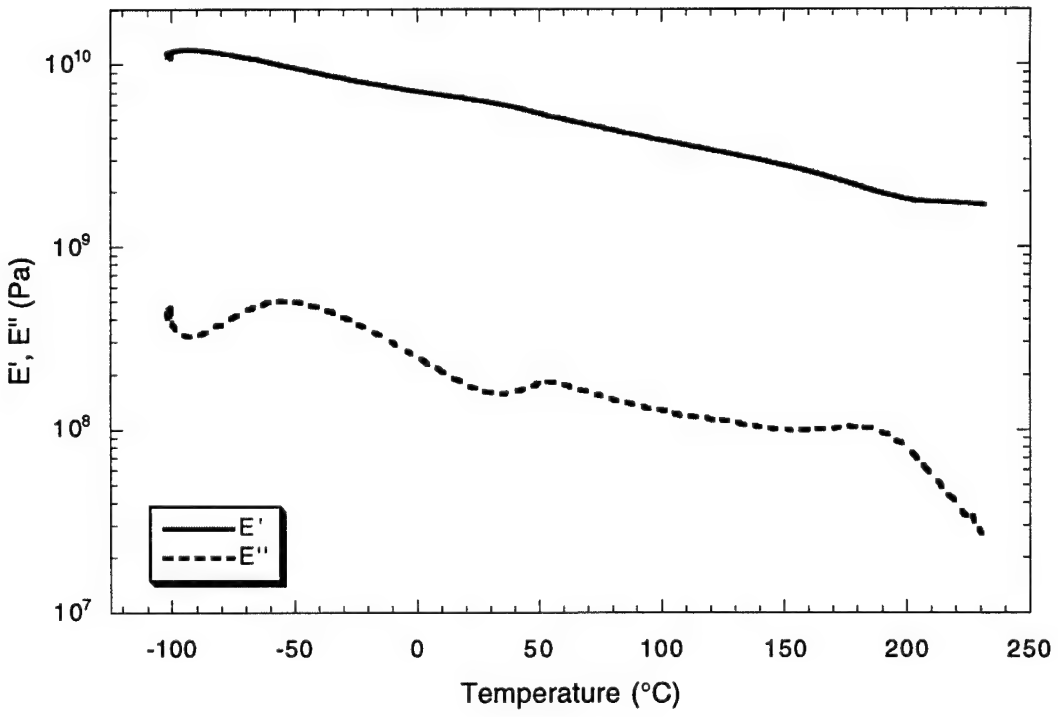

Tan δ, dynamic loss and storage modulus curves for the 0 minute b-staged, 15 Tesla sample.

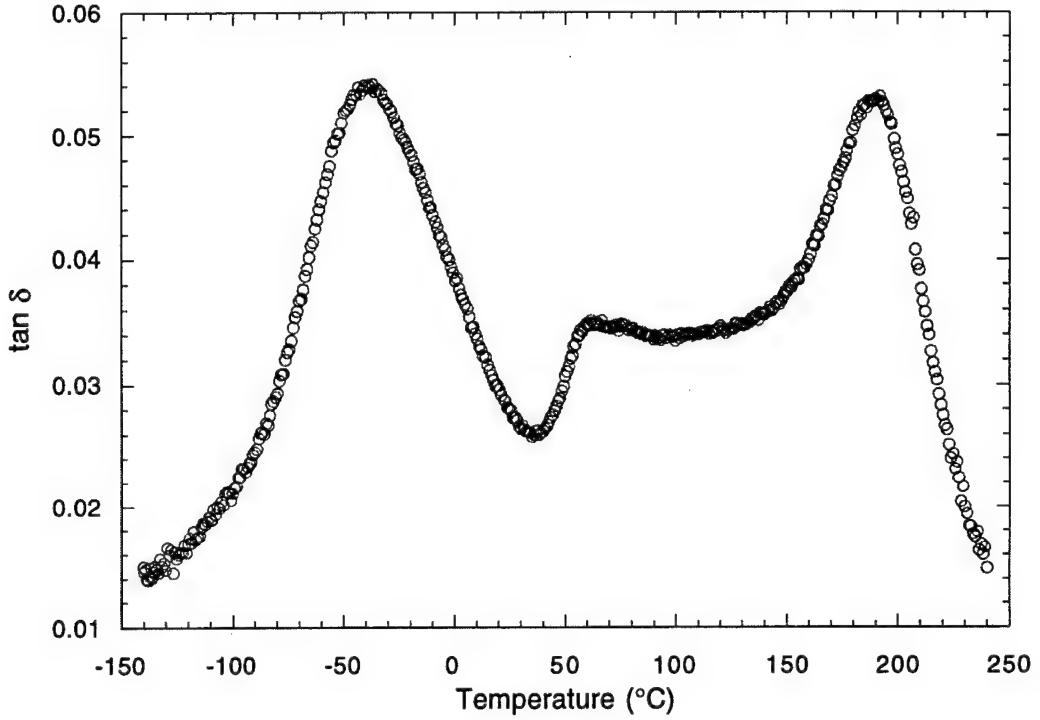

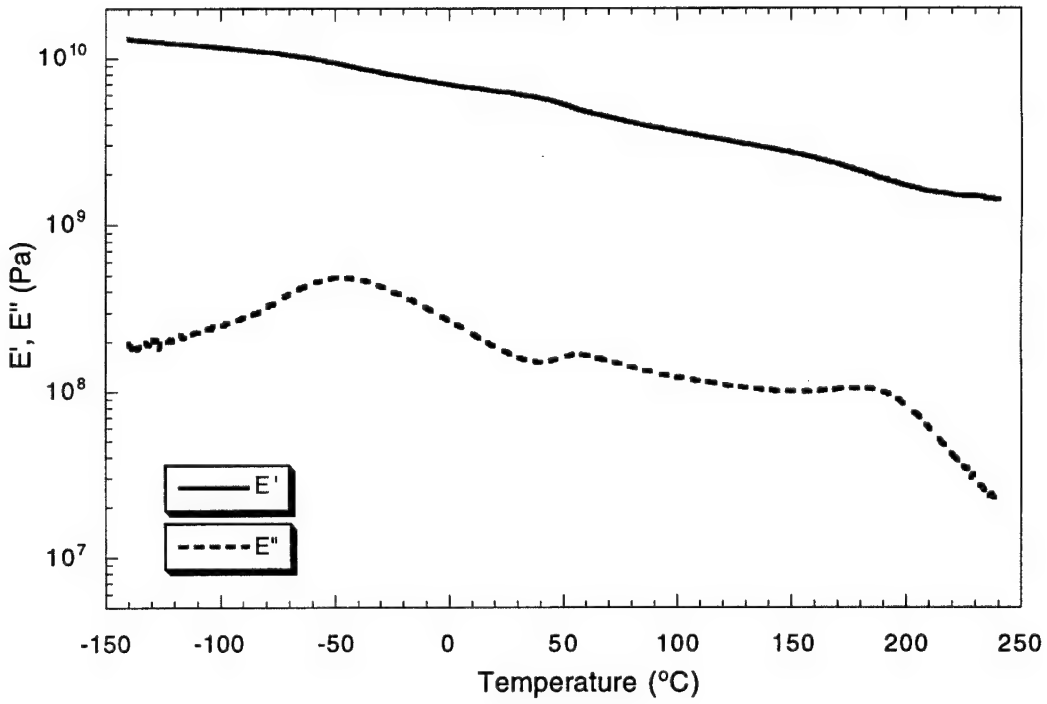

Tan δ, dynamic loss and storage modulus curves for the 120 minute b-staged, 3 Tesla sample.

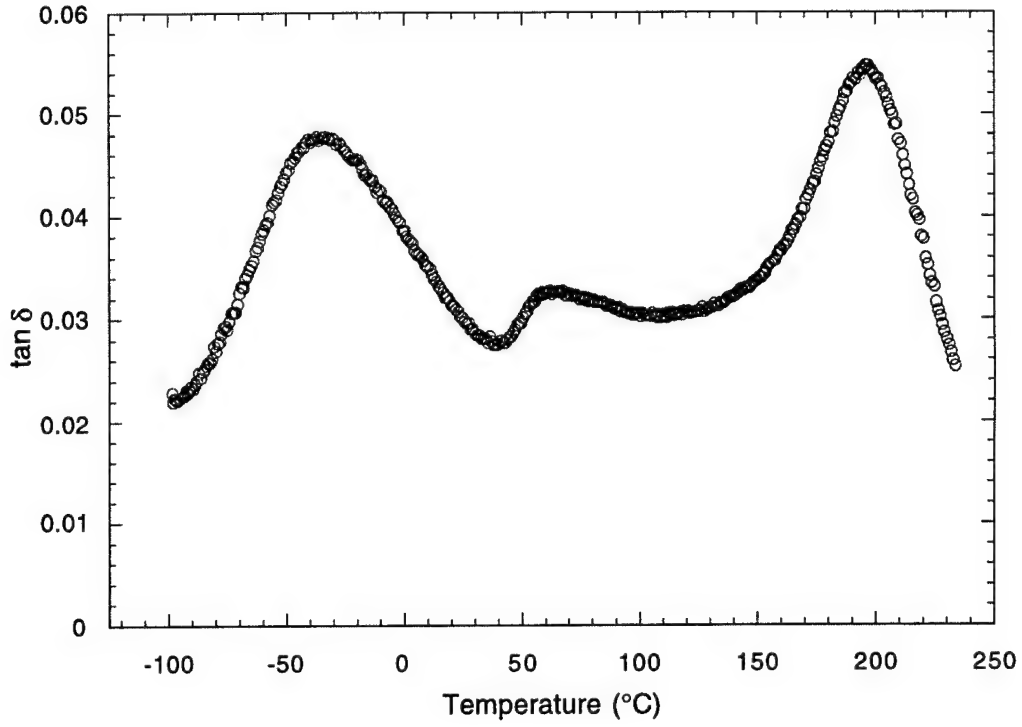

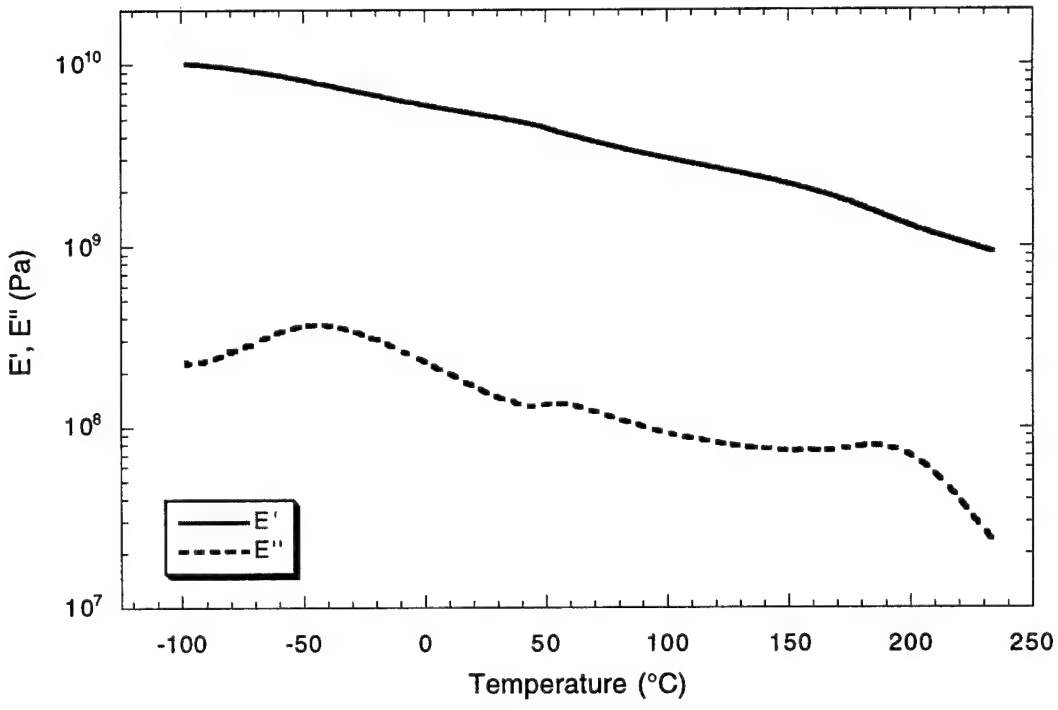

Tan δ, dynamic loss and storage modulus curves for the 120 minute b-staged, 6 Tesla sample.

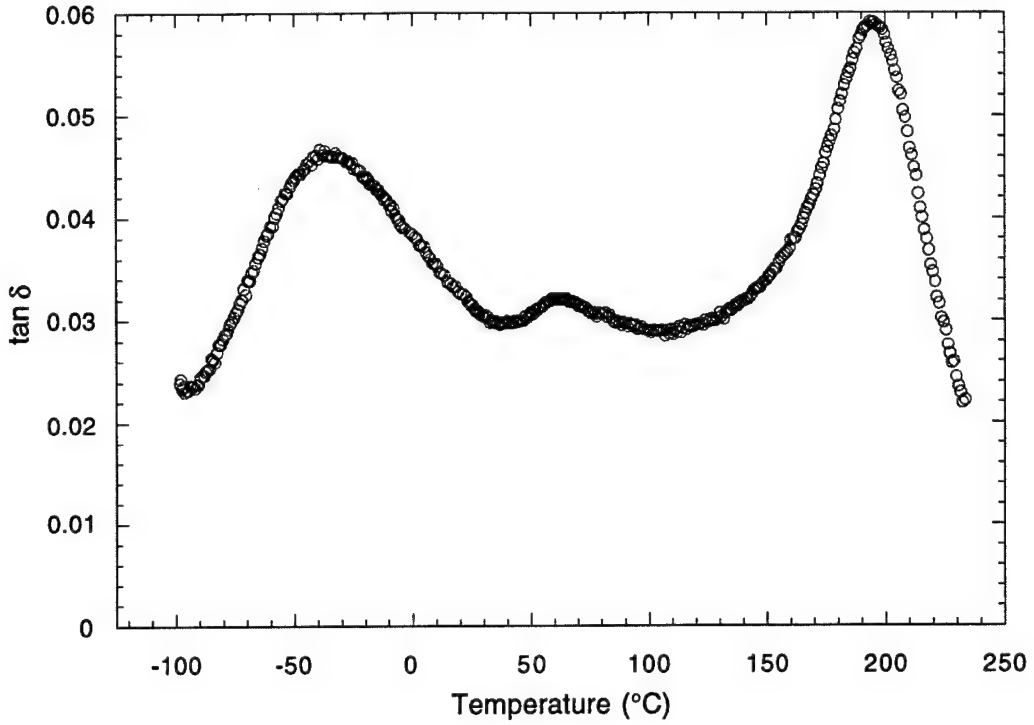

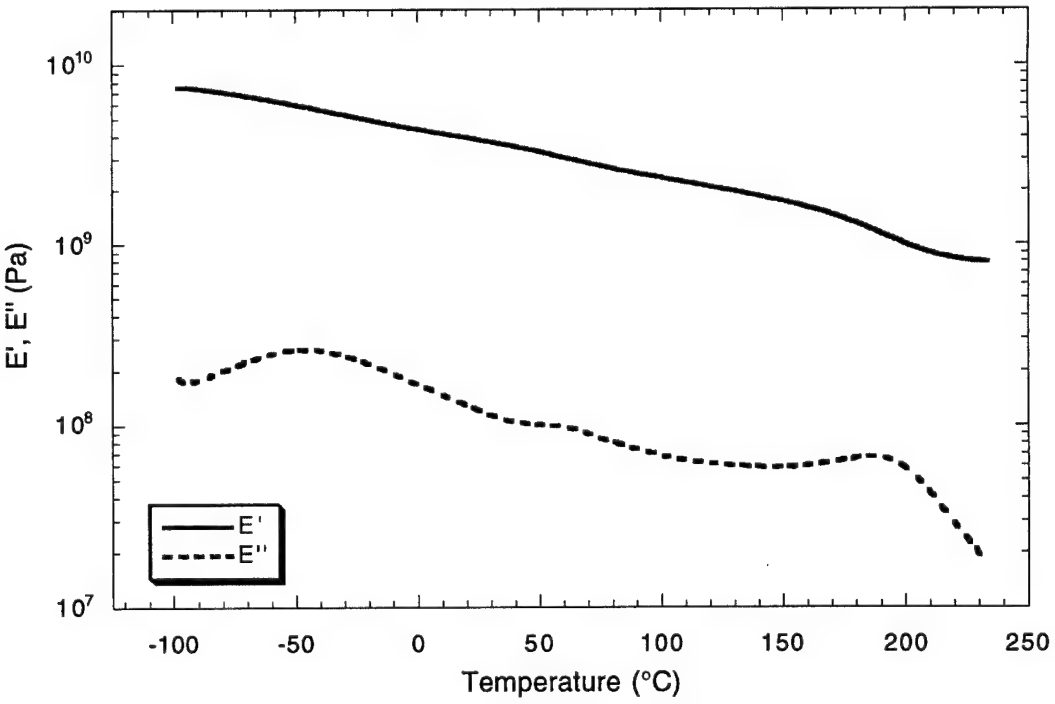

Tan δ, dynamic loss and storage modulus curves for the 120 minute b-staged, 9 Tesla sample.

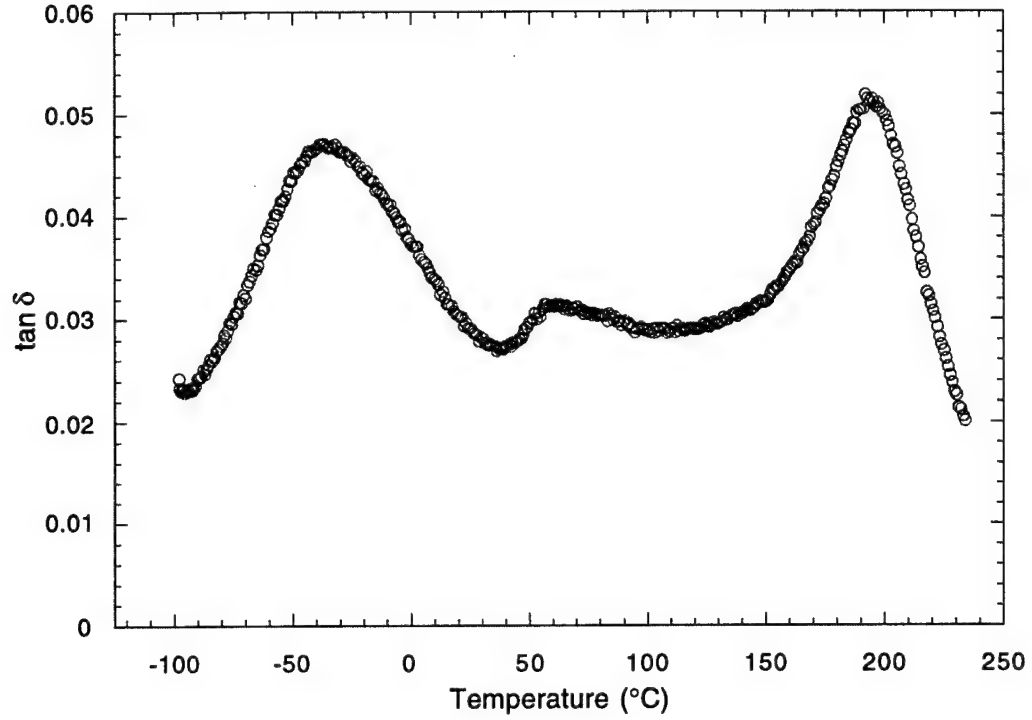

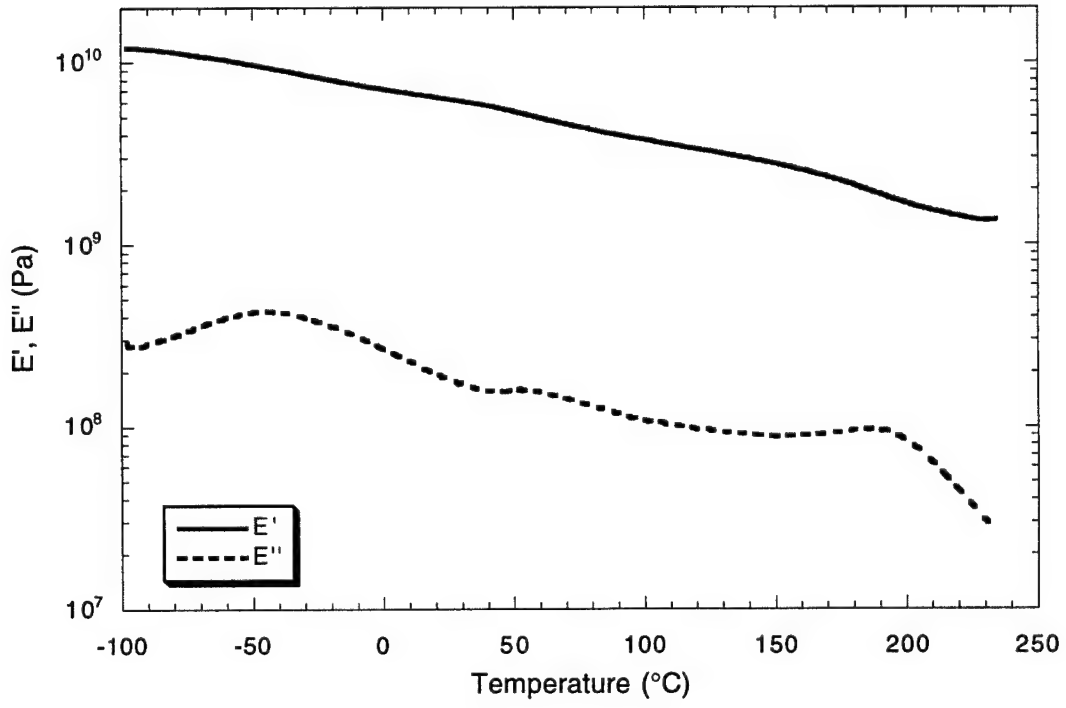

Tan δ, dynamic loss and storage modulus curves for the statistical experimental design sample #1.

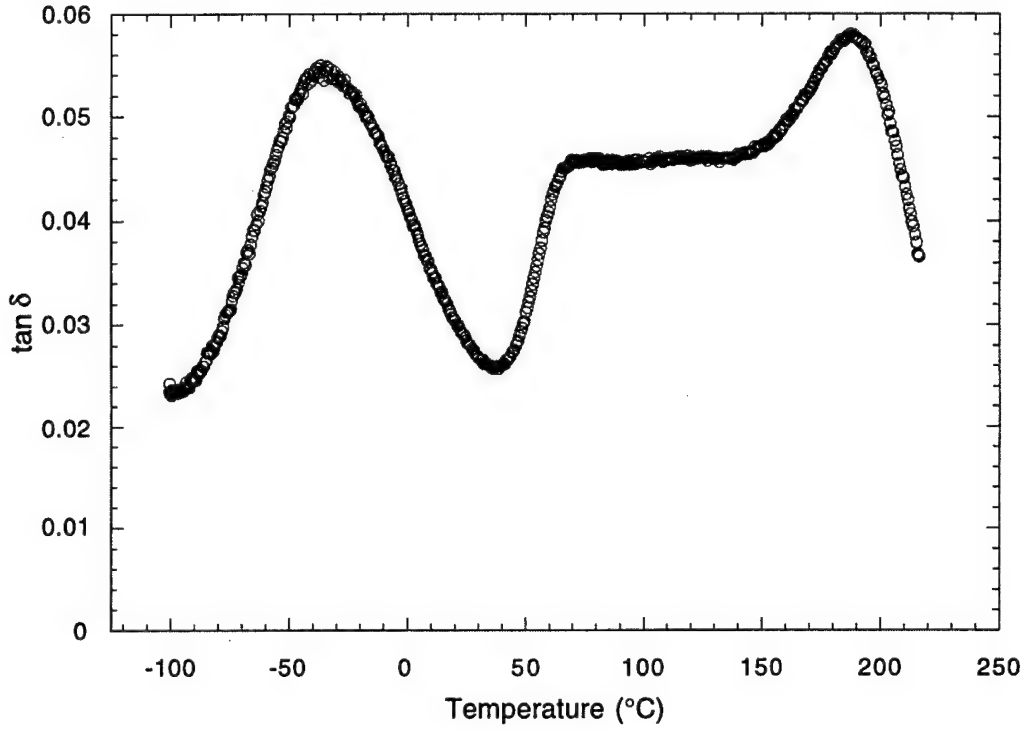

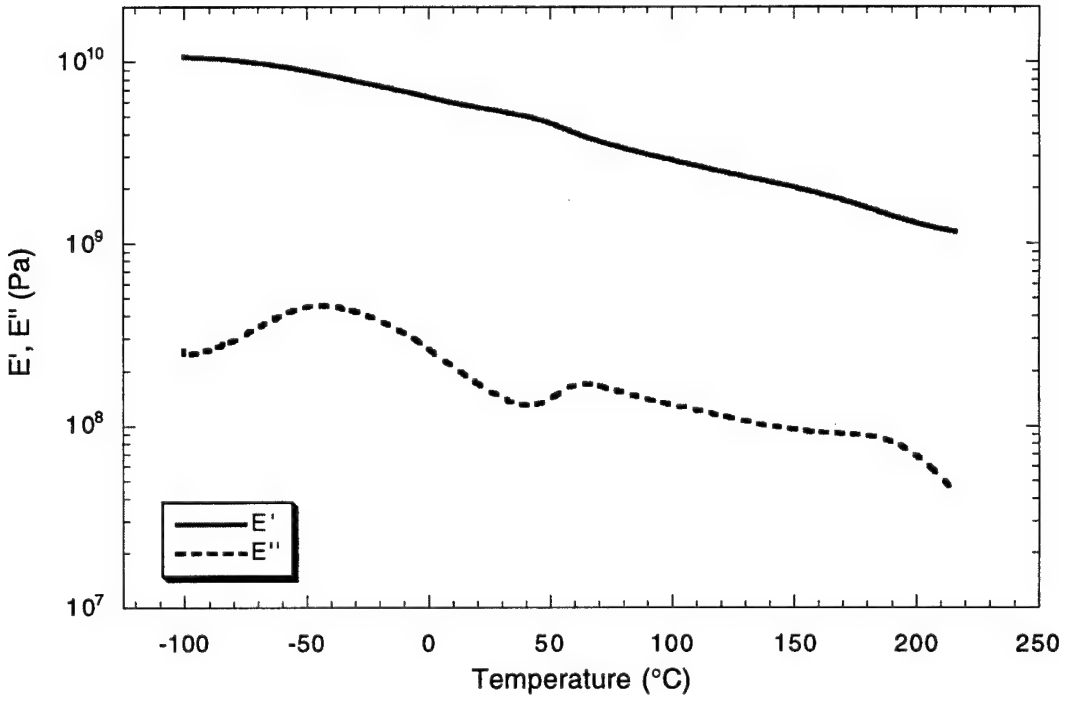

Tan δ, dynamic loss and storage modulus curves for the statistical experimental design sample #2.

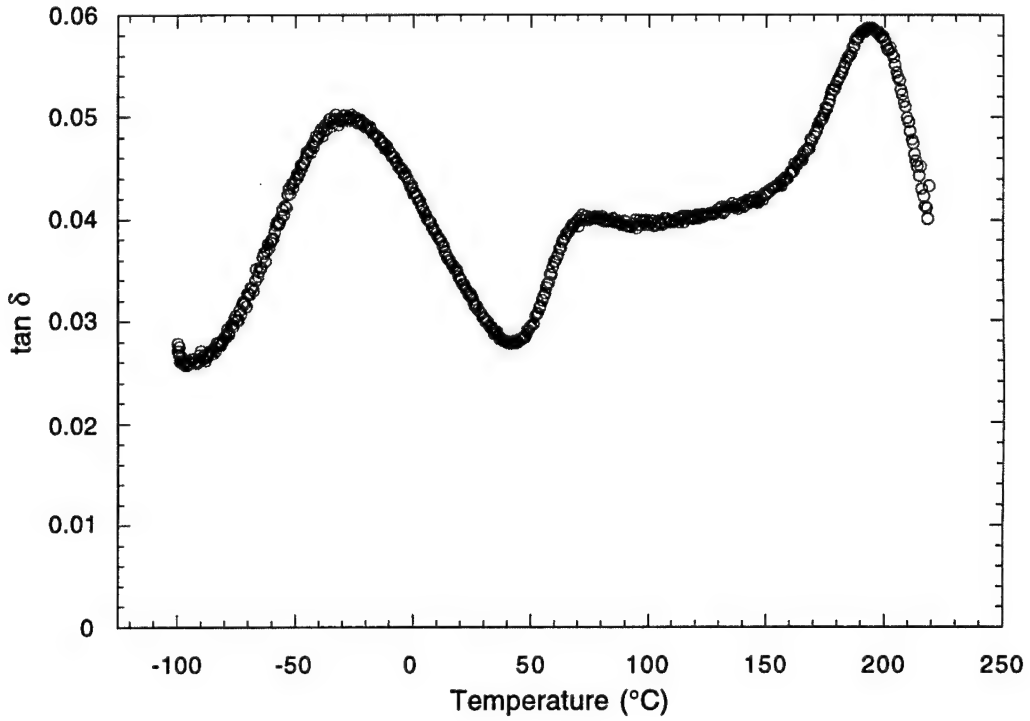

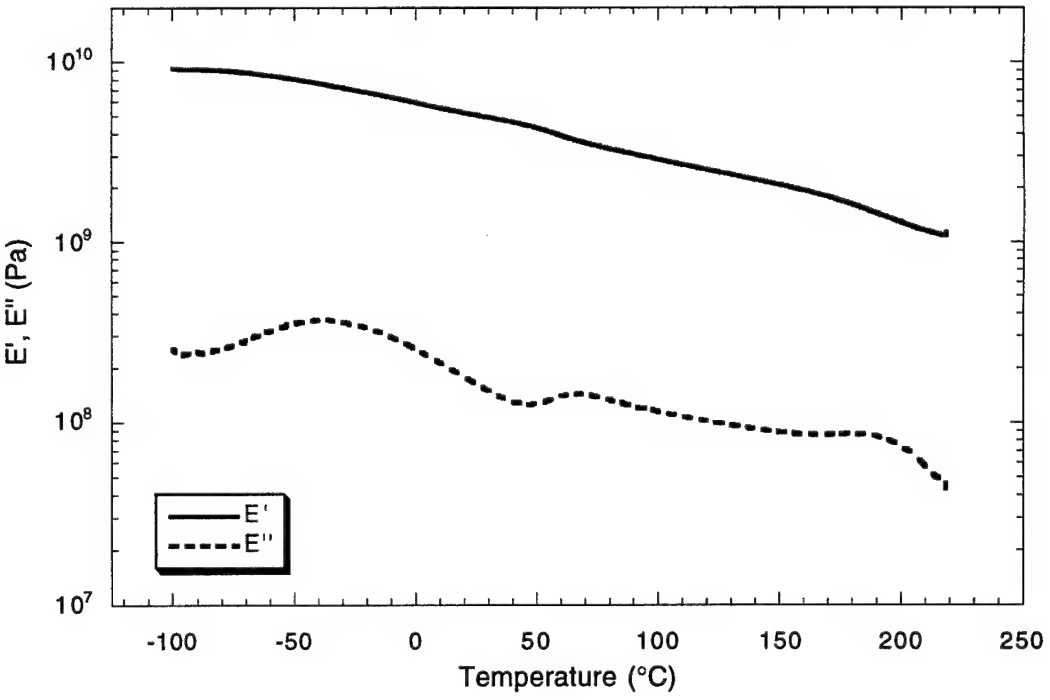

Tan δ, dynamic loss and storage modulus curves for the statistical experimental design sample #3.

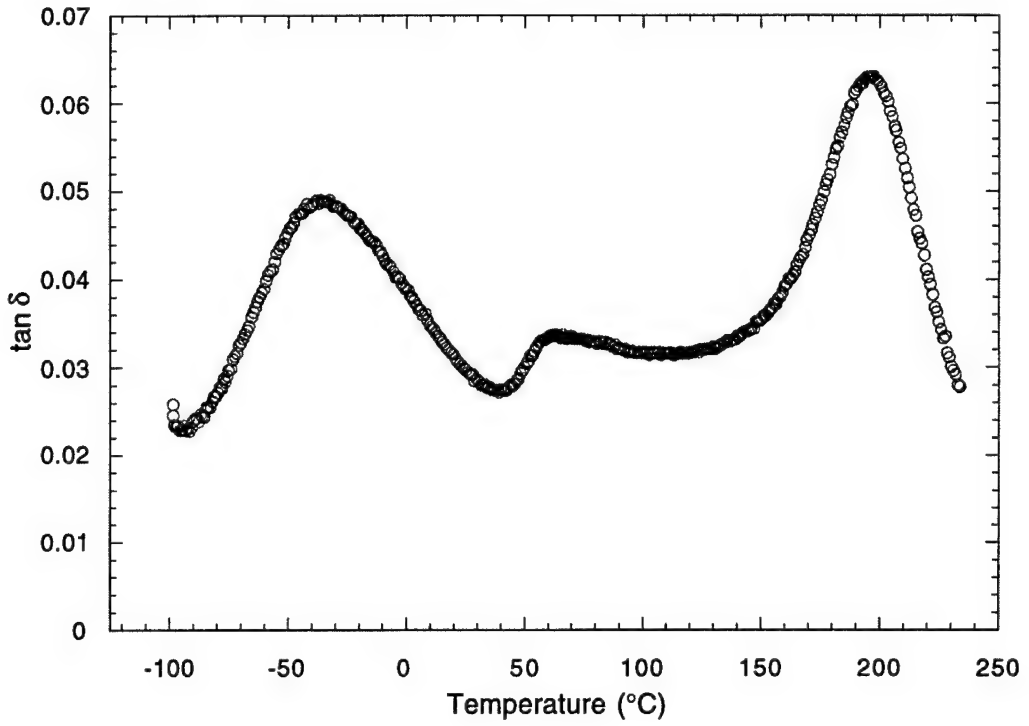

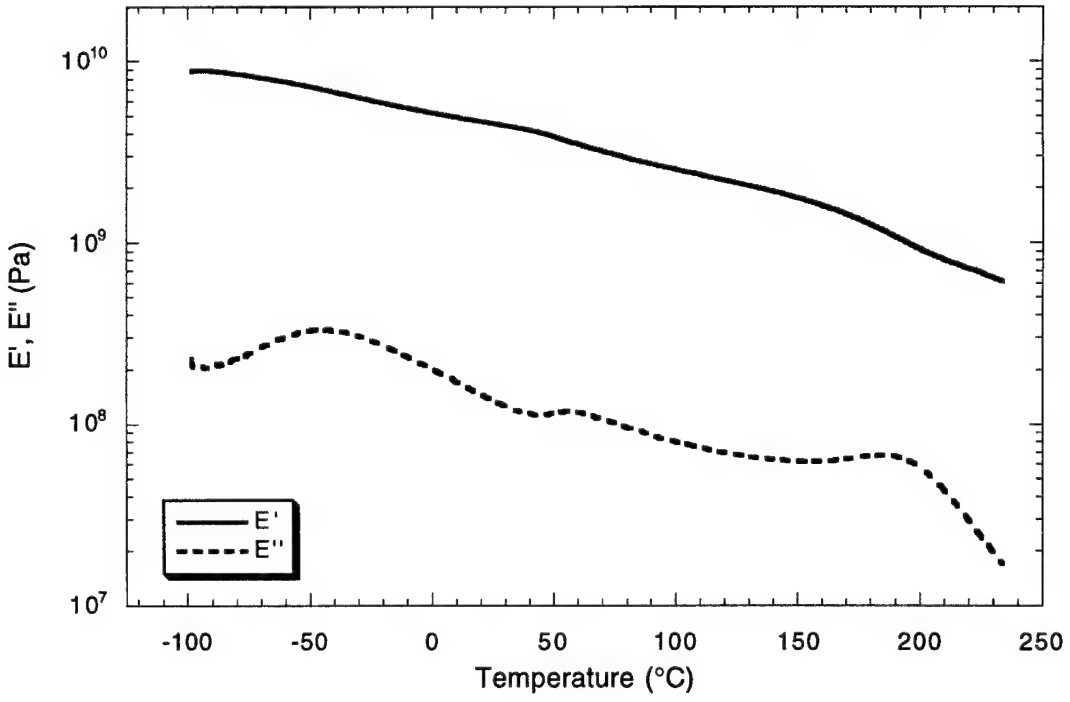

Tan δ, dynamic loss and storage modulus curves for the statistical experimental design sample #4.

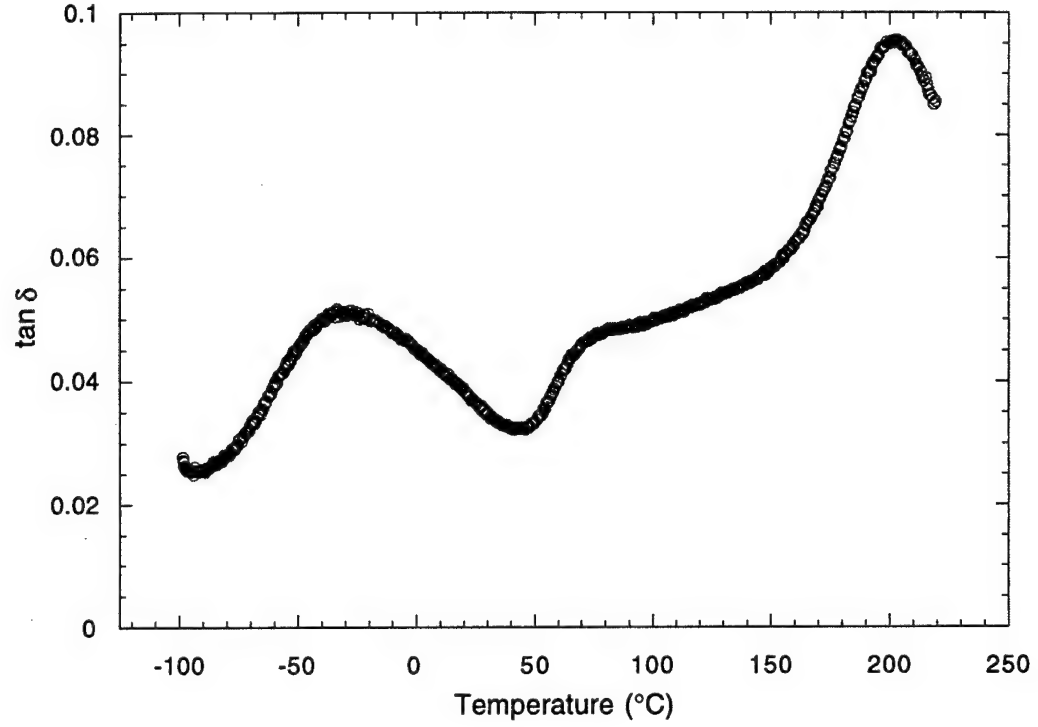

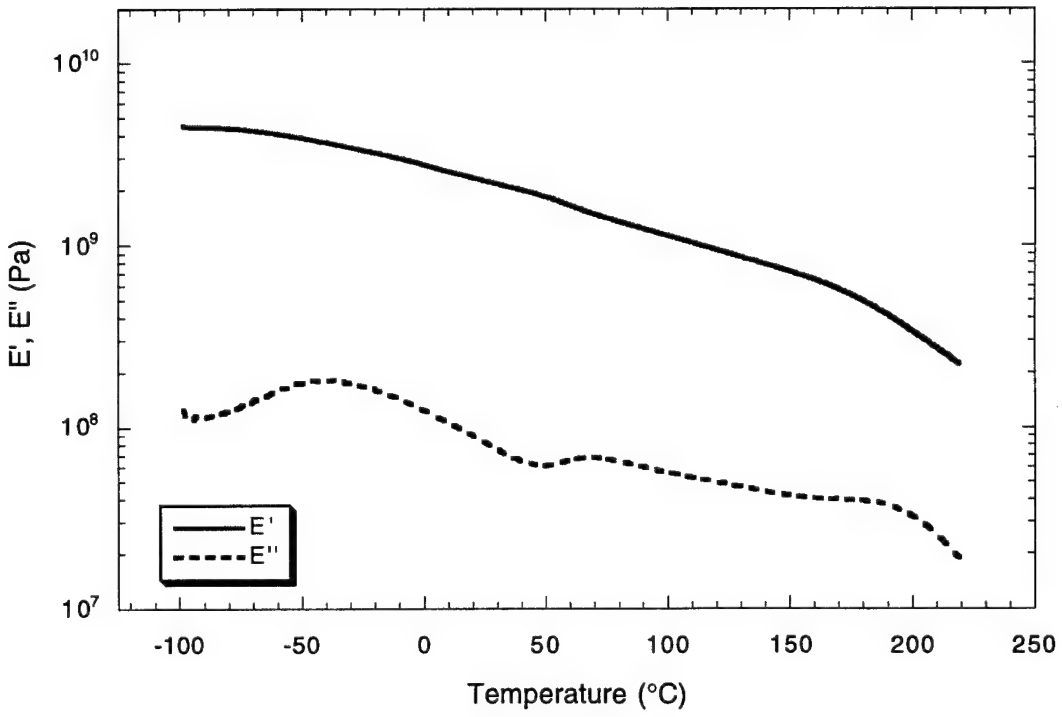

Tan δ, dynamic loss and storage modulus curves for the statistical experimental design sample #5

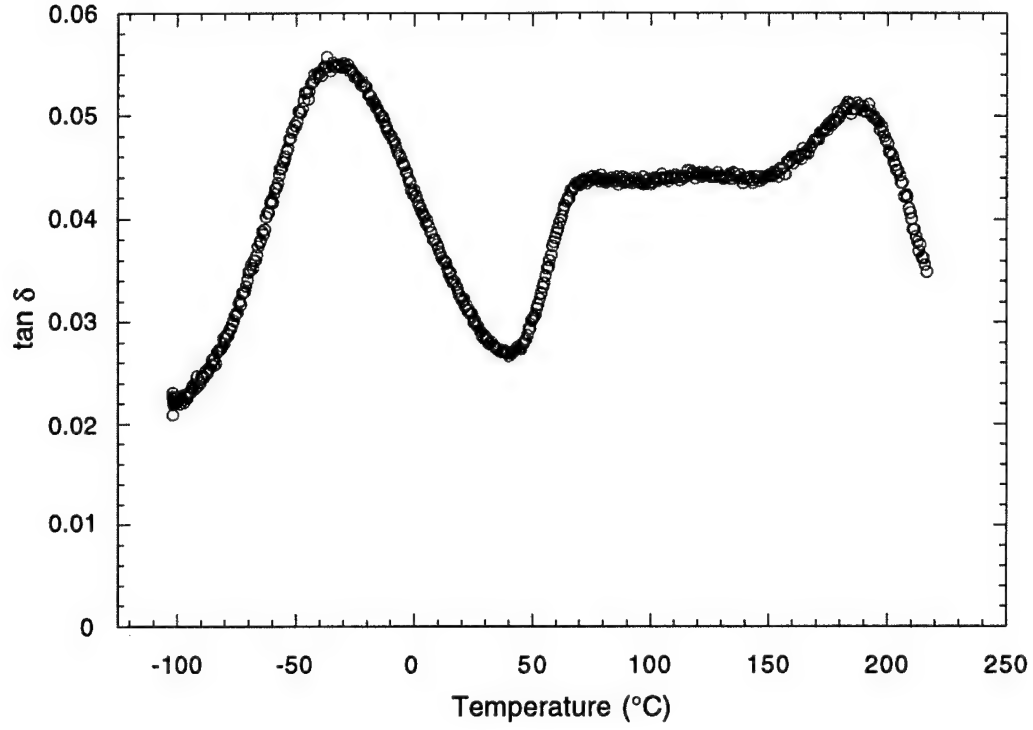

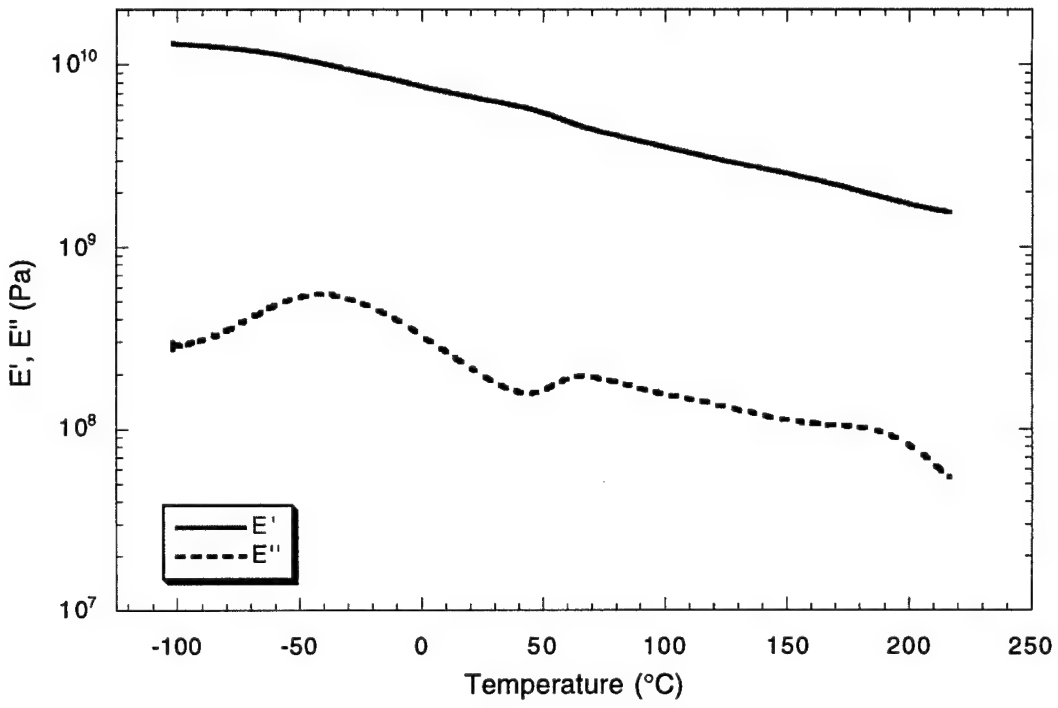

Tan δ, dynamic loss and storage modulus curves for the statistical experimental design sample #6.

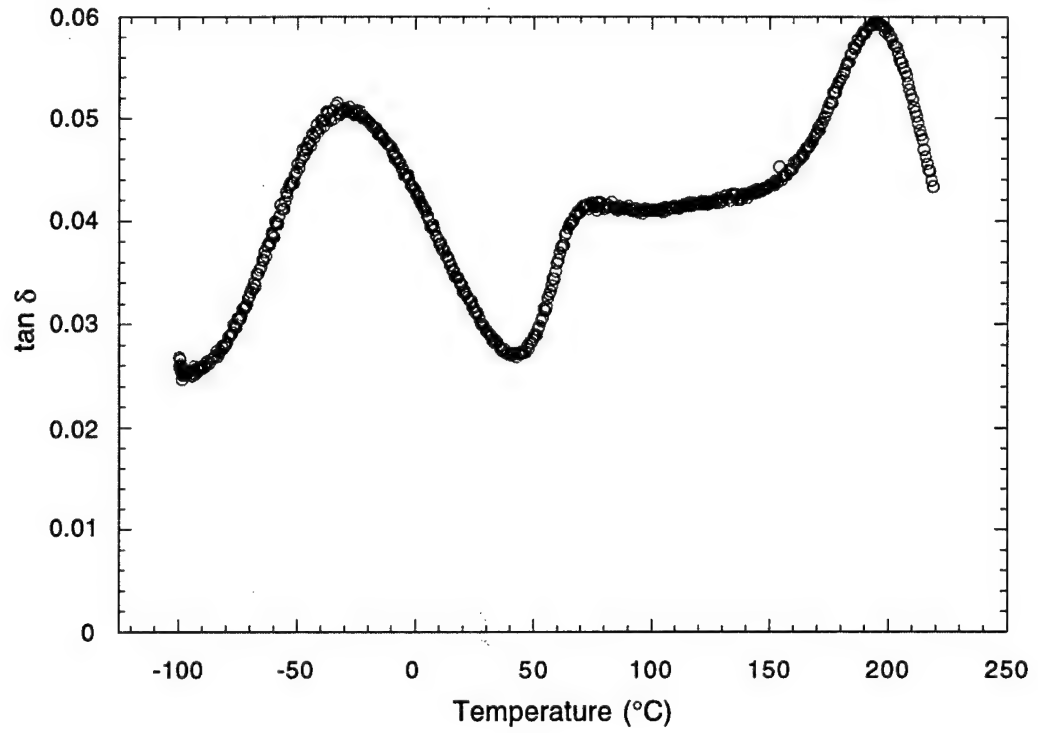

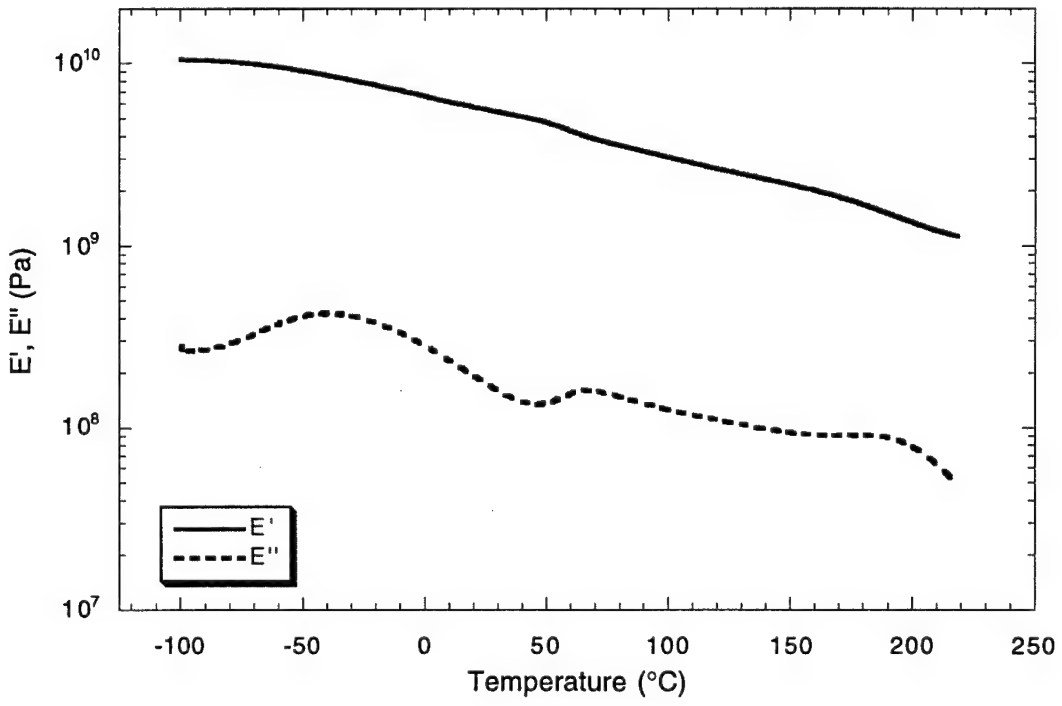

Tan δ, dynamic loss and storage modulus curves for the statistical experimental design sample #7.

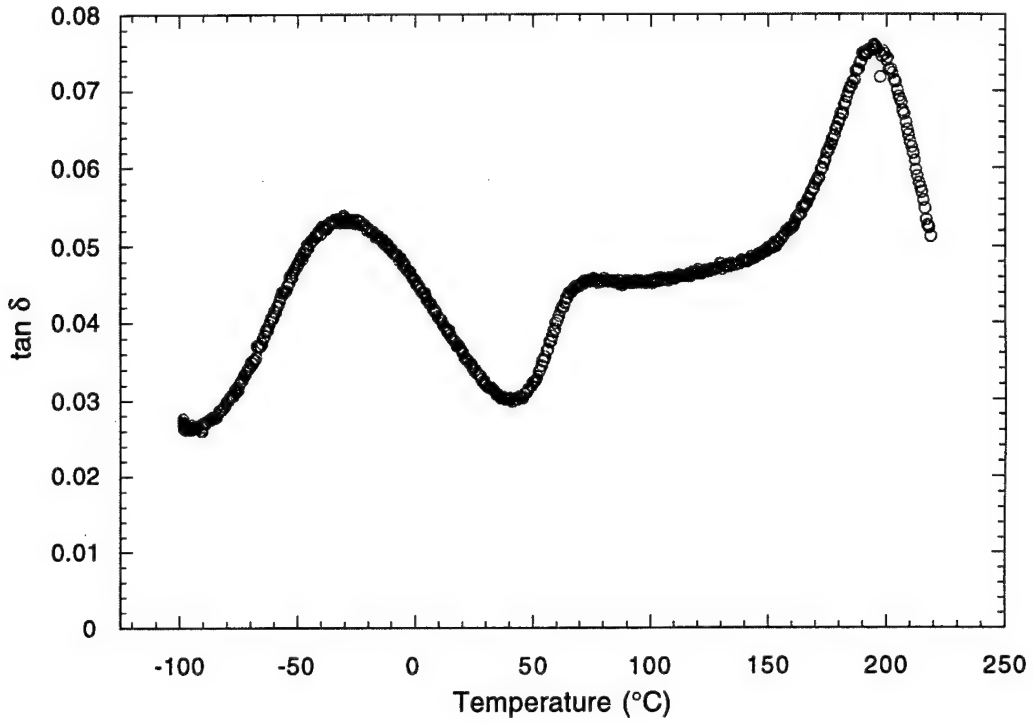

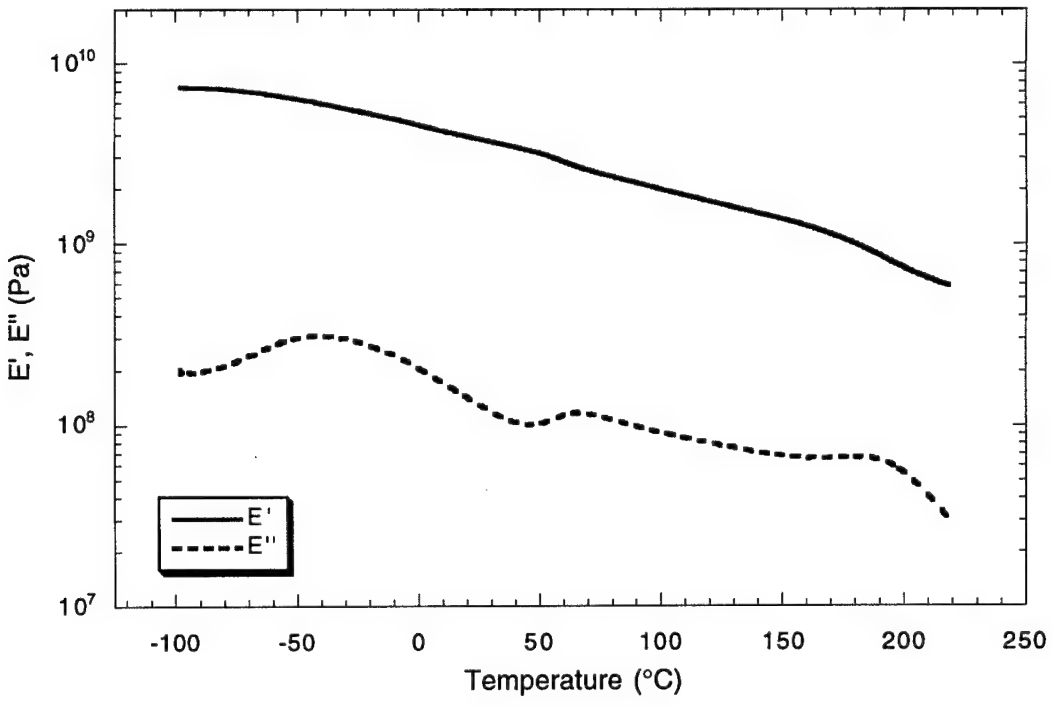

Tan δ, dynamic loss and storage modulus curves for the statistical experimental design sample #8.

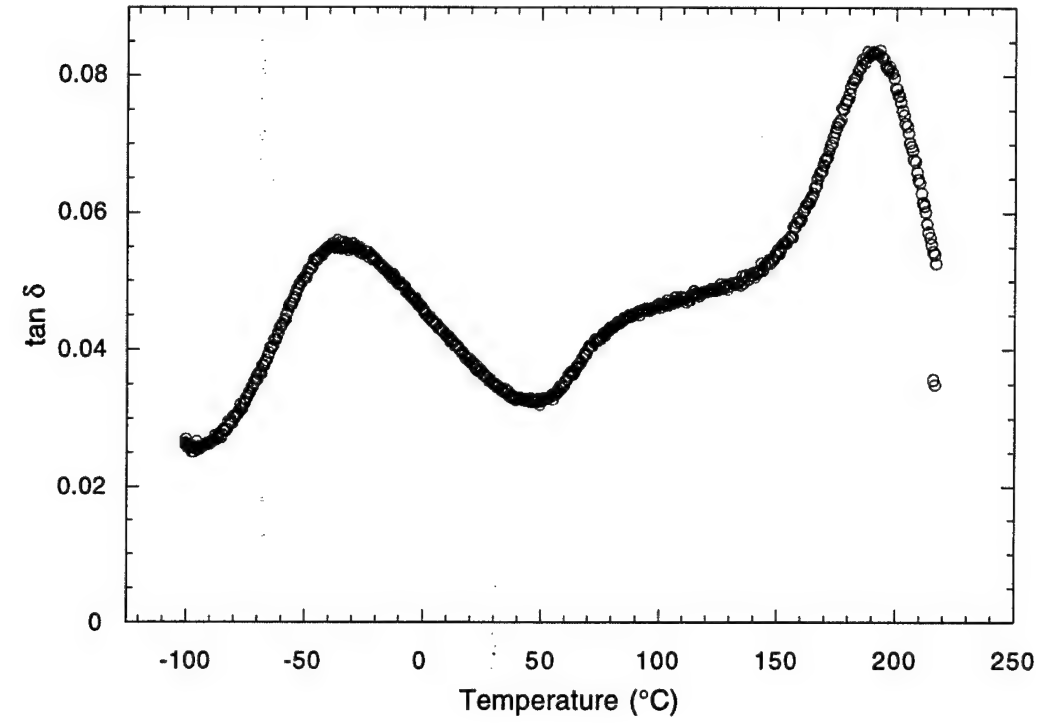

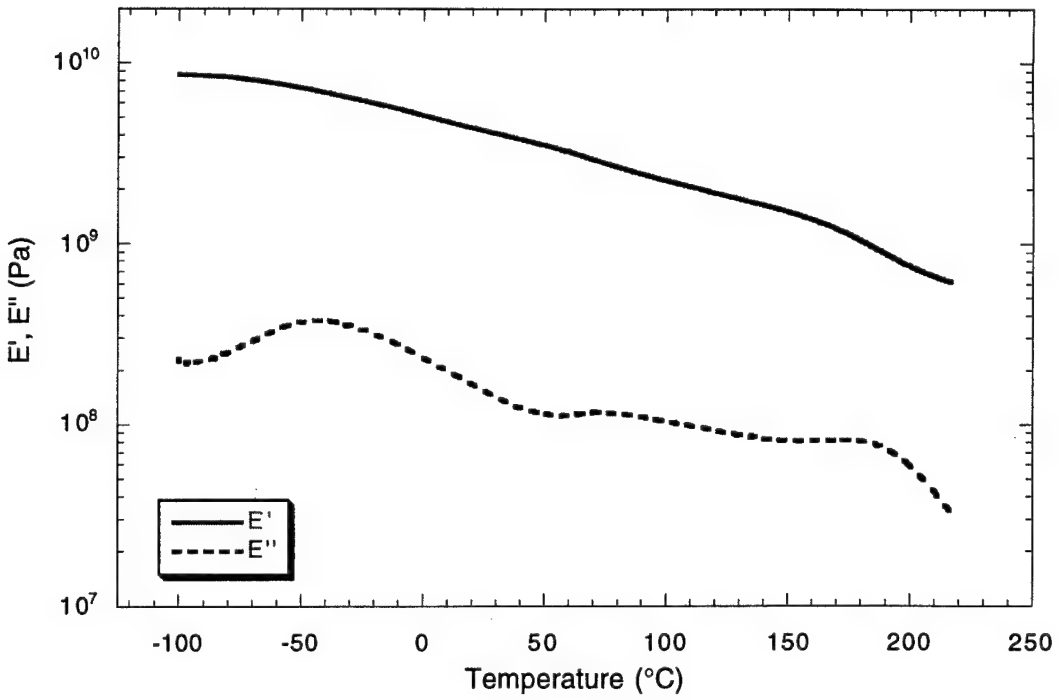

Tan δ, dynamic loss and storage modulus curves for the statistical experimental design sample #9.

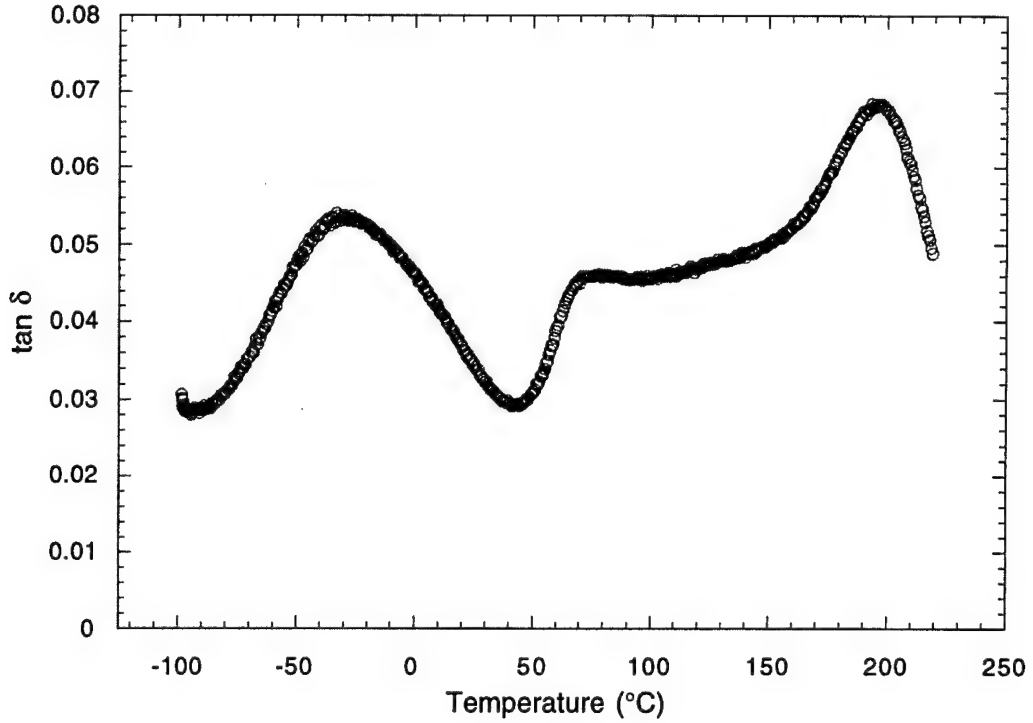

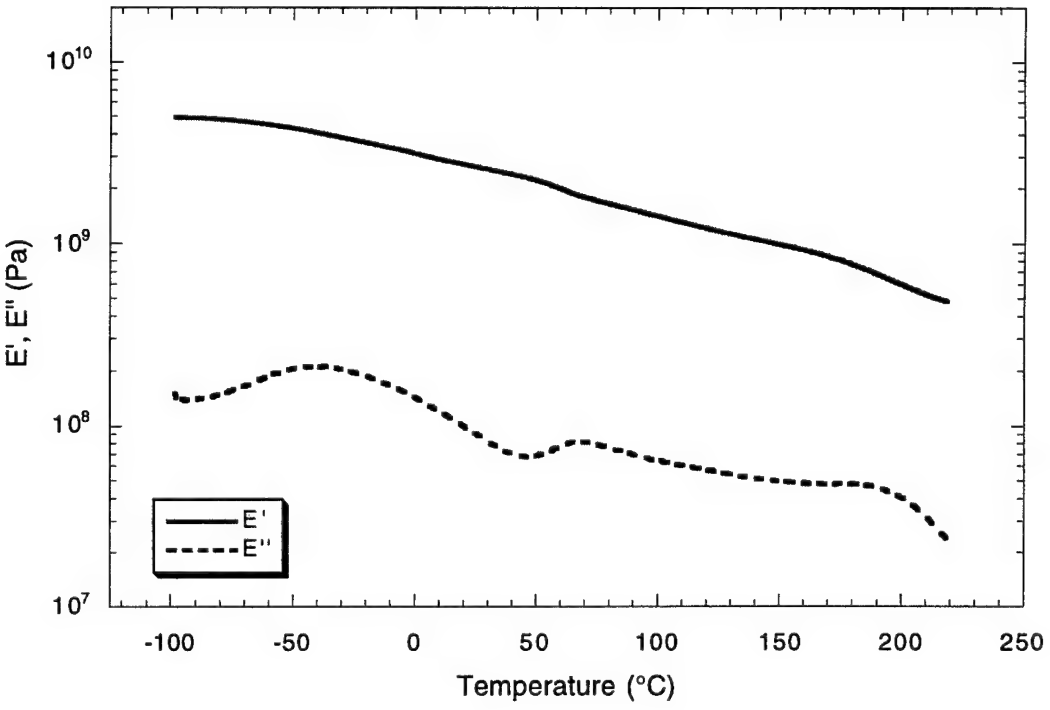

Tan δ, dynamic loss and storage modulus curves for the statistical experimental design sample #10.

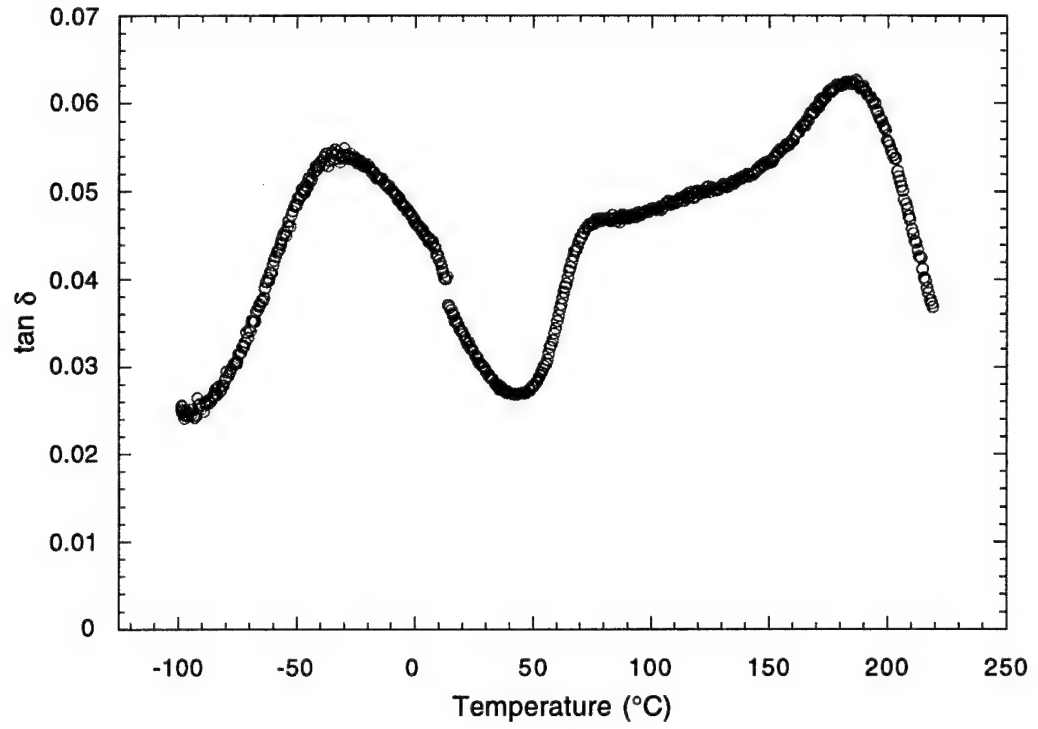

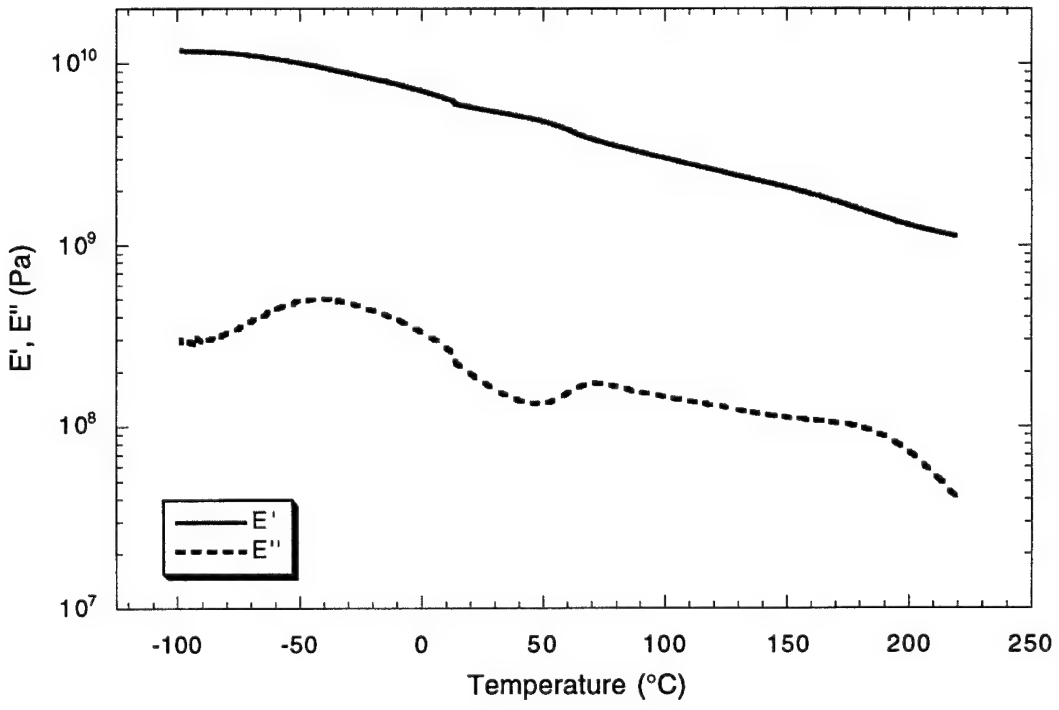

Tan δ, dynamic loss and storage modulus curves for the statistical experimental design sample #11.

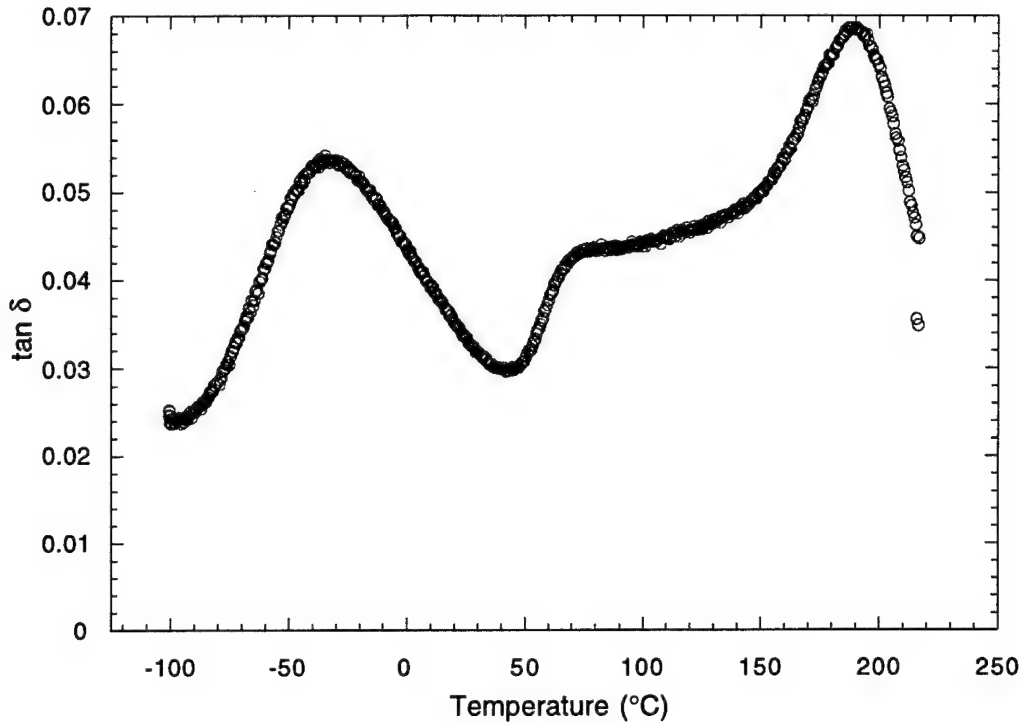

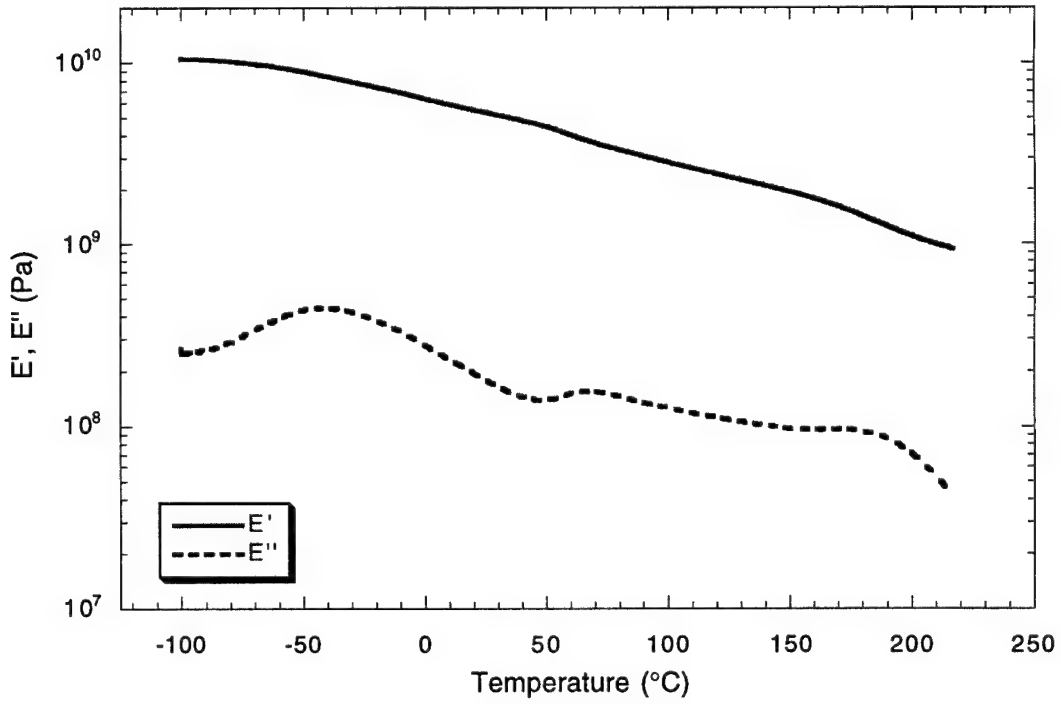

LIST OF REFERENCES

Adm78 Admur, S; Chang, A.; Wong, C.; Ehrlich, P.; Allendoerfer, D. *J. Polym. Sci. Polym. Chem. Ed.* **1978**, *16*, 407

Alt95 Alt, David J.; Hudson, Steven D.; Garag, R. O.; Fujishiro, K. *Macromolecules*. **1995**, *28*, 1575

Anw91 Anwer, Afzana; Windle, Alan H. *Polymer*. **1991**, *32*, 103

Anw93 Anwer, A.; Windle, A. H. *Polymer*. **1993**, *34*, 3347

Arr72 Arridge, R. G. C.; Speake, J. H. *Polymer*. **1972**, *13*, 443

Ass97 Assender, Hazel E.; Windle, Alan H. *Polymer*. **1997**, *38*, 677

Avi76 Aviram, A. *Polym. Sci.: Polym. Lett. Ed.* **1976**, *14*, 757

Bar92 Barclay, G. G.; McNamee, S. G.; Ober, C. K.; Papathoms, K. I.; Wang, D. W. *J. Polym. Sci.: Part A: Polym. Chem.* **1992**, *30*, 1845

Bee96 Beekmans, F.; Posthuma de Boer, A. *Macromolecules*. **1996**, *29*, 8726

Bel90 Bellenger, V.; Dhoui, W.; Verdu, J.; Boye, J.; Lacabanne, C. *Polym. Eng. Sci.* **1990**, *30*, 321

Ben92 Benicewicz, Brian C.; Hoyt, Andrea E. U.S. Patent 5,114,612 1992.

Ben98 Benicewicz, Brian C.; Smith, Mark E.; Earls, Jim D.; Priester, Ralph D.; Setz, Stefan M.; Duran, Randolph S.; Douglas, Elliot P. *Macromolecules*. submitted

Bli97 Blinov, L. M. in *Handbook of Liquid Crystal Research*. Collings, Peter J.; Patel, Jay S. Eds. Oxford University Press: New York, 1997, p. 125.

Car70 Carr, E. F. *Phys. Rev. Lett.* **1970**, *24*, 807

Car93 Carfagna, C.; Amendola, E.; Giamberini, M.; Filippov, A. G.; Bauer, R. S. *Liquid Crystals*. **1993**, *13*, 571

Car94a Carfagna, C.; Amendola, E; Giamberini, M. *Composite Structures*. **1994**, *27*, 37

Car94b Carfagna, C.; Amendola, E; Giamberini, M. *J. Mat. Sci. Lett*. **1994**, *13*, 126

Car94c Carfagna, C.; Amendola, E.; Giamberini, M. *Liquid Crystalline Polymers: Proceedings of the International Workshop of Liquid Crystalline Polymers*. Capri, Italy, June 1-4, 1993, Carfagna, C. Ed.; Pergamon Press: Oxford, UK, 1994; pp. 69-85.

Car94d Carfagna, Cosimo; Amendola, Eugenio; Giamberini, Marta. *Macromol. Rapid Commun*. **1994**, *195*, 279

Car94e Carfagna, Cosimo; Amendola, Eugenio; Giamberini, Marta. *Macromol. Chem. Phys*. **1994**, *195*, 2307

Car95 Carfagna, C.; Amendola, E.; Giamberini, M.; Mensitieri, G.; Del Nobile, M. A.; Filippov, A. G. *Polym. Eng. Sci*. **1995**, *35*, 137

Cha94 Chang, Rong-Yeu; Sjiao, Fu-Chia; Yang, Wen-Lii. *J. Non-Newtonian Fluid Mech*. **1994**, *55*, 1

Col97 Collings, Peter J.; Patel, Jay S. in *Handbook of Liquid Crystal Research*. Collings, Peter J.; Patel, Jay S. Eds.; Oxford University Press: New York, 1997, p. 1.

Cre92 Crevecour, G.; Groeninckx, G. *Polymer Composites*. **1992**, *13*, 244

deG93 de Gennes, P. G.; Prost, J. *The Physics of Liquid Crystals*. Clarendon Press: Oxford, 1993.

Dem80 Demus, D.; Richter, L. *Texture of Liquid Crystals*. VEB Deutscher Verlag für Grundstoff Industrie: Leipzig, 1980.

Dre98 Dreher, S.; Seifert, S.; Zachmann, H. G.; Moszner, N.; Mercoli, P.; Zanghellini, G. *J. Appl. Polym. Sci*. **1998**, *67*, 531

Dut90 Dutta, D.; Fruitwala, H.; Kohli, A.; Weiss, R. A. *Polym. Eng. Sci*. **1990**, *30*, 1005

Eck96 Eckert, Tobias; Finklemann, Heino. *Macromol. Rapid Commun.* **1996**, *17*, 767

Eic96 Eichorn, Klaus J.; Sahre, Karin; Jahnichen, Diefer; Tobisch, Josef; Häbler, Liane. *Macromol. Chem. Phys.* **1996**, *197*, 3729

Eng94 Engberg, K.; Strömberg, O.; Martinsson, J.; Gedde, U. W. *Polym. Sci. Eng.* **1994**, *34*, 1336

Enn83 Enns, John B.; Gillham, John K. *J. Appl. Polym. Sci.* **1983**, *28*, 2831

Fer97 Ferri, D.; Laus, M. *Macromolecules.* **1997**, *30*, 6007

Ger91 Gerzeski, Roger H. *Int. SAMPE Symp.* **1991**, *36*, 1368

Gia95 Giamberini, Marta; Amendola, Eugenio; Carfagna, Cosimo. *Macromol. Rapid Commun.* **1995**, *16*, 97

Gra83 Gray, M. E.; Harrison, I. R. *J. Appl. Polym. Sci.* **1983**, *28*, 3603

Gri91 Grillet, Anne Cecile; Galy, Jocelyne; Gerard, Jean-Francois; Pascault, Jean-Pierre. *Polymer.* **1991**, *32*, 1885

Gul72 Gul', V. E.; Trifel', Yu. B.; Abdullaev, N. A. *Mekhanika Polimerov.* **1972**, *5*, 923

Gup85 Gupta, V. B.; Drzal, L. T.; Lee, C. Y. C. *Polym. Eng. Sci.* **1985**, *25*, 812

Han96 Hanabusa, Kenji; Hashimoto, Masami; Kimura, Mutsumi; Koyama, Toshiki; Shirai, Hirofusa. *Macromol. Chem. Phys.* **1996**, *197*, 1853

Her80 Hergenrother, P. M. *J. Macromol. Chem.* **1980**, *C19*, 1

Hey93 Heynderickx, I; Paridaans, F. *Polymer.* **1993**, *34*, 4068

Hik91 Hikmet, R. A.; Broer, D. J. *Polymer.* **1991**, *32*, 1627

Hik93 Hikmet, R. A. M.; Lub, J.; Higgins, J. A. *Polymer.* **1993**, *34*, 1736

Hoy90a Hoyt, Andrea E.; Benicewicz, Brian C.; Huang, Samuel J. in *ACS Symposium Series 435*. Weiss, R. A.; Ober, C. K., Eds.; American Chemical Society: Washington, D. C., 1990, p. 198.

Hoy90b Hoyt, Andrea E.; Benicewicz, Brian C. *J. Polym. Sci.: Part A: Polym. Chem.* **1990**, *28*, 3403

Hoy90c Hoyt, Andrea E.; Benicewicz, Brian C. *J. Polym. Sci.: Part A: Polym. Chem.* **1990**, *28*, 3417

Hud90 Hudson, Steven D.; Thomas, Edwin L. *Polymer Preprints.* **1990**, *31*, 379

Iiz85 Iizuka, Eisaku. *J. of Appl. Polym. Sci.: Appl. Polym. Symp.* **1985**, *41*, 131

Jen73 Jen, S.; Clark, N. A.; Pershan, P. S.; Priestly, E. B. *Phys. Rev. Lett.* **1973**, *31*, 1552

Kis78 Kishore, P. R.; Rao, N. V. S.; Sarma, P. B. K.; Raj, T. F. S.; Avadhanlu, M. N.; Murty, C. R. K. *Mol. Cryst. Liq. Cryst.* **1978**, *45*, 231

Kis87 Kiss, Gabor. *Polym. Eng. Sci.* **1987**, *27*, 410

Kee79 Keenan, Joseph D.; Seferis, James C.; Quinlivan, John T. *J. Appl. Polym. Sci.* **1979**, *24*, 2375

Kos97 Kossikhina, S.; Kimura, T.; Ito, E.; Kawahara, M. *Polym. Eng. and Sci.* **1997**, *37*, 396

Koz89 Kozak, A.; Simon, G. P.; Williams, G. *Polym. Commun.* **1989**, *30*, 102

Kra76 Kramarenko, N. L.; Kurnosov, I. V.; Naboikin, Yu. V. *Phys. Stat. Sol. (A).* **1976**, *33*, 773

Li96 Li, Jianlin; Anderson, James E.; Hoke, Charles D.; Nose, Toshiaki; Bos, Philip J. *Jpn. J. Appl. Phys.* **1996**, *35*, 1342

Lin94 Lin, Qinghuang; Yee, Albert F.; Earls, Jimmy D.; Hefner Jr., Robert E.; Sue, Hung-Jue. *Polymer.* **1994**, *35*, 2679

Lin97 Lin, Q.; Yee, A. F.; Sue, H-J.; Earls, J. D.; Hefner Jr., R. E. *J. Polym. Sci. Part B: Polym. Phys.* **1997**, *35*, 2363

Lit93 Litt, Morton H.; Whang, Wha-Tzong; Yen, Kung-Ti; Qian, Xue-Jun. *J. Polym. Sci.: Part A: Polym Chem.* **1993**, *31*, 183

Liu97 Liu, Jingping; Wang, Chicheng; Campbell, Gregory A.; Earls, Jim D.; Priester Jr., Ralph D. *J. Polym. Sci.: Part A: Polym. Chem.* **1997**, *35*, 1105

Mar82 Maret, G.; Blumstein, A. *Mol. Cryst. Liq. Cryst.* **1982**, *88*, 295

Mar91 Marrucci, Giuseppe; Grizzuti, Nino. *Makromol. Chem. Macromol. Symp.* **1991**, *181*

Mel94 Melissaris, Anastasios P.; Litt, Morton H. *Macromolecules.* **1994**, *27*, 2675

Mel95 Melissaris, Anastsios P.; Sutter, James K.; Litt, Morton H.; Scheiman, Daniel A.; Schuerman, Marla A. *Macromolecules.* **1995**, *28*, 860

Mic86 Michl, J.; Thulstrup, E. W. *Spectroscopy with Polarized Light.* VCH Publishers: Deerfield Beach, FL, 1986.

Mik87 Mikolajczak, G.; Cavaille, J. Y.; Johari, G. P. *Polymer.* **1987**, *28*, 2023

Miy78 Miyano, K. *J. Chem Phys.* **1978**, *69*, 4807

Moo85 Moore, R. C.; Denn, M. M.; Marrucci, G. *Polym. Mat. Sci. Eng.* **1985**, *52*, 84

Moo87 Moore, J. S.; Stupp, S. I. *Macromolecules.* **1987**, *20*, 282

Moo96 Moon, Hyuk-Soo; Park, Jung-Ki; Liu, Ju-Hwan. *J. Appl. Polym. Sci.* **1996**, *59*, 489

Och85 Ochi, Mitsukazu; Iesako, Hiroshi; Shimbo, Masakis. *Polymer.* **1985**, *26*, 457

Pav88 Pavia, Donald L.; Lampman, Gary M.; Kriz, George S. *Introduction to Organic Laboratory Techniques: A Contemporary Approach.* Saunder College Publishing: Philadelphia, 1988, pp. 318-19.

Pog70 Pogany, G. A. *Polymer.* **1970**, *11*, 66

Rao76 Rao, N. V. S.; Kishore, P. R.; Raj, T. F. S.; Avadhanlu, M. N.; Murty, C. R. K. *Mol. Cryst. Liq. Cryst.* **1976**, *36*, 65

Rat80 Rato, J.; Dynes, P.; Hamermesh, C. J. *J. Polym. Sci. Polym. Chem. Ed.* **1980**, *18*, 1035

Rod91 Rodin, Yu P. *Mekhanika Kompozitnykh Metrialov.* **1991**, *3*, 490

San95 Sanz, G.; Garmendia, J.; Andes, M. A.; Mondragon, I. *J. Appl. Polym. Sci.* **1995**, *55*, 75

Sas91 Sasuga, Tsuneo; Udagawa, Akira. *Polymer.* **1991**, *32*, 402

Saw86 Sawyer, Linda C.; Jaffe, Michael. *J. of Mat. Sci.* **1986**, *21*, 1897

Shi96 Shiota, Atsushi; Ober, Christopher K. *J. Polym. Sci.: Part A: Polym. Chem.* **1996**, *34*, 1291

Shi97a Shimoda, Toshiyuki; Kimura, Tsuehisa; Ito, Eiko. *Macromolecules.* **1997**, *30*, 5045

Shi97b Shiota, Atsushi; Ober, Christopher K. *Macromolecules.* **1997**, *30*, 4278

Shi97c Shiota, Atsushi; Ober, Christopher K. *Polymer.* **1997**, *38*, 5857

Smi96 Smith, M. E.; Douglas, E. P.; Benicewicz B. C.; Earls, J. D.; Priester Jr., R. D. *Mater. Res. Soc. Proc.* **1996**, *425*, 167

Tal93 Tal'roze, R. V.; Plate, N. A. in *Liquid-Crystal Polymers.* Plate, N. A. Ed. Plenum Press: New York, 1993, p. 303.

Ven95a Venditti, R. A.; Gillham, J. K.; Jean, Y. C.; Lou, Y. *J. Appl. Polym. Sci.* **1995**, *56*, 1207

Ven95b Venditti, R. A.; Gillham, J. K. *J. Appl. Polym. Sci.* **1995**, *56*, 1687

Yam89 Yamagishi, Akio; Takeuchi, Tetsuya; Higashi, Terumasa; Date, Muneyuki. *J. Phys. Soc. Jpn.* **1989**, *58*, 2280

Yos96 Yoshiki, Kazumasa; Nakayama, Kazuo; Kyotani, Mutsumasa. *J. Appl. Polym. Sci.* **1996**, *62*, 1331

Zen85 Zentel, Rudolf; Strobl, Gert R.; Ringsdorf, Helmut. *Macromolecules.* **1985**, *18*, 960

Zha96 Zhao, Yue; Roche, Philippe; Yuan, Guoxiong. *Macromolecules*. **1996**, *29*, 4619

BIOGRAPHICAL SKETCH

Derek Lincoln was born in Denver, Colorado, on 20 January 1974. He lived in Colorado from birth until coming to the University of Florida for work on his Master of Science degree in August 1996. Prior to that he earned his Bachelor of Science degree and a commission as a second lieutenant in the United States Air Force from the United States Air Force Academy in Colorado Springs, Colorado.

Following graduation from the University of Florida he was assigned to the Air Force Material labs at Wright-Patterson Air Force Base, Dayton Ohio, to work in the Materials and Manufacturing Directorate, Non-metallic materials division, Polymer branch.

I certify that I have read this study and that in my opinion it conforms to acceptable standards of scholarly presentation and is fully adequate, in scope and quality, as a thesis for the degree of Master of Science.

Elliot P. Douglas, Chair
Assistant Professor of Materials Science and Engineering

I certify that I have read this study and that in my opinion it conforms to acceptable standards of scholarly presentation and is fully adequate, in scope and quality, as a thesis for the degree of Master of Science.

Anthony B. Brennan
Associate Professor of Materials Science and Engineering

I certify that I have read this study and that in my opinion it conforms to acceptable standards of scholarly presentation and is fully adequate, in scope and quality, as a thesis for the degree of Master of Science.

Christopher D. Batich
Professor of Materials Science and Engineering

This thesis was submitted to the Graduate Faculty of the College of Engineering and to the Graduate School and was accepted as partial fulfillment of the requirements for the degree of Master of Science.

August, 1998

Winfred M. Phillips
Dean, College of Engineering

Karen A. Holbrook
Dean, Graduate School